International
Progress Report

IPR-02-32

Äspö Hard Rock Laboratory

TRUE Block Scale project

Predictive modelling and evaluation of the Phase C tracer tests using the Posiva Streamtube approach

Posiva/VTT Processes modelling team

Antti Poteri

VTT Processes

October 2002

Svensk Kärnbränslehantering AB
Swedish Nuclear Fuel
and Waste Management Co
Box 5864
SE-102 40 Stockholm Sweden
Tel +46 8 459 84 00
Fax +46 8 661 57 19

Äspö Hard Rock Laboratory

Report no.
IPR-02-32
No.
F56K
Author
Antti Poteri
Date
Oct 2002
Checked by
Anders Winberg
Date
Jan 2003
Approved
Christer Svemar
Date
03-04-17

Äspö Hard Rock Laboratory

TRUE Block Scale project

Predictive modelling and evaluation of the Phase C tracer tests using the Posiva Streamtube approach

Posiva/VTT Processes modelling team

Antti Poteri

VTT Processes

October 2002

Keywords: Breakthrough, flow channel, matrix diffusion, modelling, predictive, streamtube

Abstract

Predictive modelling and evaluation of the Phase C tracer tests performed as part of the TRUE Block Scale project were performed using the Posiva Streamtube approach. The predictive modelling was based on the concept of a single flow channel that connects the source and the sink sections. Properties of the flow channels were estimated using the results of the Phase B tracer tests. Matrix diffusion and retardation properties of the different tracers were imported from results of the corresponding evaluation of the TRUE-1 tracer tests, the latter carried out in an interpreted single fracture. The TRUE-1 tracer tests were interpreted to provide the matrix diffusion and sorption properties along single fracture flow paths. The evaluated matrix diffusion and sorption properties were applied directly to predict the TRUE Block Scale tracer tests performed in a network of fractures. The import is based on the assumption that the characteristics of the immobile pore spaces at the TRUE-1 and TRUE Block Scale sites are similar. A comparison with *in situ* test results show that the predicted breakthrough curves are reasonably accurate for the non-sorbing tracers. For the sorbing tracers the discrepancy between the measured and predicted breakthrough curves increases with increasing sorptivity of the tracer. Following the predictive modelling, the breakthrough curves were modelled anew relative to the measured breakthrough curves to identify the processes causing the observed tracer retention. The most consistent understanding of the Phase C tracer tests was provided by a model that is based on surface sorption on the fracture surfaces combined with matrix diffusion into fault gouge. The least sorbing tracers also show retardation caused by diffusion into stagnant zones of the flow field.

Sammanfattning

Prediktiv modellering och utvärdering av Phase C-försöken, en del av TRUE Block Scale, utfördes med utnyttjade av ”Posiva Streamtube approach”. Den utförda prediktiva modelleringen baseras på konceptet att en enskild flödeskanal förbinder injiceringssektion och pumpsektion. Transportegenskaperna hos flödeskanalen har uppskattats med hjälp av resultaten från Phase B-försöken. Egenskaper som beskriver matrisdiffusion och övriga retentionsegenskaper för utnyttjade spårämnena har importerats från utvärderingen av försöken på TRUE-1-siten. Dessa försök genomfördes i en enskild spricka. Utvärderingen av TRUE-1-experimenten antogs ge de efterfrågade retentionsegenskaperna längs flödesvägar i enskilda sprickor. Dessa utnyttjades sedan direkt i prediktionen av försök i blockskala för de nätverk av sprickor som undersöktes inom ramen för TRUE Block Scale. Den utförda importen motiverades av antagandet att egenskaper och struktur hos de stagnanta zonerna längs flödesvägarna på de två platserna är likartade. Modellförutsägelser av genombrottskurvor visar överlag god överensstämmelse för icke-sorberande spårämnen. För sorberande spårämnen ökar avvikelsen mellan mätta och simulerade genombrottskurvor med ökande sorptionskapacitet. Därefter utvärderades de mätta genombrottskurvorna med hjälp av den upprättade modellen för att söka identifiera de processer som orsakat den observerade retentionen. Den mest konsistenta tolkningen av Phase C-försöken erhålls av en modell som är baserad på sorption på sprickytorna kombinerad med matrisdiffusion i finkorniga sprickfyllnader (fault gouge). Spårämnen med låg sorptionskapacitet visar också en retardation orsakad av diffusion in i stagnanta zoner längs flödesvägarna.

Executive Summary

The TRUE project is a series of in-situ tracer tests made over different distances and complexity of the flow system at the Äspö HRL. The smallest scale tested is a single fracture (detailed scale) over 5-10 m transport distance. TRUE Block Scale project is continuation of the TRUE project with application to a fracture network of multiple fractures and transport distances over several tens of meters.

This report summarises the modelling and evaluation work of the Phase C tracer tests carried out by the Posiva/VTT Processes modelling team. The field part of the TRUE Block Scale project consists of a series of dilution and tracer tests. The modelled Phase C tracer tests comprise three different tests performed using one pumping borehole and three different injection boreholes. Transport distance, calculated along the structural model, varies from about 16 m to about 90 m. Injection points have been selected such that the tracers need to migrate through several different fractures. In addition, several different tracers ranging from non-sorbing to moderately and strongly sorbing have been applied in each test. The modelling work consists of two parts: first the tracer breakthrough curves were predicted, then the transport properties along the flow paths were evaluated using the observed breakthrough curves. Evaluation of the breakthrough curves showed that other immobile pore spaces than rock matrix may have dominated the retardation in the tracer tests.

Predictive modelling is based on the concept of a single flow channel that connects the source to the sink. Properties of the flow channel have been estimated using the results of the Phase B tracer tests where tests were run in the same source-sink combination at equitable flow rate. Matrix diffusion and retardation properties of the different tracers have been taken from the matrix diffusion and sorption properties evaluated along the single fracture flow paths at the TRUE-1 site. The evaluated in-situ matrix diffusion and sorption properties were applied directly to model the TRUE Block Scale tracer tests through the network of fractures. This is based on the assumption that the structure of the immobile pore spaces at the TRUE-1 and TRUE Block Scale sites are similar.

The predicted breakthrough curves are reasonably accurate for the non-sorbing tracers. For the sorbing tracers the discrepancy between the actual measured and predicted breakthrough curve increases with increasing sorptivity.

Subsequently to the predictive modelling the breakthrough curves were modelled anew to evaluate the processes behind the tracer retention. The evaluation shows that the observed retention is quite strong along all flow paths, but especially along flow path I. This can be explained by application of elevated porosity/K_d values compared to the laboratory measurements. However, there is no clear basis for the higher K_d values, though the porosity can be higher close to the fracture. In the evaluation the physical parameters were determined by assigning an excess retention capacity compared to the laboratory measurements to the flow field properties. In practice, this means distribution of the flow into larger area than in the prediction model. The evaluation indicates that it is not reasonable to explain the retention by diffusion to the rock matrix. This would require unrealisticly wide transport channels. Diffusion to the fault gouge gives more realistic width of the transport channel.

However, in both cases, diffusion to the rock matrix or fault gouge, it is difficult to reproduce the desired retention using laboratory data on sorption and porosity.

The evaluation has not been able to resolve the governing retention processes in the Phase C tracer tests. The most consistent picture of the Phase C tracer tests is provided by the model that is based on surface sorption on the fracture surface combined with the matrix diffusion into fault gouge. It is likely that different processes have been major retention processes for non-sorbing and sorbing tracers, respectively. It also seems evident that diffusion into the rock matrix alone cannot explain the retention of the sorbing tracers. Probably, the retention follows from two processes in parallel: surface sorption and diffusion to the fault gouge, stagnant zones or rock matrix.

Within the time scale of the tracer tests the structure of the heterogeneity of the pore space as a function of the depth of the immobile zones may have caused significant effects. This heterogeneity can, for example, lead to different effective retention properties for different tracers along the same flow path implying that a model based on one single effective immobile zone cannot explain all the tracers.

Table of Content

1 Introduction 11

2 Objectives 13

3 Predictive modelling 15

3.1 Conceptual model 15

3.1.1 Processes 15

3.1.2 The flow path 16

3.2 Model description 19

3.2.1 Channel model 20

3.2.2 Matrix model 21

3.2.3 Fracture model 22

3.2.4 Velocity field 22

3.3 Transport equations 25

4 Data used 27

4.1 Velocity field 27

4.2 Matrix diffusion and sorption parameters 31

5 Predictions 35

5.1 Tracer test C1 36

5.2 Tracer test C2 38

5.3 Tracer test C3 39

6 Results of in situ experiments 41

7 Evaluation 45

7.1 Conceptual model 45

7.2 Mathematical model 48

7.2.1 Groundwater transit time distribution 48

7.2.2 Matrix diffusion 51

7.3 Evaluation process 54

7.3.1 Fitting of the parameters 54

7.3.2 Selected model parameters 56

7.3.3 Adjustment of tracer mass recovery 57

8 Results of the evaluation 63
8.1 Simulated cases 63
8.2 Transport in the advective field of the channel 64
8.3 Surface sorption 66
8.4 Matrix diffusion 68
8.4.1 Fitted breakthrough curve 69
8.4.2 Rock matrix 76
8.4.3 Fault gouge 77
8.4.4 Stagnant zones 78
8.5 Integrated retention model of the Phase C tracer tests 79
8.5.1 Flow field 79
8.5.2 Surface sorption 81
8.5.3 Rock matrix 82
8.5.4 Fault gouge 82
8.5.5 Summary 83
9 Summary and discussion 85
References 87
Appendix A: Fitted breakthrough curves of the STT-1, STT-1b and STT-2 tests 89
Appendix B: Additivity of the retention parameters u and R_a 93
Appendix C: Retention parameters fitted to the Phase C tracer experiments 97

1 Introduction

TRUE Block Scale project is a logical continuation of the tracer tests performed in an interpreted single fracture within the TRUE-1 project (Winberg et al., 2000). TRUE Block Scale includes three main phases of tracer tests carried out in a network of fractures. The last phase of the tests, Phase C, was subject to predictive modelling. Two of the predicted tracer tests, C1 and C2, were performed as weak dipole experiments. Third experiment, C3, was a pure radial converging test. The lengths of the assumed transport paths calculated along the fracture planes of the structural model vary from 16 m to about 97 m. One of the tests, C3, is interpreted to take place in a single fracture over 35 m transport distance. At least in the C1 and C2 tests the pumping and injection borehole sections are interpreted to be in different fractures. It has been estimated that the transport paths of these flow paths involve minimum of 2-3 different fractures.

Predictive modelling of the phase C tracers test injections C1, C2 and C3 was carried out by applying existing information from the TRUE-1 site with associated evaluation together with data from the Phase B tracer experiments at the TRUE Block Scale site. Application of the TRUE-1 evaluation results is based on the assumption that properties and structure of the immobile pore space along TRUE Block Scale and TRUE-1 flow paths are similar. TRUE-1 results were used to calibrate the sorption and matrix diffusion properties of the tracers. This use of the TRUE-1 data restricted the modelling of the Phase C experiments to the same tracers that were previously used at the TRUE-1 site. For this reason no predictions were calculated for the S-35 tracer of the C1 experiment. In the C2 experiment two different isotopes of the same element, Re-188 and Re-186, were used. Only Re-186 has been modelled.

Evaluation of the tracer tests is restricted only to the tracers that showed actual breakthrough in the tests. This restricts the number of tracers evaluated to six in C1, two in C2 and three in C3, cf. Chapters 6 and 7.

2 Objectives

There does not exist many tracer tests that have been performed in fractured crystalline rock over tens of meters distance and through a network of fractures. This makes the series of the TRUE Block Scale tracer experiments valuable to understanding retention processes taking place in the fractured rock. Transport calculations in the safety analysis are usually based on assumptions that are not fully tested by the tracer experiments. Matrix diffusion, for example, is a process that is not easy to verify using in-situ experiments. One of the objectives of modelling the TRUE Block Scale tracer experiments is to test the basic simplifications and assumptions that are usually applied, or that are important for the transport calculations also at the performance analysis scale.

Modelling work in the TRUE Block Scale project is aimed to test in advance a series of hypotheses. There are three hypotheses concerning a) the structural model of the TRUE block, b) influence of the heterogeneity on the flow and transport and finally c) on network effects on transport and retention (Winberg, 2000). The modelling approach we apply concentrates only on the hypothesis, which is related to transport. This hypothesis is tested by applying data from single fracture transport experiments (TRUE-1) to predict transport through the fracture network at the TRUE Block Scale site. For this reason the general transport retention hypothesis is reformulated to the following two hypotheses:

- There is no fundamental difference in the tracer retention between transport through a network of fractures and a single fracture flow path.
- Distribution of the flow rate plays an essential role in determining the coupling of the transport and retention processes.

3 Predictive modelling

3.1 Conceptual model

The basic assumption in the conceptual model is that it is possible to model the transport of the tracers by considering a streamtube that connects the source and sink. In this report the streamtube is also called a flow or transport channel and it is understood as a collection of streamlines.

3.1.1 Processes

We first examine purely advective transport. In this case the flow paths of the tracer particles coincide with the streamlines (in the steady state flow field). Each individual tracer particle travels along one-dimensional streamlines. The particle transit time distribution that determines the breakthrough curve is characterised by the lengths of the streamlines and the flow velocities of the particles. Generally, the properties of the streamlines should be calculated using a flow model. In the phase C tracer tests this is not necessary since the same flow paths have been tested in earlier tracer tests of the Phase B experiment using the same sink strength (pump rate). This means that we know the non-sorbing tracer residence time distribution in the advective flow field of the Phase B tests. The residence time distributions for the Phase C test are estimated by scaling the Phase B residence time distributions using to the known difference in the pumping conditions of the Phase B and Phase C tracer tests.

The Phase C tracer tests are performed in a network of fractures. This means that the tracer particles need to pass fracture intersection lines. This increases the probability of the tracer particles going to some other place than the sink is higher than in a single fracture tracer test.

In reality the flow paths of the tracer particles do not follow streamlines because of the molecular diffusion. All particles arriving at the sink have visited several neighbouring streamlines. This means that an individual tracer particle arriving at the sink does not represent the typical transit time of a single streamline. Statistically the transit times of the tracer particles represent integrated transit times along streamlines that are geometrically close to each other. The molecular diffusion averages the transit time distribution compared to the transit time distribution that is based solely on the advective flow field.

An important special case of the molecular diffusion to the neighbouring streamlines is the case when the particles diffuse to a region where the flow rate is very small, or the water in practice is stagnant, i.e. to the regions that do not really belong to the advective flow path. This kind of region may be in the fracture plane, in the rim zone, in the fault gouge or in the rock matrix. Visiting these regions always cause retardation and affects the tracer residence time distribution. In this report this retardation process is called “matrix diffusion” regardless of the environment where the stagnant pore space exist. Later, in the Section 3.3 it will be noted that the diffusive connection to the immobile zones (in the fracture, fault gouge or rock matrix) is determined by the groundwater flux together with the width and length of the flow channel.

3.1.2 The flow path

The geometry of the flow path or transport channel can be examined qualitatively for the flow fields, radial converging and dipole, that were used in the tracer experiments. Also, the characteristics of the flow path in the heterogeneous fractures can be assessed at a general level.

First, let us examine the geometry of the flow channel connecting the source and sink section in the homogeneous fracture. In the radial converging experiment the streamlines from the injection borehole to the pumping borehole are straight lines that converge forming a triangular flow channel in the plane. The Darcy velocity increases when the pumping borehole is approached that cause the density of the streamlines to increase in the vicinity of the sink. In this case the width of the transport channel is equal to or, smaller than, the diameter of the injection borehole (Figure 3-1).

The dipole flow field changes the shape of the flow channel. The injection flow rate pushes tracer into the fracture and the streamlines diverge. The distance between the streamlines passing through the injection area varies much more than in the radial converging case (Figure 3-2).

Taking heterogeneity into account does not change the general concept and appearance. The difference to the homogeneous case is that in the heterogeneous fracture the width of the channel varies in accordance the variation in the hydraulic properties of the fracture (Figure 3-3).

Modelling is based on the assumption that tracer transport in all the cases above can be reproduced using a model based on integrated channel properties. The integrated properties can be replaced by constant or effective properties along geometrically simplified channel.

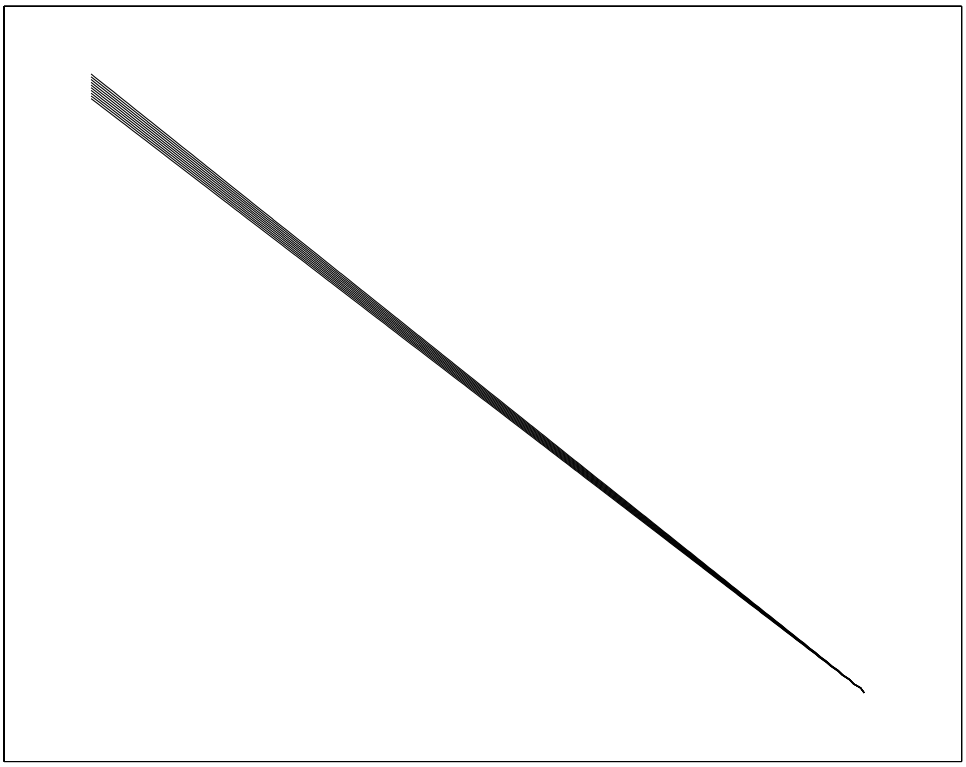

Figure 3-1. *Flow channel in homogeneous fracture and applied radial converging flow field (injection at upper left corner and pumping at lower right corner).*

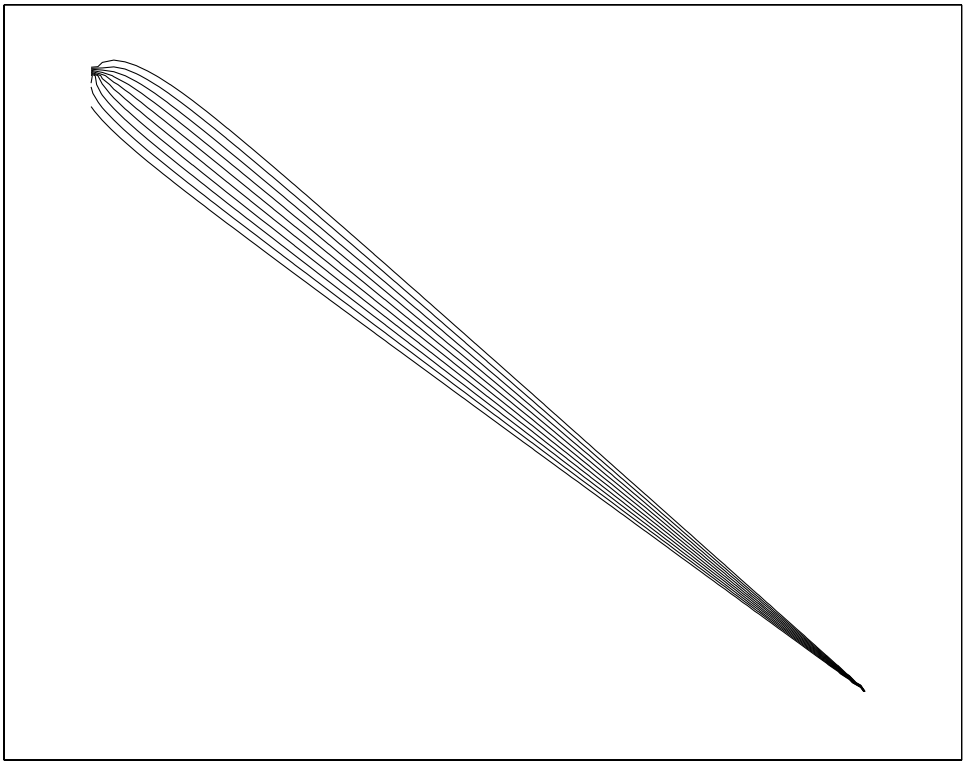

Figure 3-2. *Flow channel in homogeneous fracture and applied dipole flow field. The strength of the dipole is 1:44 (injection at upper left corner and pumping at lower right corner) that is approximately the ratio of the dipole strength in the C1 test.*

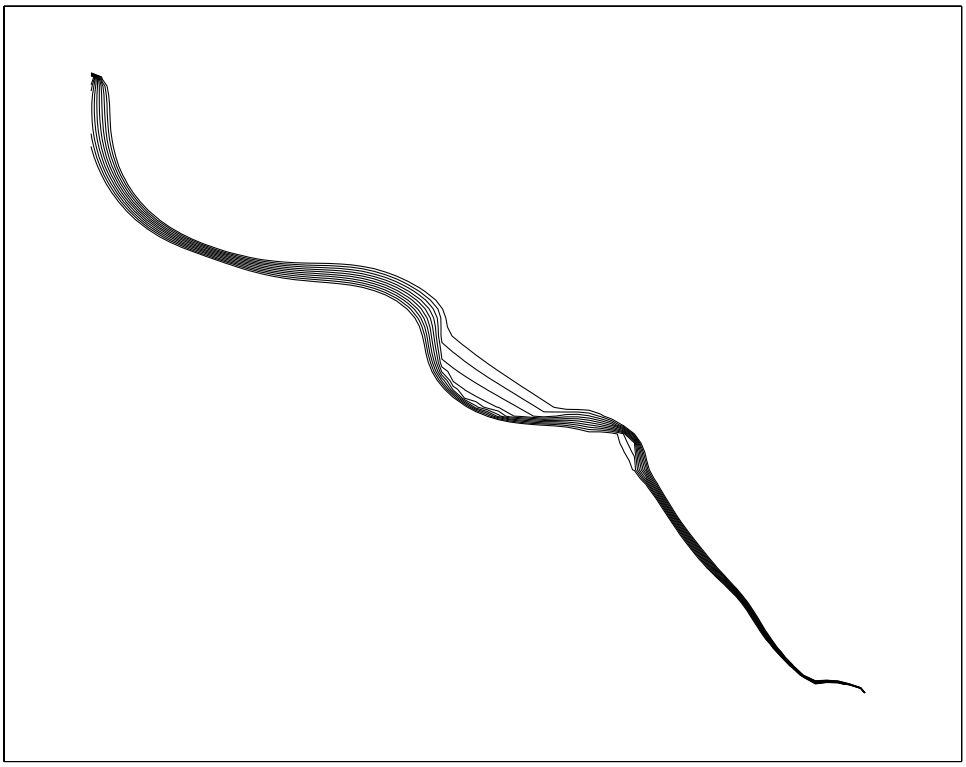

Figure 3-3. *Flow channel in heterogeneous fracture and dipole flow field (injection at upper left corner and pumping at lower right corner). The strength of the dipole is the same as in Figure 3-2.*

Based on the reasoning presented above our conceptual model, the Posiva Streamtube approach, is based on the single transport channel connecting the source and sink. Simplification of the actual streamtube to the transport channel that gives the same effective properties is presented schematically in the Figure 3-4.

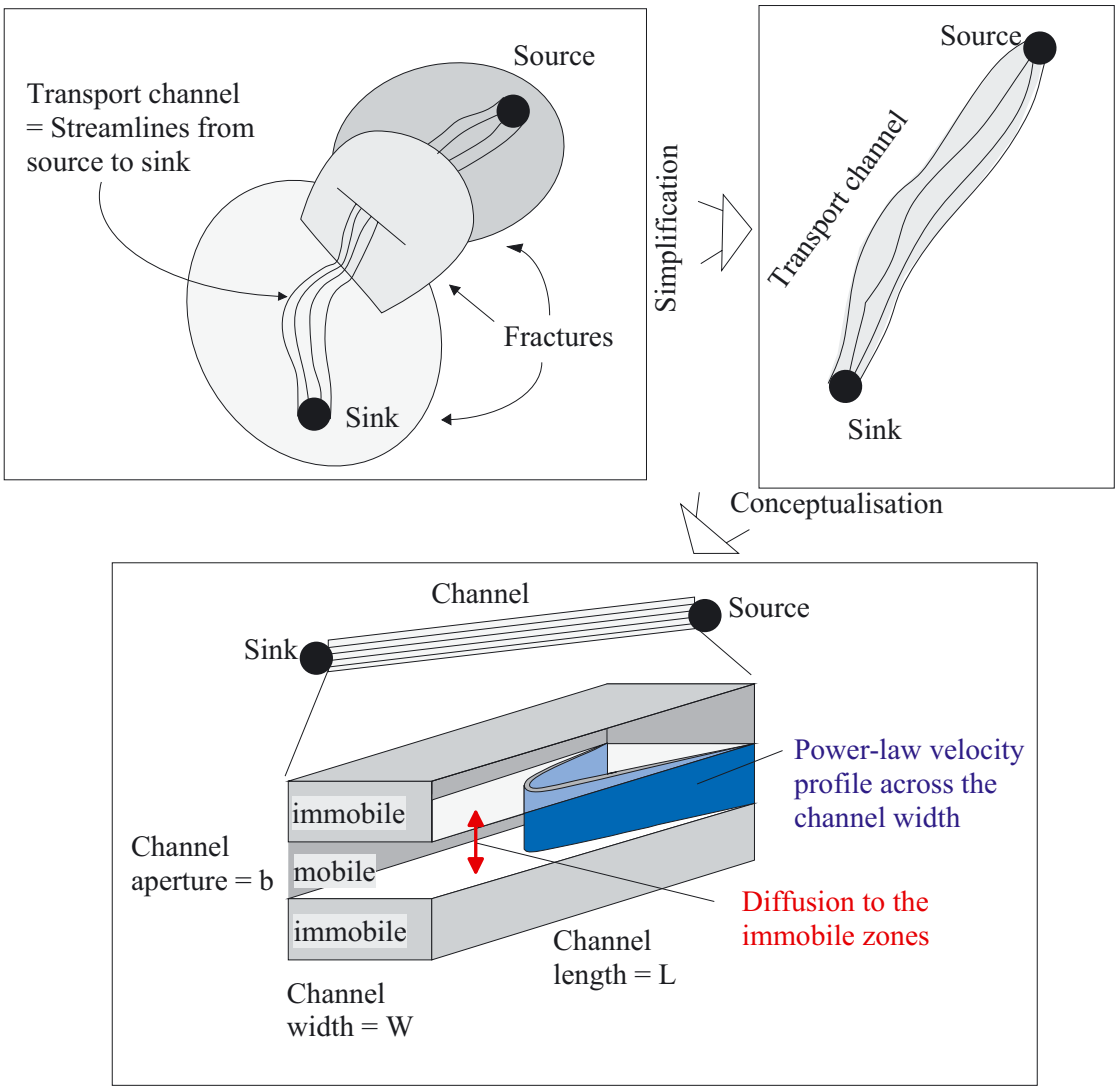

Figure 3-4. *Conceptual model used to calculate predictions of the Phase C tracer tests.*

3.2 Model description

The *transport model* comprises three different parts. These are the *flow channel model (mobile zone*), the *immobile zone model* and the *fracture model*. The immobile zone model implies usage of effective properties (from the tracer retention point of view) of the pore space that surrounds the mobile part of the transport channel and where tracer particles may visit only by diffusion. The fracture model is very simple; it accounts only for the retention that is caused by the surface sorption on the fracture surface. The channel model includes both geometrical representation of the transport channel and the assumed flow field.

The channel and immobile zone properties are assigned using the grouped parameter that controls the retention caused by the matrix diffusion. The definition of this parameter (u) is presented later in Section 3.3.

3.2.1 Channel model

The transport calculations are based on the assumption that all streamlines from the source will find their way to the pumping borehole. This means that the flow through the injection section characterises the transport channel. The flow rate through the channel is fixed for the experiment and the volume of the channel roughly determines the transit time for the non-sorbing tracers. For sorbing tracers the interaction between tracer and the immobile pore space is important (rock matrix or rim zone/fault gouge/fault breccia). The properties of the immobile zones and the width of the flow channel together with the flow rate determine the retention.

In addition, it is assumed that the distribution of the non-sorbing tracer breakthrough times stems from different fluxes in different parts of the channel, but the aperture of the channel is approximately the same all over the channel.

Basically, the channel properties are properties of the tested flow field (streamtube). The channel dimensions are not resulting from geometrical constraints that are typical for the investigated rock type or fracture system. The channel is a collection of streamlines that start from the source area end at the sink. Basically the flow field determines the geometry of the channel and under different boundary conditions the channel properties are likely to change because of the changing flow field.

In the case of tracer transport both the flow field ("geometry") and matrix (sorption coefficient, porosity and diffusivity) properties influence to the retention. If the flow properties are changed it is not possible to keep the overall retention unchanged without making corresponding changes in the matrix properties.

Later in Section 3.3 it is noted that the retention due to the matrix diffusion can be described using a parameter u

$$u = \sqrt{D_e \ \varepsilon \ R_p}\ \frac{t_w}{2b}\ , \qquad (3\text{-}1)$$

where t_w is the groundwater transit time, $2b$ is the channel aperture, D_e is the effective diffusion coefficient, ε is the porosity and R_p is the retardation coefficient in the matrix. The last part of the parameter u, $t_w/(2b)$, can be presented also as WL/Q, where W is the width of the channel, L is the length of the channel and Q is the flux through the channel. In this case the distribution of the u values is governed by the distribution of the ratio Q/W, i.e. flow rate per channel width. It is noted that in many cases an approximate value of this parameter can be calculated from the dilution measurement (gives Q) in the source borehole (borehole diameter gives W) without the need to know the aperture or groundwater transit time (of course estimates of the transport distance, L, are needed). It is still stressed that groundwater transit time distribution t_w alone does not tell much about retention properties along the flow path. It should always be coupled with aperture. In this sense the expression WL/Q describes retention behaviour more realistically because the flow rate is always measured over some length scale (W).

Equation (3-1) clearly indicates that the matrix properties (square root part) and the geometry of the channel are grouped together. Evaluation of the Equation (3-1) applying possible combinations of the physical parameters D_e, ε, R_p and b can be used to determine the applicability of the selected parameter u. This is done in the evaluation of the tracer tests in Sections 7 and 8.

The streamtube is composed of several streamlines that have different transit times. Different transit times can follow from variations in the lengths of the streamlines, boundary conditions or apertures. If it is assumed that the aperture (b) is same for all streamlines then the distribution of the u values that corresponds to the flow field (t_w distribution) can easily be calculated. The assumption of a fixed aperture means that the differences in the transit times primarily are caused by different flow rates through different parts of the flow field. In principal, this is consistent with the cubic law dependence of the transmissivity on the aperture, i.e. insignificant change in the aperture cause significant change in the flow rate. From this follows that the distribution of u can be scaled from the distribution of t_w using a fixed factor. It is now possible to write Equation (3-1) as

$$u = \frac{\sqrt{D_e \varepsilon R_p}}{2b} t_w = U_t \, t_w \ . \qquad (3\text{-}2)$$

The scaling factors U_t for the different tracers are taken from the evaluated tracer tests that were performed at the TRUE-1 site (see Appendix A and Table 4-3). In the first version of the predictions the parameter U_t values were scaled using the L and Q values of the Block Scale and TRUE-1 experiments, respectively. In principal the scaling of the U_t is equivalent to the differences in matrix properties or aperture. Data on different tracers have been collected from different TRUE-1 tests and scaling leads inconsistencies in the scaled U_t data. In addition, it is difficult to motivate different matrix properties for the TRUE-1 and TRUE Block Scale sites. For this reason predictions are presented for the case where the scaling is omitted.

Applying the following assumptions the statistical properties of the streamlines in Phase C can be determined using the Phase B results:

- Earlier tracer tests (Phase B) assured to activate the same flow paths as the Phase C tests.
- The advective flow field governs the non-sorbing breakthrough in the Phase B tests.
- Effects of the matrix diffusion and diffusion to the stagnant zones in the non-sorbing tests of the Phase B are not taken into account. This leads to overestimation of the residence times that are caused by the advection only and therefore possibly overestimation of the matrix diffusion, especially for the sorbing tracer.

The groundwater transit time distributions for predicting the Phase C tests are scaled from the Phase B test results that were carried out between the same injection and withdrawal points as the Phase C tests. The scaling is performed by first representing the residence time distribution in the Phase B tests using a velocity profile over the transport channel and then scaling the velocity profile using the known difference in the withdrawal flow rates between the Phase B and the Phase C tests. The applied velocity profile is explained in more detail in the Section 3.2.4.

3.2.2 Matrix model

In the present model retention is only assured caused by surface sorption or matrix diffusion. The matrix diffusion properties are given using the grouped parameter u (Equation (3-1)). The parameter u values that are applied in the predictive modelling of the Phase C tests have been transferred from analysis of the in-situ tests performed at the TRUE-1 site by assuming that the matrix properties (D_e, ε and R_p) are same at the

TRUE-1 and True Block Scale sites. In addition, it has been assumed that the apertures of the transport channels in the Phase C tests and in the STT-1b tests of the TRUE-1 are the same.

The transport equation (Section 3.3) is solved for the infinite and homogeneous matrix.

3.2.3 Fracture model

The fracture model includes only the sorption properties of the fracture surface. Surface retardation coefficient has been fitted using TRUE-1 data simultaneously to fitting the matrix diffusion parameter u (Appendix A). The retardation of the tracers in the TRUE-1 tests is assumed to originate both from matrix diffusion and surface sorption. In the interpretation of the TRUE-1 tests these two retention processes have been treated such that as much as possible of the noted retention has been attributed to the surface sorption and the remaining part to the matrix diffusion.

Usually the same tracer has been applied in several different experiment of the TRUE-1. The evaluation of the different experiments have been treated such that consistency between different tests is maintained as far as possible.

3.2.4 Velocity field

It is assumed that the transit time distribution of the non-sorbing tracer is characterised by the velocity field over the channel width. This velocity field is assumed to originate from the applied flow field (i.e. pumping) and from the properties of the channel. The channel properties do not change between different tests if the same channel is activated but the flow field varies according to the applied pumprate. This is the basis for the application of the velocity profile. The velocity profile for the Phase C tests can be scaled from the Phase B velocity profiles using the known pumping flow rates. The Phase B tests can also be used to calibrate the shape of the velocity profile.

The same velocity profile can then be used to calculate the breakthrough curve with two different boundary conditions. It can be assumed that there are well mixed conditions at the injection point, which means that the mass released to a streamline depends on the flow velocity, or that the same mass is released for each streamline. We may assume that flow velocity is highest at the centre of the flow channel and that it is zero at the channel walls. An arbitrary power law velocity profile can be written as

$$v = v_0 \left\{ 1 - \left(\frac{y}{a} \right)^x \right\} \quad , \qquad (3\text{-}3)$$

where a is the half-width of the channel, y is the position in the lateral direction across the channel, v_0 is the maximum flow velocity at the centre of the channel and x is the arbitrary exponent of the velocity profile that can be selected, or fitted using Phase B tracer test data.

If it is assumed that the mass released to the streamlines depends on the flow velocity (i.e. flow rate, this is the case of well mixed injection) then the cumulative mass at the collecting point for a sudden release of the tracer mass m_0 is

$$m(t) = m_0 \frac{\left(1 - \frac{t_0}{t}\right)^{\frac{1}{x}} \left(\frac{t_0}{t} + x\right)}{x} \quad , \tag{3-4}$$

where $t_0 = l/v_0$ is the first arrival time. The tracer discharge is obtained by taking the time derivative of Equation (3-4):

$$\dot{m}(t) = m_0 \frac{{t_0}^2}{t^3} \left(\frac{t - t_0}{t}\right)^{\frac{1-x}{x}} \frac{1+x}{x^2} \quad . \tag{3-5}$$

Similarly, the cumulative mass at the collecting point can be calculated for the case when the same mass is released for every streamline. In this case the cumulative mass is

$$m(t) = m_0 \left(1 - \frac{t_0}{t}\right)^{\frac{1}{x}} \quad , \tag{3-6}$$

and the tracer discharge is

$$\dot{m}(t) = m_0 \frac{t_0}{t^2} \left(1 - \frac{t_0}{t}\right)^{\frac{1-x}{x}} \frac{1}{x} \quad . \tag{3-7}$$

The predictions are calculated using a box-type source function and choosing the exponent $x = 1/2$. The groundwater residence time distribution for this case is presented in Equation (3-8) (unit mass release).

$$b(t) = \begin{cases} \left(\frac{v_0 * t - l}{v_0 * t}\right)^2 \frac{1}{dt}, \; l/v_0 < t \le l/v_0 + dt \\ \left(\left(\frac{v_0 * t - l}{v_0 * t}\right)^2 - \left(\frac{v_0 * (t - dt) - l}{v_0 * (t - dt)}\right)^2\right) \frac{1}{dt}, \; t > l/v_0 + dt \end{cases} \quad , \tag{3-8}$$

where l is the length of the channel, v_0 is the maximum flow velocity and dt is the duration of the injection.

In the predictions of the Phase C tests the residence time distribution is calculated using Equation (3-6), that assumes the same mass of tracer for every streamline. It may be argued that the assumption of well-mixed concentration at the injection point (Equation (3-4)) is more realistic. However, the deviation in residence times distribution compared to the well-mixed case having exponent x=0.27 is not that large. The breakthrough curves for the non-mixed injection applied in the predictions (Equation (3-7), x=1/2) and the mixed injection (Equation (3-5), x=0.27) are presented in Figure 3-5. The shape of the velocity field is also quite similar in both cases. This is illustrated in Figure 3-6. This means that although the selected model the advective transport is for the non-mixed injection it is possible to find a closely similar result amongst the mixed injection cases.

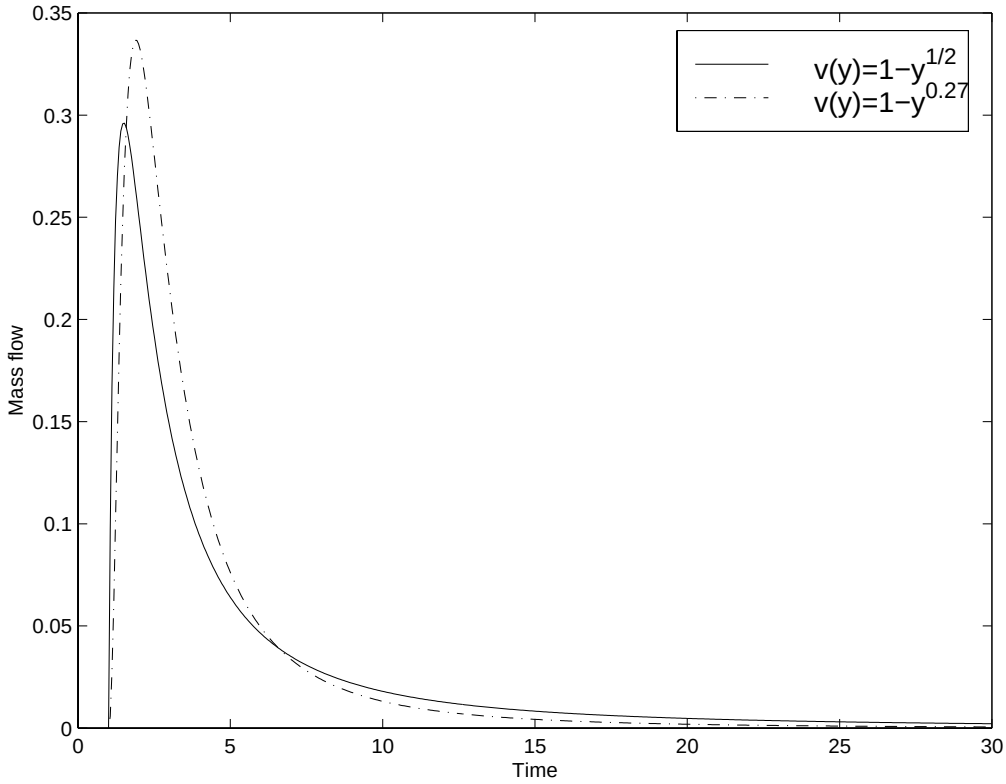

Figure 3-5. *Breakthrough curves for mixed and non-mixed injections when the exponent of the power law velocity field is* x*=1/2 (non-mixed, Equation (3-7)) and* x*=0.27 (mixed, Equation (3-5)).*

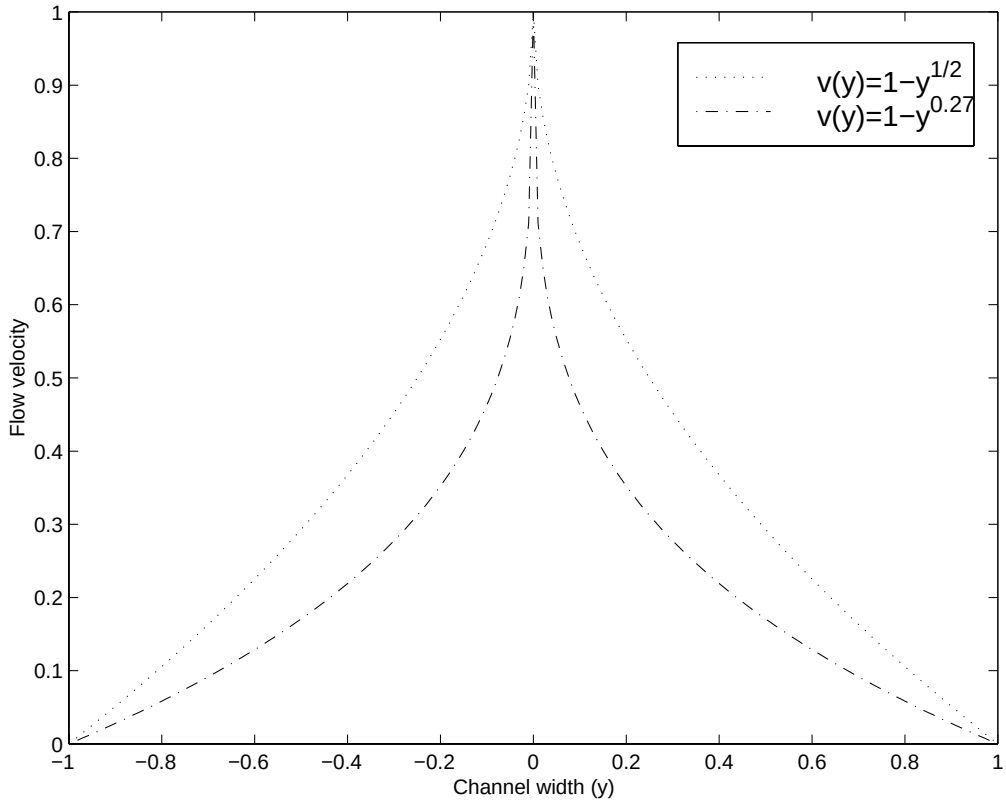

Figure 3-6. *Shapes of the velocity field in the flow channel for the mixed and non-mixed injections when the exponent of the power law velocity field is* x*=1/2 (non-mixed, Equation (3-7)) and* x*=0.27 (mixed, Equation (3-5)).*

3.3 Transport equations

The governing equations for the transport in case of advection and matrix diffusion are

$$\begin{aligned} & R_a \frac{\partial c_f}{\partial t} + v \frac{\partial c_f}{\partial x} - 2 \frac{D_e}{2b} \frac{\partial c_m}{\partial z}\bigg|_{z=0} = 0 \\ & R_p \frac{\partial c_m}{\partial t} - D_p \frac{\partial^2 c_m}{\partial z^2} = 0 \end{aligned} \quad , \tag{3-9}$$

where c_f is the solute concentration in the fracture, R_a is the retardation coefficient in the fracture (surface sorption), v is the groundwater flow velocity, $2b$ is the aperture, D_e is the effective diffusion coefficient into matrix, R_p is the retardation coefficient in the matrix, D_p is the pore diffusion coefficient in the pore water of the rock matrix and c_m is the concentration in matrix. Equation (3-9) is written for a homogeneous fracture and matrix, but it is later shown that the results are applicable also for the heterogeneous case. Boundary conditions that are usually applied for Equation (3-9) comprise instantaneous release of the tracer mass m_0, continuity of the tracer concentration at the matrix boundary and infinite depth of the matrix. These boundary conditions are presented in Equation (3-10).

$$\begin{aligned} & c_f = \frac{m_0}{v\ 2b} \delta(t)\ , x = 0 \\ & c_m = c_f\ ,\ z = 0 \\ & \lim_{z->\infty} c_m = 0 \end{aligned} \quad . \tag{3-10}$$

Equations (3-9) with boundary conditions (3-10) can be solved using e.g. Laplace transformation. In the Laplace domain the solution for tracer concentration in the fracture is

$$\ell\left\{\frac{c_f\ v\ 2b}{m_0}\right\} = \ell\left\{\frac{\dot{m}}{m_0}\right\} = \exp\left(-\frac{R_a x}{v} p\right) \exp\left(-2\frac{D_e x}{v2b}\sqrt{\frac{R_p}{D_p}}\sqrt{p}\right) , \tag{3-11}$$

Where p is the variable at the Laplace transformed space and $\dot{m}$ is the tracer discharge. The solution (3-11) can be simplified by introducing two parameters

$$\begin{aligned} & t_w = \frac{x}{v} \\ & u = \frac{D_e x}{v2b}\sqrt{\frac{R_p}{D_p}} \end{aligned} . \tag{3-12}$$

The parameter u determines the strength of the matrix diffusion and t_w gives the groundwater transit time. Applying the parameters in (3-12) to Equation (3-11) gives

$$\ell\left\{\frac{\dot{m}}{m_0}\right\} = \exp\left(-R_a t_w\ p\right) \exp\left(-2u\sqrt{p}\right) . \tag{3-13}$$

Inversion of the Laplace transformation in Equation (3-13) gives

$$\frac{\dot{m}}{m_0} = H(t - R_a t_w)\frac{u}{\sqrt{\pi}\left(t - R_a t_w\right)^{3/2}} e^{-\frac{u^2}{t - R_a t_w}}, \qquad (3\text{-}14)$$

where H is the Heaviside's unit function, $\dot{m}$ is the tracer discharge, m_0 is the released mass, R_a is the retardation coefficient in the fracture and u and t_w are defined in Equation (3-12). The strength of the matrix diffusion defined by parameter group u can be expressed in different forms according to the equation

$$u = \frac{D_e}{v}\frac{x}{2b}\sqrt{\frac{R_p}{D_p}} = \sqrt{D_e \varepsilon R_p}\,\frac{t_w}{2b} = \sqrt{D_e \varepsilon R_p}\,\frac{W\,x}{Q}, \qquad (3\text{-}15)$$

where W is the channel width, x is the channel length and Q is the flow rate through the channel.

It is shown in the Appendix B that the parameters u and t_w are additive along the transport paths. This means that also heterogeneous cases can be modelled using the same parameters. In the heterogeneous case the parameter groups u and t_w represent the effective values integrated along the flow path.

It is also noted that the same aperture along all streamlines leads to the interpretation presented in Equation (3-16) (cf. Equation (3-2)), i.e. the u distribution can be determined from the t_w distribution. However, it is again stressed that the transit time distribution t_w does not give information on the retention properties unless assumptions are made on the aperture. Application of the t_w distribution is only convenient because the breakthrough curves are presented as a function of time.

$$u = \frac{\sqrt{D_e \varepsilon R_p}}{2b} t_w = U_t\, t_w \text{ , where } U_t = \frac{\sqrt{D_e \varepsilon R_p}}{2b} \qquad (3\text{-}16)$$

4 Data used

The applied input data comprise two different entities: the properties of the flow field and properties of the rock matrix along the transport paths. Information from the TRUE-1 site has an essential role in determining the properties of the matrix. The tracer experiments that were carried out using sorbing tracers in TRUE-1 (STT-1, STT-1b and STT-2 experiments, Winberg et al., 2000) have been used to determine the retention properties of the different tracers. TRUE-1 tracer tests were analysed as a part of the present modelling by deconvoluting TRUE-1 breakthrough curves and fitting analytical solution, Equations (3-14) and (3-16), to the deconvoluted breakthrough curves (Appendix A). This gives U_t and R_a for each tracer.

The key assumption has been that the surface sorption on the fracture surfaces and the matrix diffusion are the most important retention processes both in the TRUE-1 experiments and in the Block Scale tracer experiments. The term "matrix diffusion" is here used to describe all the different diffusion processes that can take place from the mobile zone to the rim zone, fault gouge, or even to the stagnant pools of the mobile zone. Selection of the matrix diffusion parameters is presented in the Section 4.2

The flow field has an essential and direct influence on the residence times of the tracer particles. Combined with the matrix properties, the flow field also controls diffusion processes through which the tracers interact with the pore space that surrounds the flow path. The mobile zone is represented using a distribution of different flow velocities. The selection of the velocity profile is discussed in the Section 4.1.

4.1 Velocity field

The Phase C tracer experiments in TRUE Block Scale were preceded by several pre-tests that were carried out to investigate the alternative flow paths for the tracer tests. The Phase A experiment (Andersson, 2000a) was a set of crosshole interference and tracer dilution tests. This phase was followed by the Phase B experiments (Andersson, 2000b) where potential flow paths were tested using non-sorbing tracers with the purpose of showing sufficiently high tracer recovery for source-sink pairs of interest. Especially the Phase B experiments are useful because some of injections were performed using the same pumping configuration as in the subsequent Phase C experiment (Andersson et al., 2001).

The Phase B experiments B-2b, B-2d and B-2g were performed between the same source and sink points as the predicted Phase C tests C1, C2 and C3, respectively. These tests were also performed using almost the same pumping rates as the corresponding Phase C tests. If the background flow field remains unchanged it is reasonable to assume that the non-sorbing tracer residence time distribution in the predicted Phase C experiments can be scaled from the corresponding Phase B experiments. The pumping configurations of the selected Phase B tests and Phase C tests are presented in Table 4-1.

Table 4-1. Pumping configurations of the Phase B experiments that are closely corresponding to the predicted Phase C tests. The column "Tracer" indicates the tracers that were used to calculate the injection flow rate. The forced injection flow rates of the dipole tests have been C1 2700 ml/h, B-2g 2700 ml/h, C2 600 ml/h and B-2d 600 ml/h.

	Pumped section		Injection section		Tracer	Transport distance [m]*)	
Experiment		[ml/min]		[ml/h]			
C1	KI0023B:P6	2000	KI0025F03:P5	1450	Na-24, K-42	16	Dipole
B-2g	KI0023B:P6	2100	KI0025F03:P5	2040	Naphtionate	16	Dipole
C2	KI0023B:P6	2000	KI0025F03:P7	507	Re-188	97	Dipole
B-2d	KI0023B:P6	2100	KI0025F03:P7	504	Gd-DTPA	97	Dipole
C3	KI0023B:P6	2000	KI0025F02:P3	112	HTO	35	Passive injection
B-2b	KI0023B:P6	2100	KI0025F02:P3	96	NaReO4	35	Passive injection

*) Estimated along the interpreted structures of the March'00 hydrostructural model.

The flow field dependent part can also be expressed using the residence times in the flow field together with the fracture aperture (parameter u, Equation (3-15)). To calculate the tracer residence time distribution of the Phase C tests we need to know the detailed structure of the velocity field or the non-sorbing tracer residence time distribution. The spatial structure of the velocity field has influence on the breakthrough curves because of molecular diffusion between the streamlines. This effect is already built-in in the non-sorbing tracer residence time distribution.

For illustrative reasons the non-sorbing tracer residence time distributions of the Phase B tests are interpreted by a velocity profile across the transport channel. This also makes it clear how to scale the residence time distribution in the Phase B tests to the Phase C flow conditions. The change in the residence time distribution can be done by scaling the velocities by the known difference in the pumping conditions of the Phase B and Phase C tests. Later in the evaluation stage (Chapter 7) the molecular diffusion in the flow field is taken into account. In that case it is important to apply the concept of the velocity profile and the spatial structure of the flow velocities to obtaining correct description of the Taylor dispersion in the breakthrough curves.

The residence time distribution that is corresponding to the velocity profile used is presented in Equation (3-8). The velocity profile is a power law distribution having highest flow velocity at the centreline of the channel and zero velocity at the channel edges. The shape of the velocity distribution follows the square root function so that the flow concentrates in the middle of the channel being stronger than in the linear velocity profile. This flow field produces residence time distributions that closely agree with the measured breakthrough curves of the Phase B experiments.

It should be noted that the fitting of the velocity profile is performed using only one fitting parameter (apart from the selected square root shape of the velocity profile). The fitting parameter is the maximum flow velocity at the centreline of the channel.

Equation (3-8) also includes the length of the channel. The length is taken from the structural model calculated in-plane distances between source and sink and because the fitting is made to the measured breakthrough curve (i.e. tracer transit times) the uncertainty in distance is also assigned to the flow velocity.

Fitting of the velocity profile to the Phase B experiments is been carried out by applying the following procedure. The source terms of the Phase B tests follow decaying injection curves. The "decay constants" of the source terms were determined from the experimental injection curves. Then the source term was described by exponentially decaying concentration at the source point. Equation (3-8) was applied to calculated breakthrough curves for the different Phase B tests. Both calculated and measured breakthrough curves were normalised to unit mass and they were compared. The maximum flow velocity was adjusted to make the calculated and measured breakthrough curves to fit. The calculated and measured breakthrough curves are presented in Figure 4-1.

The injection flow rates used in the predictions are based on the tracer injection data. In the C1 experiment the injection flow rate calculated from the tracer injection data is about 1450 ml/h and in the B-2g test 2040 ml/h. These flow rates give the maximum flow velocity of 1450/2040 * 3.2 m/h= 2.3 m/h in C1, where 3.2 m/h is the fitted maximum flow velocity in the B-2g test. Similarly for the C2 experiment the calculated injection flow rate is 507 ml/h (from Re-188) and in the B-2d test 504 ml/h. This gives for the C2 test a maximum flow velocity of 507/504 * 2 m/h ~ 2 m/h, where 2 m/h is the fitted maximum flow velocity in the B-2d test. Finally, in the C3 test the calculated injection flow rate is 112 ml/h (from HTO) and in the B-2b test 96 ml/h giving the maximum flow velocity in the transport channel of 112/96 * 0.3 m/h = 0.35 m/h, where 0.3 m/h is the fitted maximum flow velocity in the B-2b test. The flow field parameters of the Phase C experiment are summarised in Table 4-2.

For the predictions the scaling was performed using the flow rates that were calculated from the dilution of the tracers in the injection section. For the C1 and C2 tests these flow rates can be compared with the forced flow rate of the dipoles. The result is that these do not coincide with the injection pumprates of the tests. For example, in the C1 test was performed using forced injection flow rate of 2700 ml/h and the tracer decay of the tracer Na-24 and K-42 show injection flow rate of 1490 ml/h and 1410 ml/h, respectively. Similar behaviour has also been reported from the earlier tests. The reason for this might be that the tracer concentration in the injection section is not homogeneous enough. This indicates that it might have been more appropriate to apply forced injection flow rates for the dipole tests.

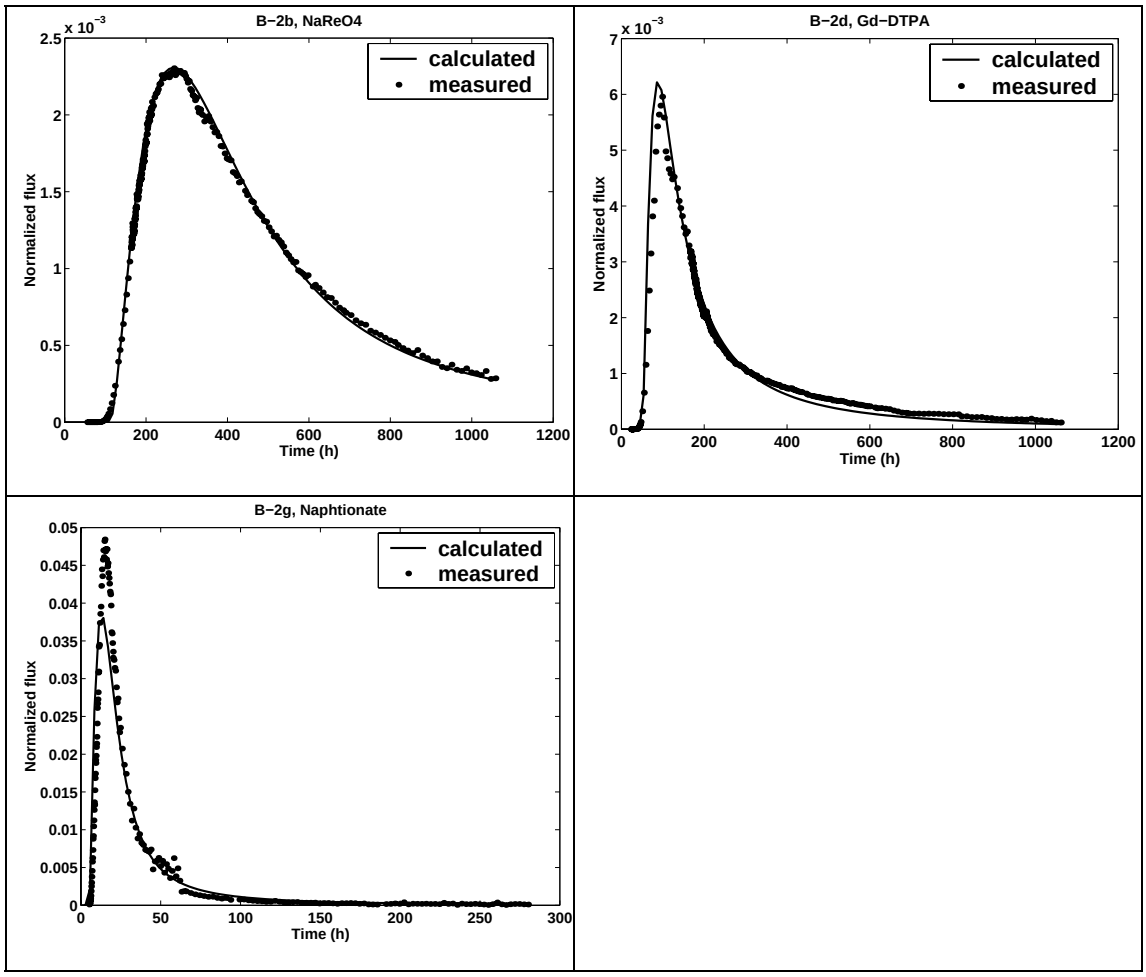

Figure 4-1. *Fitting of the experiments B-2b, B-2d and B-2g using the only the injection curves and the advective flow field.*

Table 4-2. Parameters of the fitted velocity profiled in the Phase B experiments.

Experiment	Channel Length [m] *)	Maximum Flow velocity [m/h]
B-2g	16	3.2
B-2d	97	2.0
B-2b	35	0.3

*) See Table 4-1.

4.2 Matrix diffusion and sorption parameters

The matrix dependent part of the retention properties is presented for scaling factor U_t (cf. Equation (3-16)). The matrix diffusion parameters have been calculated from the data of the TRUE-1 tracer experiments STT-1, STT-1b and STT-2. Analysis of the TRUE-1 experiments was carried out as a part of the present modelling by deconvoluting STT-1, STT-1b and STT-2 breakthrough curves and fitting the analytical solution (Equations (3-14) and (3-16)) to the deconvoluted breakthrough curves. Fitted parameters are given in Table 4-3.

All breakthrough curves of the STT-1, STT-1b and STT-2 tests were deconvoluted to get the unit response functions of the breakthrough curves. The unit response functions (i.e. deconvoluted breakthrough curve) of Uranine were taken to represent the breakthrough due to the advective flow field. The surface retardation coefficients (R_a) and matrix diffusion parameters (U_t) were determined for each tracer by fitting the Uranine breakthrough curves to the deconvoluted tracer breakthrough curves.

Usually, there are different flow rates through the different flow tubes. This can be interpreted as having parallel transport channels with different flow velocities and the same aperture. If the velocity distribution is known then the importance of the different transit times can be scaled using Equation (3-15) (assuming that the aperture ($2b$) is fixed). This also means that to each different breakthrough time of the non-sorbing tracers can be assigned different parameter u value.

Most of the tracers used in Phase C were also applied in two or three different experiments among the STT-1, STT-1b and STT-2 tests. The results of the fitting of the tracer properties are presented in Table 4-3. If the surface sorption and matrix diffusion are expected to be the only mechanisms affecting the transport, then the fitted U_t and retardation coefficient values should be the same for the same tracer in every experiment. However, there seems to be variation in these values among the STT experiments, especially for the strongly sorbing tracers cesium, rubidium and strontium (cf. Table 4-3). Finally, the STT-1 and STT-1b experiments were applied because the fits were better and the dual peak nature of the STT-2 experiment resulted in higher uncertainties in the estimated STT-2 parameters. It should be noted that the fitting of the retardation coefficient and parameter U_t values was not unique. Some degree of freedom exists to choose which one, U_t or retardation coefficient R_a, was the primary contributor to retention. In the fitting the retardation coefficient (R_a) has been selected to be the primary parameter. This means that as much as possible of the retention was first attributed to the retardation coefficient and if possible using consistent values for the different experiments with the same tracer. The results of the fitting to the deconvoluted TRUE-1 breakthrough curves are presented in Appendix A.

Estimation of the parameter U_t values using TRUE-1 sorbing tracer tests and the results for the Phase B non-sorbing uranine includes an implicit assumption that the diffusive processes have negligible influence on the uranine breakthrough curve. Strictly, this may be incorrect and the parameter u values may be underestimated. In addition, this approach does not enable estimation of the parameter u for the non-sorbing tracers (HTO and Re), the latter employed in C3 and C2, respectively. For these tracers, the parameter U_t values were calculated using Equation (3-15) (note that $t_w/(2b) = WL/Q$) and D_e=10^{-13} m^2/s, ε = 0.01, W = 0.05 m. Path lengths (L) and flow rates (Q) were selected according to the modelled Phase C experiment.

Table 4-3. Fitted retention properties of the tracers used in the TRUE-1 sorbing tracer tests. Parameters that are highlighted were applied in the Phase C predictions.

Experiment	Injection flow rate [ml/h]	Transport length [m]	Tracer	U_t [$h^{-1/2}$]	Surface retardation coef. (R_a)
STT-2	29	4.68	Ba-131	0.27	5.00
STT-1	33	4.68	Ba-133	0.50	5.00
STT-2	29	4.68	Ba-133	0.27	5.00
STT-2	29	4.68	Br-82	0.05	1.10
STT-1	33	4.68	Ca-47	0.18	2.10
STT-2	29	4.68	Ca-47	0.13	2.20
STT-2	29	4.68	Cs-134	1.90	95.00
STT-1	33	4.68	Cs-137	1.90	75.00
STT-1b	60	5.03	K-42	0.38	1.90
STT-1	33	4.68	Na-22	0.07	1.35
STT-1b	60	5.03	Na-22	0.07	1.35
STT-2	29	4.68	Na-22	0.05	1.30
STT-1	33	4.68	Rb-86	1.10	9.00
STT-1b	60	5.03	Rb-86	1.10	4.50
STT-2	29	4.68	Rb-86	1.10	7.00
STT-1	33	4.68	Sr-85	0.20	2.00
STT-1b	60	5.03	Sr-85	0.15	1.80
STT-2	29	4.68	Sr-85	0.25	5.00

In the first predictions the fitted parameter U_t values were scaled for the different length of the transport path and different flow rates. The logic behind this was that the flow field dependent part of the parameter u was written as WL/Q, where W is the width of the flow channel, L is the length of the channel and Q is the flow rate. Assuming that the width of the flow channel is the same at the TRUE-1 and TRUE Block Scale sites suggest that the parameter U_t should be scaled by the length and flow rate of the channel. However, if the u parameter is written according to the Equation (3-16) then the scaling of the U_t clearly indicates change in the aperture or immobile zone properties. The scaling applied in the first predictions indicate 8-15 times larger aperture for C1, 1.4 times smaller aperture for C2 and 2-3.5 times smaller aperture for C3 compared to the apertures in TRUE-1 if the immobile zone properties are unchanged. The final predictions were calculated by assuming both same aperture and immobile zone properties, i.e. the same U_t..

The set of retention parameters applied both in the first and final predictions are presented in Table 4-4. It has been assumed that the whole injection flow rate has gone to the single transport channel in the weak dipole experiments (C1 and C2). In reality, the effective width of the transport channel in the dipole tests may be larger than it has been in the radially converging STT-tests of TRUE-1. However, due to the heterogeneity of the fractures at the TRUE Block Scale site it is very difficult to estimate projected channel widths in the dipole tests. As mentioned above the parameter u values for Re-186 and HTO were calculated directly using Equation (3-15).

Table 4-4. Transport parameters applied in the Phase C predictions. Note that in the corrected predictions both U_t and R_a are taken directly from Table 4-3.

Experiment	Tracer	Injection [ml/h]	Transport length [m]	U_t [$h^{-1/2}$] corrected predictions	U_t [$h^{-1/2}$] 1st predictions	Retardation coef. R_a
C1	Br-82	1450	16	0.05	0.003	1.10
C1	Ca-47	1450	16	0.18	0.014	2.10
C1	Cs-134	1450	16	1.90	0.15	75.00
C1	K-42	1450	16	0.38	0.05	1.90
C1	Na-24	1450	16	0.07	0.009	1.35
C1	Rb-86	1450	16	1.10	0.15	4.50
C2	Ba-131	507	97	0.50	0.68	5.00
C2	Ca-47	507	97	0.18	0.24	2.10
C2	Cs-137	507	97	1.90	2.6	75.00
C2	Re-186	507	97	0.018	0.018	1
C3	Ba-133	112	35	0.50	1.04	5.00
C3	HTO	112	35	0.028	0.028	1
C3	Na-22	112	35	0.070	0.25	1.35
C3	Rb-83	112	35	1.10	3.9	4.50
C3	Sr-85	112	35	0.15	0.53	1.80

5 Predictions

The predictions were calculated by assuming that the main processes during the transport are advection along the flow field, sorption on the fracture surface, diffusion to the matrix pore space and sorption in the matrix pores space. The advective flow field was estimated using results of the Phase B tracer tests that were made under the same pumping configuration as the predicted C1, C2 and C3 experiments. This also means that it has been assumed that the same flow paths are activated in the C1, C2 and C3 experiments as in the earlier Phase B tests.

Transport calculations are based on the transport channel model. A single channel connects the source and sink but there are different flow velocities at different positions along the channel. The flow field in the channel is assumed to be two-dimensional. In the model there are no velocity (or concentration) differences normal to the fracture plane (i.e. in the direction of the channel aperture). In the transverse direction the flow field is assumed follow the general behaviour of the viscous flow. This means that the flow velocity is highest at the centerline of the channel, it is zero at the transverse boundaries of the flow channel and that the flow velocity changes continuously in the transverse direction.

The evaluation of the Phase B tracer tests indicated that for the non-sorbing tracers this kind of velocity field alone can explain the breakthrough curves rather well. The pumping configuration in the Phase C tracer tests does not differ very much from the pumping configuration in the Phase B tracer experiments (B-2b, B-2d and B-2g). It was considered reasonable to assume that the flow field in the Phase C tracer tests could be approximated using the Phase B tests.

Representation of the Phase B tracer tests using a velocity profile over the transport channel incorporates the effect of the molecular diffusion in the flow channel in the representation of the flow field. This does not affect the results because eventually the residence time distribution of the tracer particles in the flow field has meaning for the retention processes. However, the selected approach also incorporate the matrix diffusion effects that may exist in the Phase B breakthrough curves in the velocity profile. Strictly, this is not correct and it leads to overestimation of the matrix diffusion in the Phase C predictions. However, the non-sorbing tracer breakthrough curve gives the closest approximation of the residence time distribution of the tracer particles in the advective field of the transport channel.

The modelling procedure may be summarised by following steps:

1. Estimation of the velocity field using Phase B tests B-2b (for C3), B-2d (for C2) and B-2g (for C1). Scaling of the velocity fields to the Phase C pumping conditions.

2. Estimation of the surface sorption and matrix diffusion parameters using the TRUE-1 experiments STT-1, STT-1b and STT-2 (cf. Table 4-4).

3. Scaling of the matrix diffusion parameters from the TRUE-1 flow conditions to the TRUE Block Scale Phase C conditions (Not in the corrected predictions).

4. Calculation of the breakthrough for the Phase C experiment by applying unit (Dirac) injection and the velocity field only.

5. Adding matrix diffusion and surface sorption effects to the advective breakthrough curves (i.e. step 4 result).

6. Taking the actual injection function into account by convoluting the injection functions with the advection-matrix diffusion (and sorption) unit response function (step 5 result).

According to the definition of the modelling task the predictions were calculated by not taking into account the radioactive decay. The predictions have been calculated both for the Dirac pulse source term and for the measured injection source term

First predictions included an error that caused the scaling of the matrix diffusion parameters to take place twice. Explicit scaling of the matrix diffusion parameters as indicated above in step 3 is not necessary if it is assumed that the matrix and channel properties are the same in the TRUE-1 and TRUE Block Scale experiments. However, both first and corrected predictions are presented. The results that involve the scaling error may serve as useful sensitivity cases that indicate the importance of the matrix properties in the transport. Difference in matrix properties between the first and corrected predictions can be determined by comparing values of U_t in Table 4-4 and using Equation (3-16).

5.1 Tracer test C1

The definition of the modelling task did include recommendations for the time span of the predictions. It was selected more or less arbitrarily to calculate the first predictions until approximately 2 000 hours and show the corrected predictions until 10 000 hours. According to the modelling results all tracers high mass recoveries.

Predictive results for tracer test C1 gave rather high mass recoveries for most of the tracers. Predicted recoveries are presented in Table 5-1 both for the original predictions that include the scaling error (in parentheses) and for the corrected predictions in Table 5-2. In the C1 experiment the correction clearly increased the effect of matrix diffusion by a factor that varies form 8 to 15. Recovery of the Rb-86, for example, decreased from the 81 % to 59 % although the simulation time was increased from 2 000 h to 10 000 h. Predicted cumulative recoveries are presented in Figure 5-1.

Table 5-1. Performance measures of the C1 tracer experiment (first predictions).

	Dirac source term			**Measured source term**			**Recovery at 1 998 h**
Tracer	**t 5% [h]**	**t 50% [h]**	**t 95% [h]**	**t 5% [h]**	**t 50% [h]**	**t 95% [h]**	
Br-82	9	25	304	11	34	314	99 %
Ca-47	18	53	935	20	58	939	97 %
Cs-134	661	-	-	715	-	-	45 %
K-42	14	62	-	20	68	-	92 %
Na-24	11	33	545	14	37	549	98 %
Rb-86	44	220	-	48	226	-	81 %

Table 5-2. Performance measures of the simulated C1 tracer experiment (corrected predictions).

	Dirac source term			Measured source term			Recovery at 9 997 h
Tracer	**t 5% [h]**	**t 50% [h]**	**t 95% [h]**	**t 5% [h]**	**t 50% [h]**	**t 95% [h]**	
Br-82	10	43	5638	12	55	5648	96 %
Ca-47	25	197	-	27	201	-	88 %
Cs-134	1227	-	-	1331	-	-	41 %
K-42	37	645	-	41	651	-	80 %
Na-24	13	61	-	15	65	-	94 %
Rb-86	195	5048	-	201	5054	-	59 %

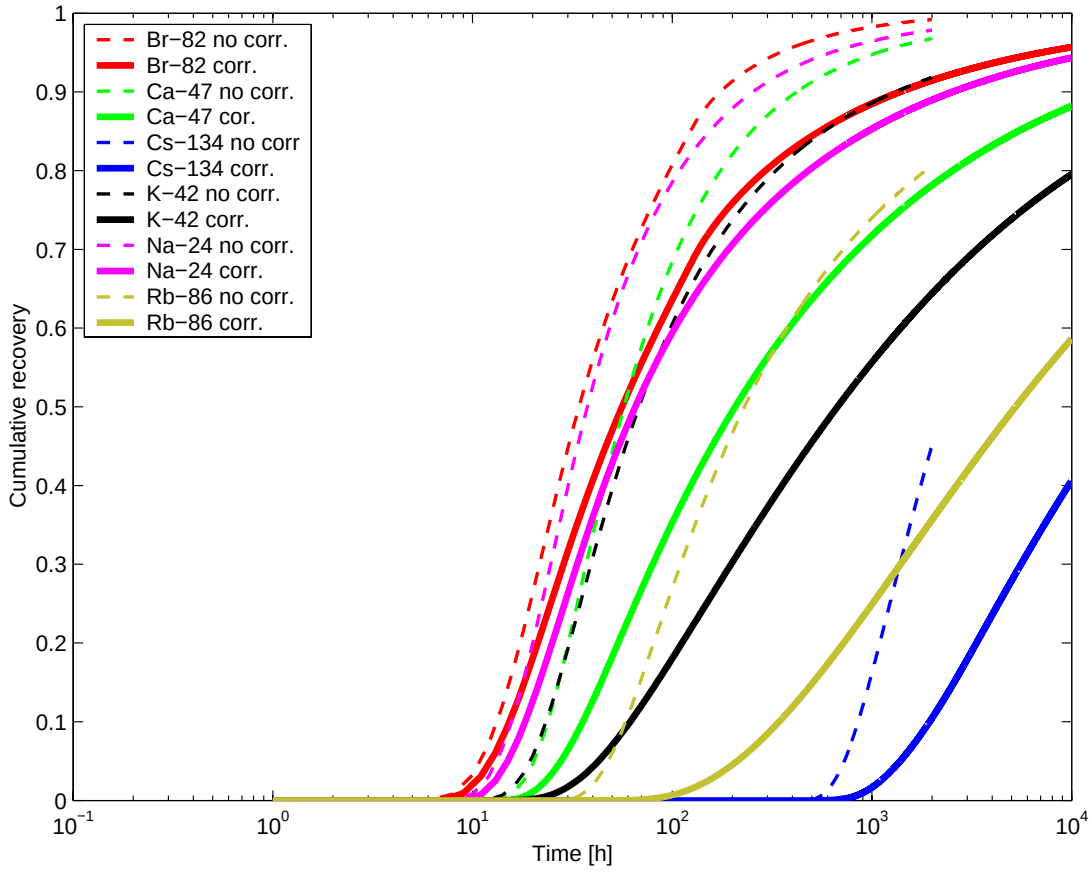

Figure 5-1. *Predicted cumulative recoveries for the simulated C1 test. First predictions are presented with dotted lines and corrected predictions are presented with solid lines.*

5.2 Tracer test C2

The definition of the modelling task did not have recommendations for the time span of the predictions. It was selected more or less arbitrarily to calculate the first predictions until approximately 5 000 hours and the corrected predictions until 15 000 hours.

Predictive modelling of the tracer test C2 gave poor mass recovery for the Cs-137 and Ba-131. Other tracers gave reasonable mass recoveries. The cumulative recoveries of the tracers are presented in Figure 5-2. The same scaling error as in C1 predictions occur also in the C2 predictions. The correction of the scaling of the matrix diffusion parameter decreased the parameter by a factor 1.3. However the influence of the matrix diffusion in the C2 test is smaller than in C1 and C3. For the non-sorbing tracer (Re-186) the correction did not change the breakthrough curve indicating that the matrix diffusion is not important in the predictive modelling of C2. Generally, the scaling error worked in the C2 test to opposite direction as in the C1 test. The performance measures of the C2 test for the first predictions are presented in Table 5-3. Corrected predictions and performance measures are accounted for in Table 5-4.

Table 5-3. Performance measures of the simulated C2 tracer experiment (first predictions).

	Dirac source term			Measured source term			Recovery at 4 995 h
Tracer	**t 5% [h]**	**t 50% [h]**	**t 95% [h]**	**t 5% [h]**	**t 50% [h]**	**t 95% [h]**	
Ba-131	2793	-	-	2813	-	-	10 %
Ca-47	485	-	-	501	-	-	37 %
Cs-137	-	-	-	-	-	-	0 %
Re-186	65	255	-	73	270	-	89 %

Table 5-4. Performance measures of the simulated C2 tracer experiment (corrected predictions).

	Dirac source term			Measured source term			Recovery at 14 997 h
Tracer	**t 5% [h]**	**t 50% [h]**	**t 95% [h]**	**t 5% [h]**	**t 50% [h]**	**t 95% [h]**	
Ba-131	1715	-	-	1733	-	-	33 %
Ca-47	335	6324	-	349	6338	-	61 %
Cs-137	-	-	-	-	-	-	1 %
Re-186	67	255	-	77	281	-	93 %

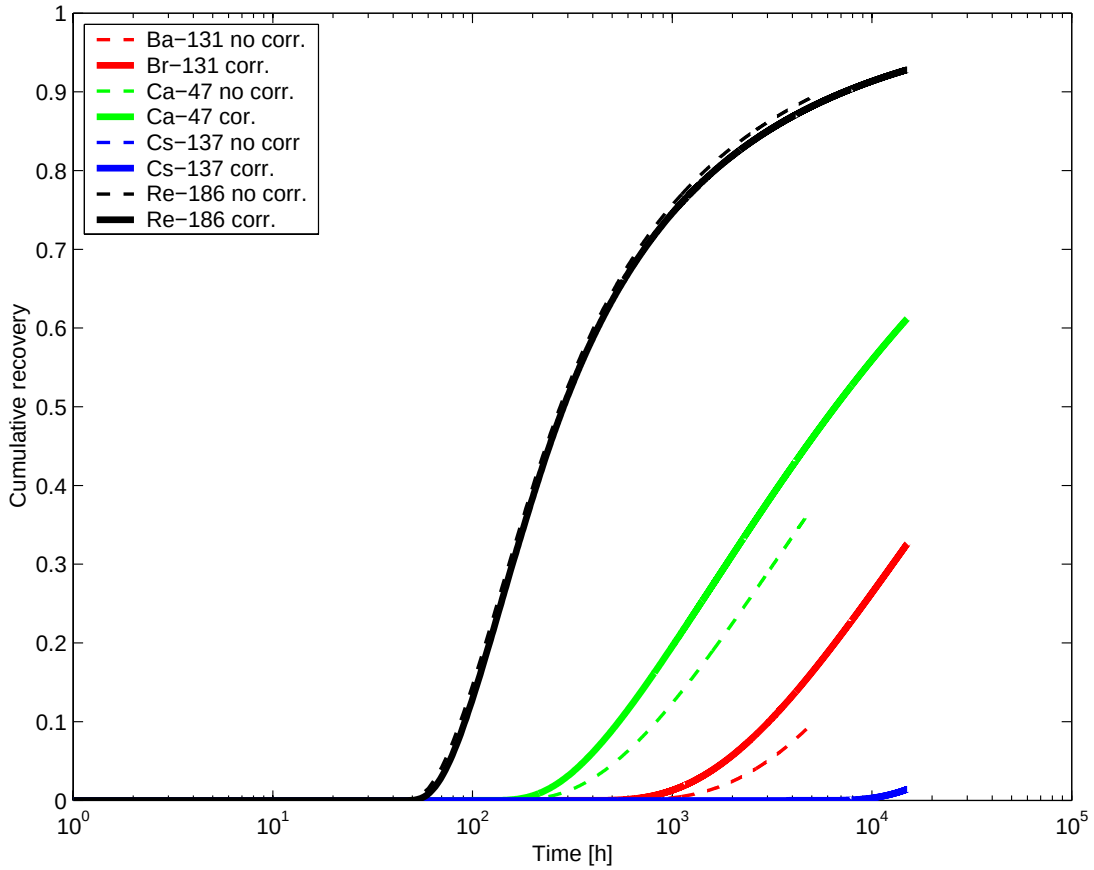

Figure 5-2. *Predicted cumulative recoveries in C2 test. First predictions are presented with dotted lines and corrected predictions are presented with solid lines.*

5.3 Tracer test C3

The definition of the modelling task did not have recommendations for the time span of the predictions. It was selected more or less arbitrarily to calculate the first predictions until approximately 4 000 hours and the corrected predictions until 14 000 hours.

The predictive modelling of tracer test C3 gave very poor mass recovery for the Ba-133, Rb-83 and Sr-85. Recovery of the HTO was rather high and Na-22 moderate. The cumulative recoveries of the tracers employed in C3 are presented in Figure 5-3. The correction of the scaling of the matrix diffusion parameter decreased the matrix diffusion parameter by a factor of 3.5. As in the case of the C2 test the effect of the matrix diffusion for the non-sorbing (Na-22) is very small and correction of the matrix diffusion parameter does not influence this breakthrough curve. For the more sorbing tracers (e.g. Rb-83) the effect of the correction is clearly noticeable.

The performance measures for the first predictions are presented in Table 5-5 and for the corrected predictions in Table 5-6.

Table 5-5. Performance measures of the simulated tracer experiment C3 (first predictions).

	Dirac source term			Measured source term			Recovery at 3 996 h
Tracer	**t 5% [h]**	**t 50% [h]**	**t 95% [h]**	**t 5% [h]**	**t 50% [h]**	**t 95% [h]**	
Ba-133	-	-	-	-	-	-	0 %
HTO	152	877	-	200	957	-	74 %
Na-22	1433	-	-	1506	-	-	15 %
Rb-83	-	-	-	-	-	-	0 %
Sr-85	-	-	-	-	-	-	2 %

Table 5-6. Performance measures of the simulated tracer experiment C3 (corrected predictions).

	Dirac source term			Measured source term			Recovery at 13 997 h
Tracer	**t 5% [h]**	**t 50% [h]**	**t 95% [h]**	**t 5% [h]**	**t 50% [h]**	**t 95% [h]**	
Ba-133	5798	-	-	5870	-	-	13 %
HTO	155	953	-	205	1033	-	83 %
Na-22	301	3886	-	363	3964	-	67 %
Rb-83	-	-	-	-	-	-	2 %
Sr-85	731	-	-	805	-	-	47 %

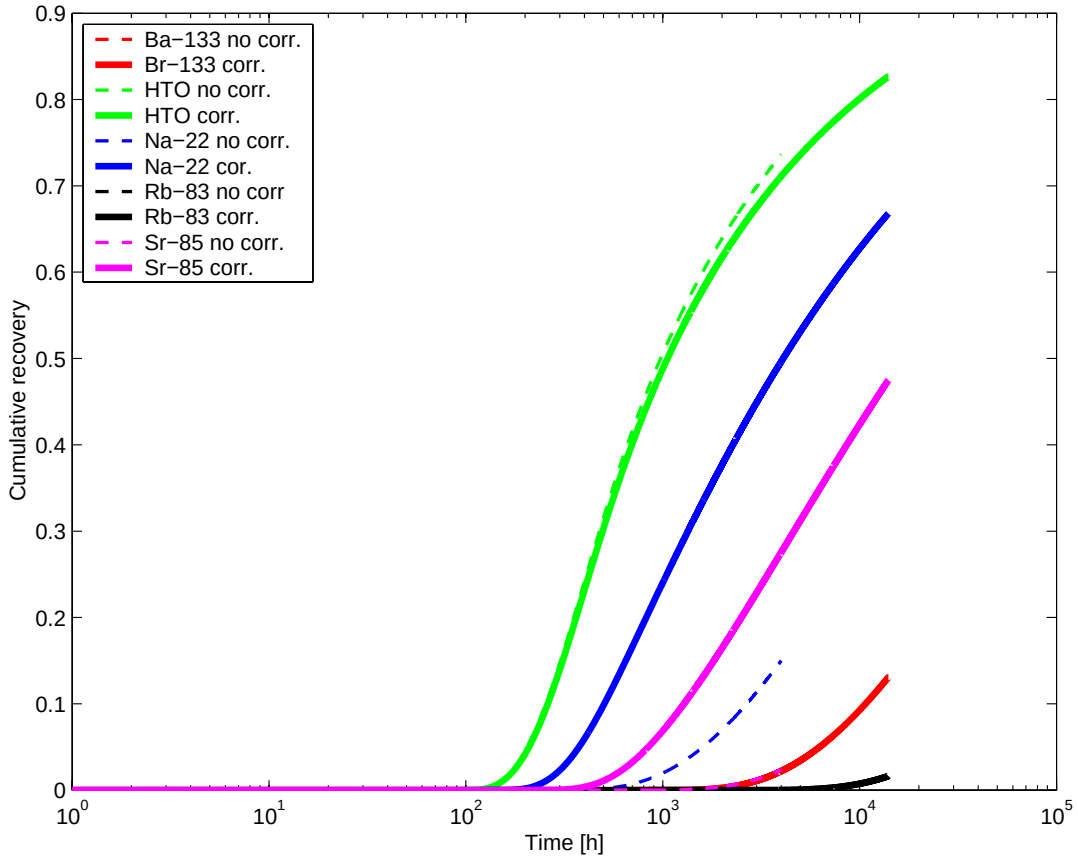

Figure 5-3. *Predicted normalised mass flow for the simulated tracer test C3.*

6 Results of in situ experiments

The experimental results showed recovery for six tracers in C1, two tracers in C2 and three tracers in C3 at time of termination of official monitoring (3300 hours). Generally the performance of the tracer test predictions relative to the experimental results was better for non-sorbing tracers than for the sorbing ones. Experimental results are here compared against the final corrected predictions.

For the tracer test C1 the measured breakthrough of Cs-134 differed considerably from the predicted breakthrough. The predicted breakthrough starts too late and the width of the predicted curve is narrower than the measured one. For the other tracers the first breakthrough times and the shape of the tailing were quite correct, but in some cases (e.g. Rb-86) the shape at the peak arrival time was sharper in the predictions than in the measured curves.

For the tracer test C2 it was correctly predicted that only Re-186 and Ca-47 would be recovered during the first 900 hours. However, the predicted behaviour of the Ca breakthrough does not follow the measured behaviour. The measured first breakthrough is at later time than predicted and the shape of the measured peak arrival time is much sharper than the predicted one.

In tracer test C3 it was correctly predicted that Ba-133 and Rb-83 do not show recovery during the first 3000 hours. According to the predictions it was expected that also the recovery of Sr-85 would be low, but that was not the case in the experiment. Generally, the predictions gave too wide breakthrough curves.

It may be noted that the predicted results for the HTO and Re-186 were quite good both in C2 and C3. These tracers were the only ones for which the parameter u were calculated directly from Equation (3-15) and not transferred from the TRUE-1 tests. Overall, the accuracy of the predictions seems to be better for C2 and C3 than in C1. However, this may result simply from the fact that the tracers recovered in C1 represent much wider spread of the sorption properties. The more sorbing tracers that were poorly predicted in C1 were not recovered at all during C2 and C3. The performance of the predictions for C1 compared to the other tests cannot thus be entirely determined.

The measured and predicted results are presented in Figures 6-1 through 6-3. The breakthrough curves are not normalised in any way. They are plotted by converting the measured breakthrough concentrations to the mass flow by multiplying the measured concentration by the pumping rate of 1.96 l/min (=117.6 l/h). Performance measures of the C1, C2 and C3 tests are presented in Table 6-1. They are collected from the Tables 6-2, 6-3 and 6-4 from Andersson et al. (2002a).

Table 6-1. Performance measures of the in situ experiments (from Andersson et al., 2002a)

Test No.	Distance [m]	R (%)	First arrival [h]	Mean travel time [h]	Dispersivity [m]
C1	14	100	4.5	18	2.3
C2	97	80	38	282	24
C3	33	>73	114	514	9.6

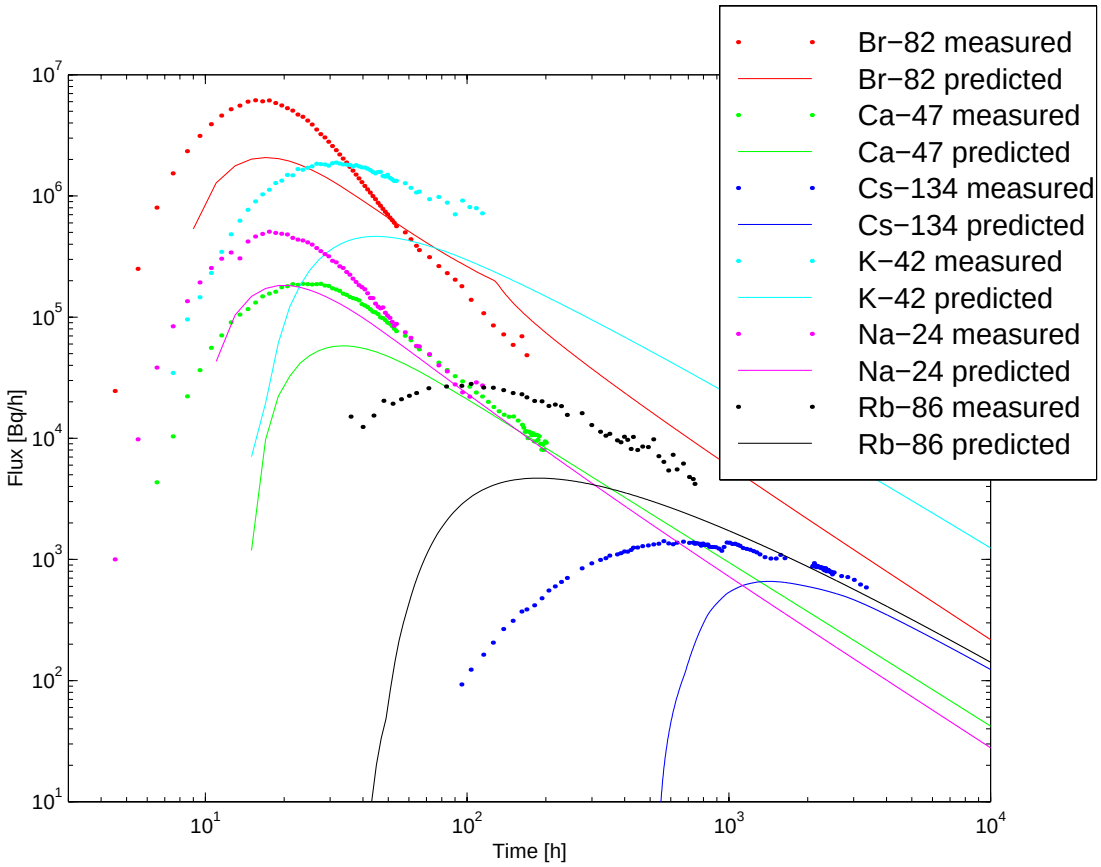

***Figure 6-1**. Predictions compared to the measured breakthrough curves for the tracer test C1.*

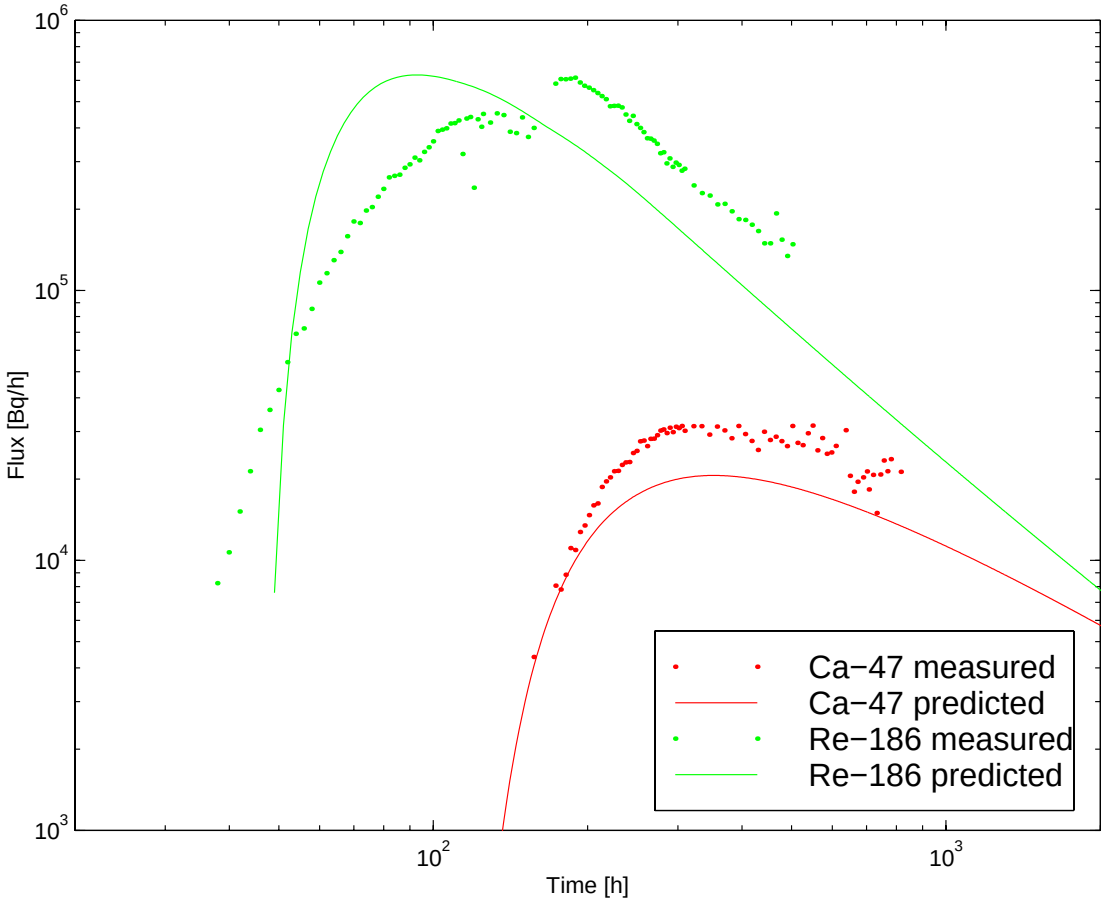

Figure 6-2. *Predictions compared to the measured breakthrough curves for the tracer test C2.*

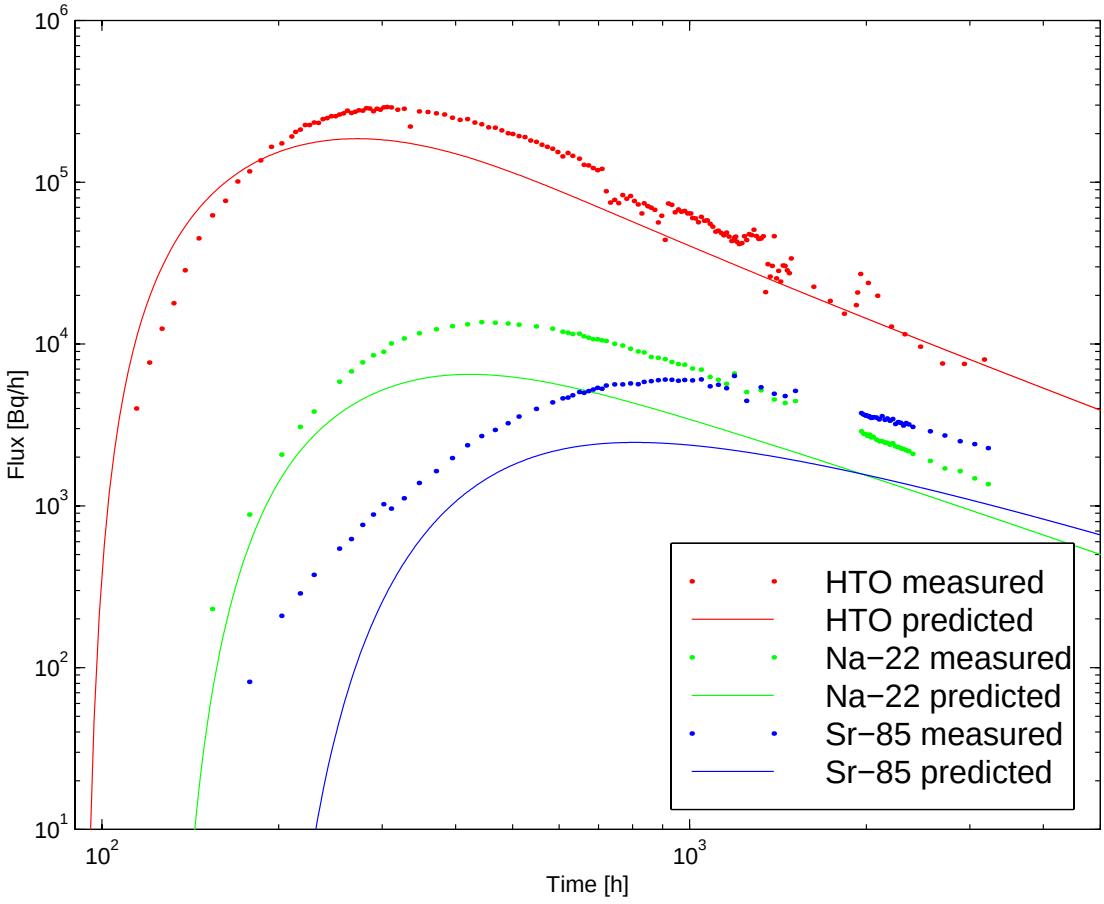

Figure 6-3. *Predictions compared to the measured breakthrough curves for the tracer test C3.*

7 Evaluation

The evaluation of the tracer tests is based on the data available from the measured breakthrough curves of the Phase C tests. In the evaluation the goal has been to find out an explanation for the observed breakthrough curves that is also consistent with the other independent information available from the site. Basic questions addressed are; what kind of pore structure there exists along the tested flow paths? What is the role of the advective flow field? And does there exist indications of the matrix diffusion (diffusion to the immobile pore space) in the breakthrough curves?

Laboratory measurements are available for the sorption properties and porosity of the rock samples from the test area (e.g. Andersson et al., 2002b and Byegård et al., 1998). In the predictions it was assumed that the matrix diffusion properties along the block scale flow paths are similar as along the TRUE-1 flow paths. Comparison of the predictions with the in situ results show that fine-tuning of the matrix diffusion properties is needed. In the evaluation sorption coefficients, porosity and geometric factor of the pore diffusivity are changed but in such a way that the corresponding laboratory measurements tried to be taken into account. This is useful because tracer retention is a result of several different processes/properties that cannot be determined uniquely using the measured breakthrough curves. In practice, constraining the immobile zone properties shifts the fitting of the observed retention to the fitting of the geometry of the flow channel.

The modelling approach applied in the evaluation is basically the same that was applied in the prediction phase. The only significant difference to the prediction model is found in the description of the advective transport. The molecular diffusion in the transport channel is now taken into account and the velocity profile in the channel is linear. Together these steps lead to the model of the generalised Taylor dispersion of the advective transport. In the prediction phase the velocity profile was a square root function fitted to the non-sorbing Phase B tests and the molecular diffusion in the channel was not taken into account.

7.1 Conceptual model

As in the prediction model (Figure 3-4), it is here assumed that a single flow path connects the source to the sink. The flow path may visit different fractures, but it is not possible to infer properties of the individual fractures from the breakthrough curves. This concept can be taken even further by arguing that, in principal, it is not possible to see from the breakthrough curve whether the channel has heterogeneous or homogeneous retention properties along the flow path (i.e. immobile zone porosity, K_d, K_a, D_e, channel width and aperture). This means that in the model calculations it is appropriate to apply only equivalent or averaged homogeneous properties along the flow path. The conceptual transport model applied in the evaluation of the tracer tests is presented in Figure 7-1.

The approach applied in the evaluation can be summarised by following main points:

- Transport of the tracers takes place along a channel that connects the source and the sink. A single channel model has its limitations. It can be applied to examine the shape of the tracer residence time distribution, but in general, it cannot be used to calculate the recovered cumulative tracer mass because the whole tracer mass eventually goes to the sink.

- Tracers may diffuse into the immobile pore space surrounding the transport path and tracers can sorb on the fracture surface, or on the surfaces of the immobile pore space.

- The flow field between the source and sink is characterised by the linear distribution of different flow velocities from zero to maximum velocity. The flow field is characterised by the maximum flow velocity and a correlation length that determines the transverse scale over which the flow velocities vary. Molecular diffusion in the flow field is taken into account

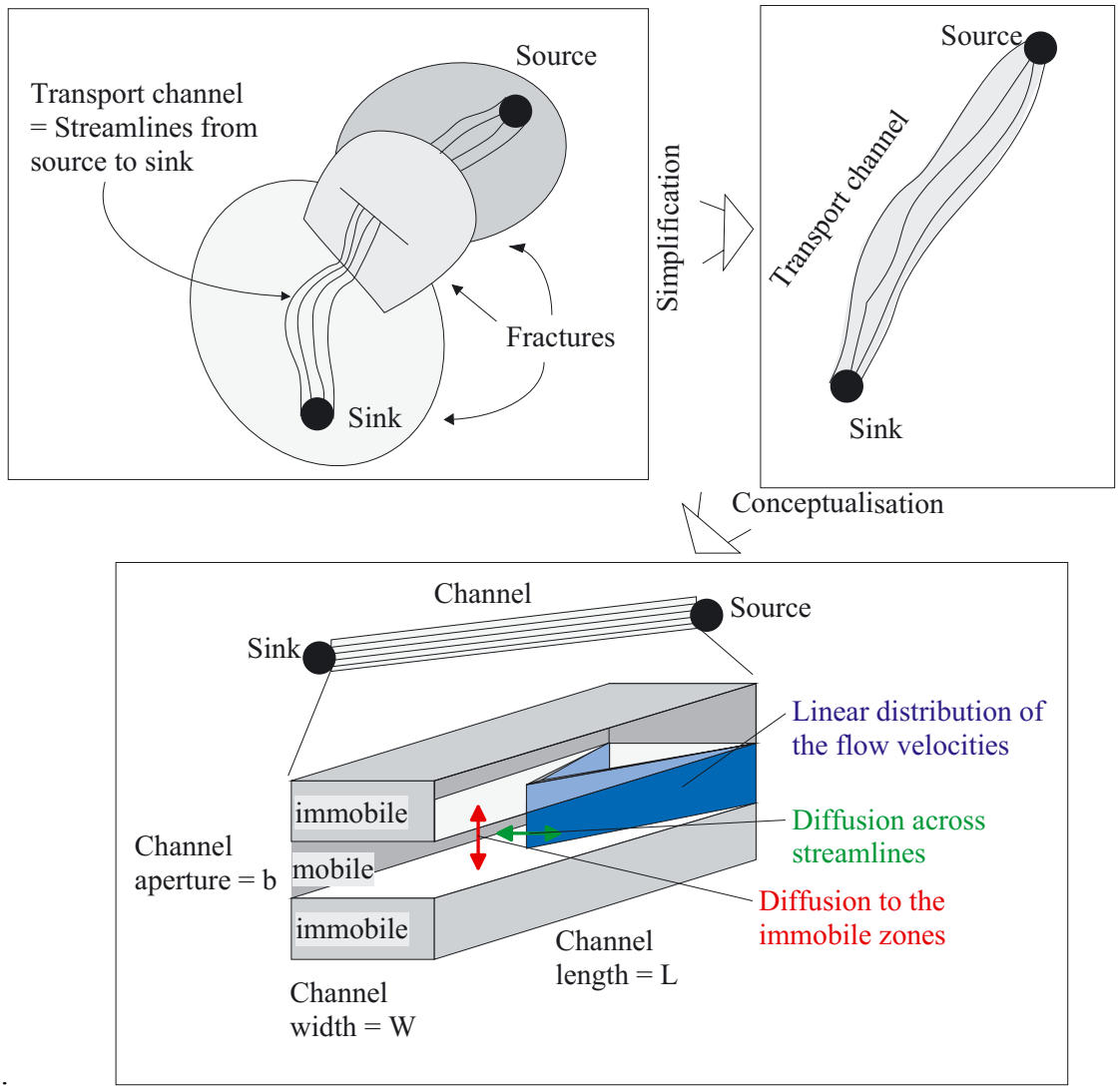

.

Figure 7-1. *Conceptual model of the tracer transport from source to sink using the single channel model.*

The immobile zone pore structure along the transport path has a significant influence on the transport. Therefore different alternatives of the immobile pore space structures surrounding the flow path have been applied/tested. In the first alternative there is no fault gouge, and the tracers may only diffuse directly to the rock matrix. The second alternative includes fault gouge on the fracture surface and diffusion takes place only to the fault gouge (Figure 7-2). Fault gouge has not been collected from the intercepts contained in the Phase C injection sections. However, such material is found in the other locations of the structures that were tested in the Phase C tests (Andersson et al., 2002b).

The third alternative diffusive mass exchange process is diffusion to the stagnant zones of the flow field. The stagnant zones are regions of the flow field where the flow velocity is very small, but at the same time the volume of the region is sufficiently large so that it does not get saturated during the experiment. These kind of regions can develop, for example, in the areas of the low transmissivity.

It is assumed in all three alternative models that the tracer particles collected during the time frame of the tracer experiments have not seen any boundary in the immobile pore space. This means that the diffusion depth in the immobile zone is always assumed infinite.

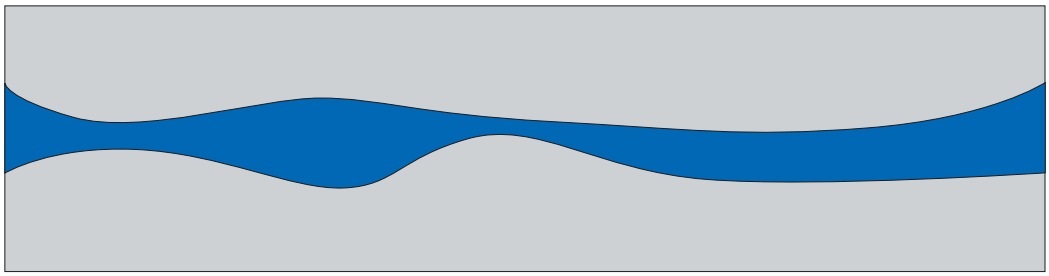

Alternative 1. No fault gouge

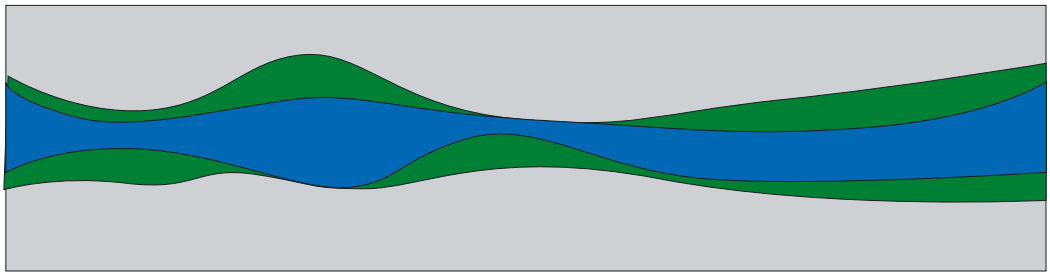

Alternative 2. Fault gouge on the fracture surface

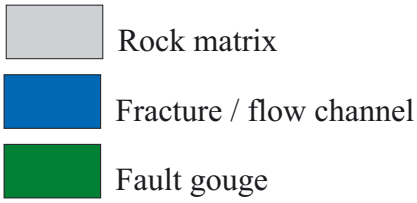

Figure 7-2. *Alternative conceptual models of the immobile pore space in geological material along the transport channel (vertical view across the transport channel). In addition to the geological material also stagnant zones of the flow field are examined in the modelling.*

7.2 Mathematical model

7.2.1 Groundwater transit time distribution

Groundwater transit time distribution is represented using a linear distribution of the flow velocities from zero to maximum velocity and molecular diffusion across the streamlines. The maximum flow velocity and correlation length of the velocity field parameterises the flow field. The groundwater transit time distribution includes the effect caused by the molecular diffusion in the flow field but it does not include diffusion to the immobile pore space (rock matrix, fault gouge or stagnant zones). This distribution can also be conceived as the residence time distribution of the water molecules in the case that the fracture surfaces are acting as boundaries for the water molecules.

It is assumed that there is no velocity or concentration variation in the normal to the fracture plane (in the void space of the fracture). The residence time distribution of the ideal non-sorbing tracer (no matrix diffusion) is a result of the different flow velocities and the transverse molecular diffusion over the flow field in the transport channel. The channel is presented conceptually in Figure 7-3. In the figure the correlation length of the velocity variation is half of the channel width. The development of the released concentration plume is illustrated at three different time steps using different grey scales. The actual width of the transport channel can also be much larger than the correlation length of the velocity variation (*a* in Figure 7-3). In that case the transport channel is simply composed of a variable velocity field that have several maximum and minimum points. In Figure 7-4 the correlation length is one sixth of the channel width.

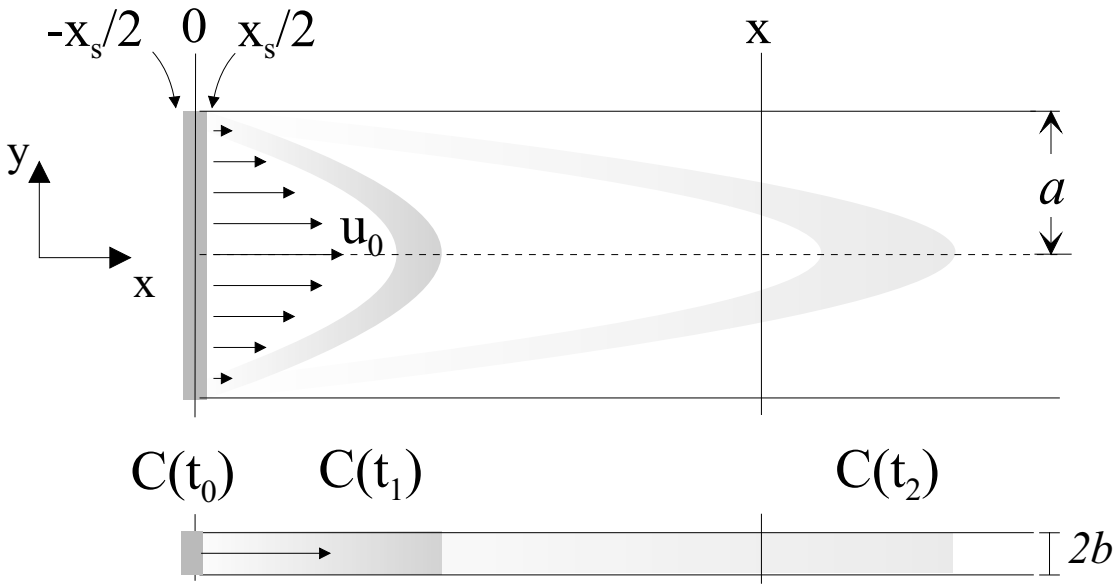

Figure 7-3. *Conceptual figure of the flow field in the transport channel used for the evaluation. The lower part of the figure is a vertical cross-section and the upper part is horizontal cross-section. The released tracer plume is illustrated at three different time steps using different grey scales. Aperture of the channel is 2b and the correlation length of the velocity variation is a.*

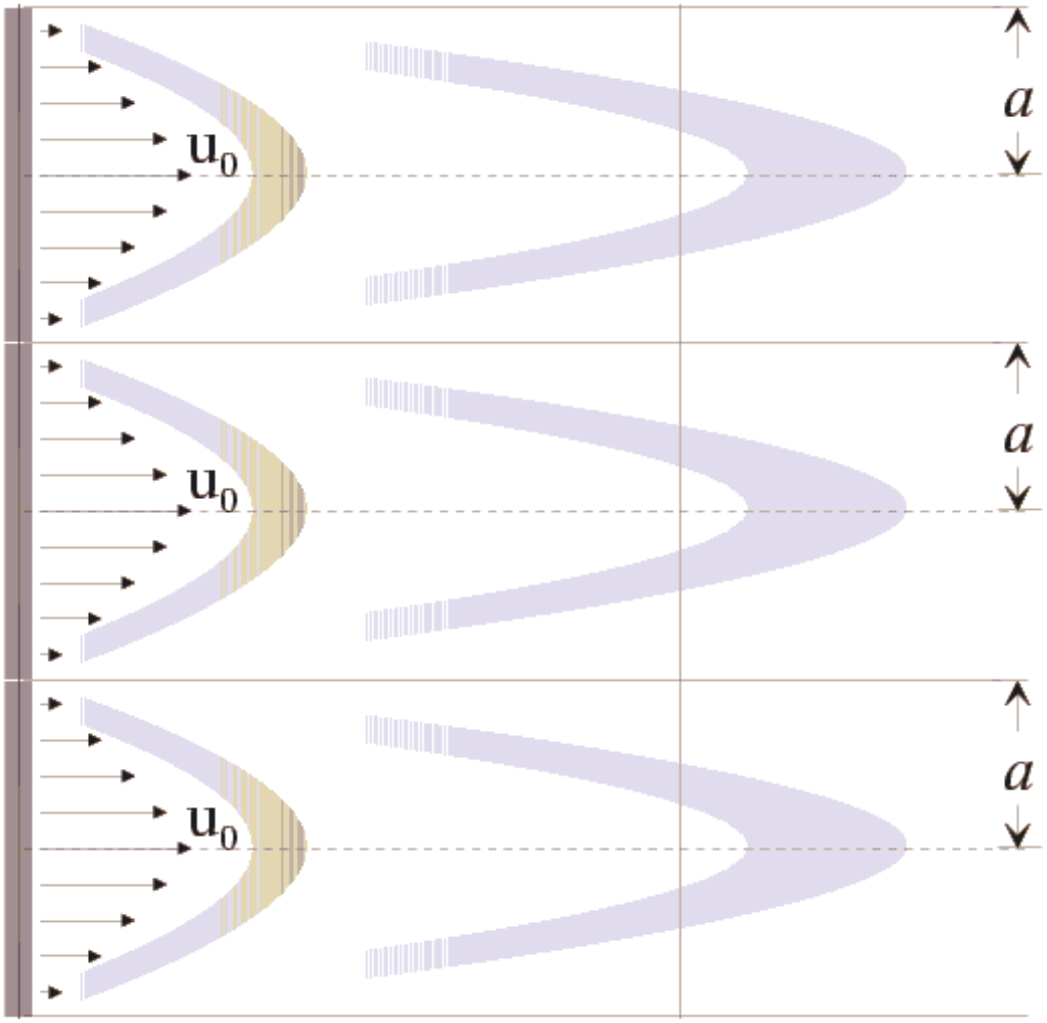

Figure 7-4. *An example of the transport channel in the case the correlation length of the flow velocity variation is much smaller than the channel width. The released tracer plume is illustrated at three different time steps using different grey scales.*

The mean concentration across the channel can be solved analytically. Here only the solution for the mean concentration is given. A more detailed discussion is given by Hautojärvi and Taivassalo (1994). The mean concentration across the velocity field for a narrow box-function release is given in Equation (7-1).

$$C_m = \frac{1}{2}\left(erf\left[\frac{\frac{1}{2}X_s + X + \xi_1}{2\sqrt{\xi_2}}\right] + erf\left[\frac{\frac{1}{2}X_s - X - \xi_1}{2\sqrt{\xi_2}}\right]\right);$$

$$\xi_1 = -\frac{1}{2}\tau;\ \xi_2 = \left(\frac{1}{(Pe)^2} + \frac{1}{120}\right)\tau - 8\sum_{n=0}^{\infty}\frac{1-e^{-(2n+1)^2\pi^2\tau}}{(2n+1)^8\pi^8}; \qquad (7\text{-}1)$$

$$\tau = \frac{Dt}{a^2};\ X = \frac{Dx}{a^2 v_0};\ X_s = \frac{Dx_s}{a^2 v_0};\ Pe = \frac{a v_0}{D}$$

where D is the molecular diffusion coefficient in water, a is the correlation length of the velocity variation, x_S is the initial width of the tracer plume (see Figure 7-3), u_0 is the maximum flow velocity, t is the time and x is the position along the channel.

The solution in (7-1) cannot be applied if the dimensionless parameter X (given in Equation (7-1)) is very small. In that case the residence time distribution approaches the purely advective case and the dispersion caused by diffusion between the streamlines becomes negligible. This case has been taken into account by replacing the solution (7-1) by the purely advective transit time distribution if $X \leq 0.1$.

The breakthrough curve of the linear velocity profile using only the advective flow field is presented in Equation (7-2). It can be calculated using Equation (3-7) and substituting x=1 (linear profile). Equation (7-2) assumes that the tracer mass released to different streamlines is proportional to the flow rate equitable to good mixing at the injection point.

$$\dot{m}(t) = 2m_0 \frac{t_0^{\,2}}{t^3} \quad . \qquad (7\text{-}2)$$

The behaviour of the groundwater transit time distribution is illustrated in Figure 7-5. For values X>0.5 the resulting transit time distribution is a typical symmetric advection-dispersion breakthrough curve. The longitudinal diffusion is here not taken into account. This means that as X increases the transit time distribution gets narrower and approaches plug flow (see Figure 7-5). For small values of X the transit time distribution becomes governed by the advective field (i.e. the transit time distribution given in Equation (7-2)). This is illustrated in Figure 7-5 by showing the purely advective transit time distribution for $X \leq 0.1$.

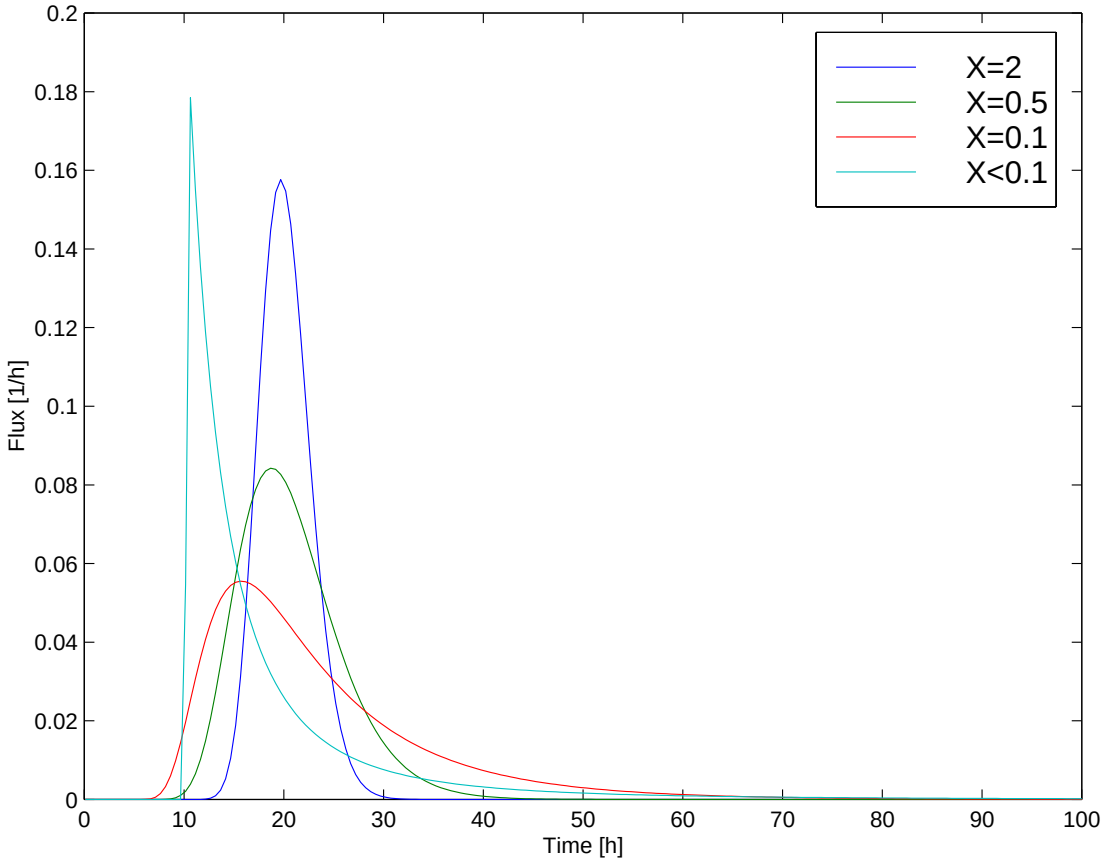

Figure 7-5. *Groundwater transit time distributions calculated using Equations (7-1) and (7-2) and parameter values* $m_0 = 1$, $t_0 = 10$ *and* X=*2,* X=*0.5,* X=*0.1 and* X<*0.1.*

7.2.2 Matrix diffusion

The advection-matrix diffusion transport equation has been presented earlier in Equation (3-9) and the solution is presented in Equation (3-14). According to Equation (3-14) the tracer discharge at the end of the transport channel for the delta function release can be written as

$$j(t,t_w,u,R_a) = H(t-R_a t_w)\frac{u}{\sqrt{\pi}\left(t-R_a t_w\right)^{3/2}} e^{-\frac{u^2}{t-R_a t_w}}, \qquad (7\text{-}3)$$

Where parameter u determines the strength of the matrix diffusion, t_w is the groundwater transit time and R_a is the surface retardation coefficient. The matrix diffusion property (u) for different parts of the streamtube are connected to the transit time distribution (t_w) according to the Equation (3-16), i.e. $u=u(t_w)=U_t\, t_w$. This is based on the assumption that the differences in transit times are due to different flow rates through different parts of the channel, although the aperture is the same throughout the channel (this is reasoned, among other things, by the fact that flow rate depends on the third power of the aperture, i.e. the aperture variation is minor compared to the corresponding flow rate change). The tracer transit time distribution for the matrix diffusion case can now be calculated by integrating the discharge function of the delta function release over the groundwater transit time distribution according to Equation (7-4).

$$k(t) = \int_0^t j(t, t_w, U_t\, t_w, R_a) b(t_w) dt_w \quad , \qquad (7\text{-}4)$$

where $b(t_w)$ is the groundwater transit time distribution. Equation (7-4) gives the breakthrough curve for instantaneous release of a unit mass of the tracer. The actual injection curve is taken into account by convoluting the function $k(t)$ in Equation (7-4) with the injection function $s(t)$,

$$c(t) = \int_0^t s(t') k(t - t') dt' \quad . \qquad (7\text{-}5)$$

In this kind of approach the source term for different parts of the channel (i.e. different t_w) is the same. It is noted, that making the integrations (7-4) and (7-5) in the reversed order enables application where the source term over the channel varies, e.g. following the flow rate distribution. However, this has not been done in the present evaluation.

Inspection of the solution in Equation (7-3) shows that the surface sorption causes the residence time distribution to shift towards later breakthrough time without changing the overall shape of the curve. This means that for tracers having different surface sorption coefficients the R_a determines the time when first arrival occur for the sorbing tracer (reactive). This can also be seen by plotting Equation (7-3) using different R_a's. This is illustrated in Figure 7-6 by presenting $j(t,tw,u,Ra)$ for two pairs of u and R_a.

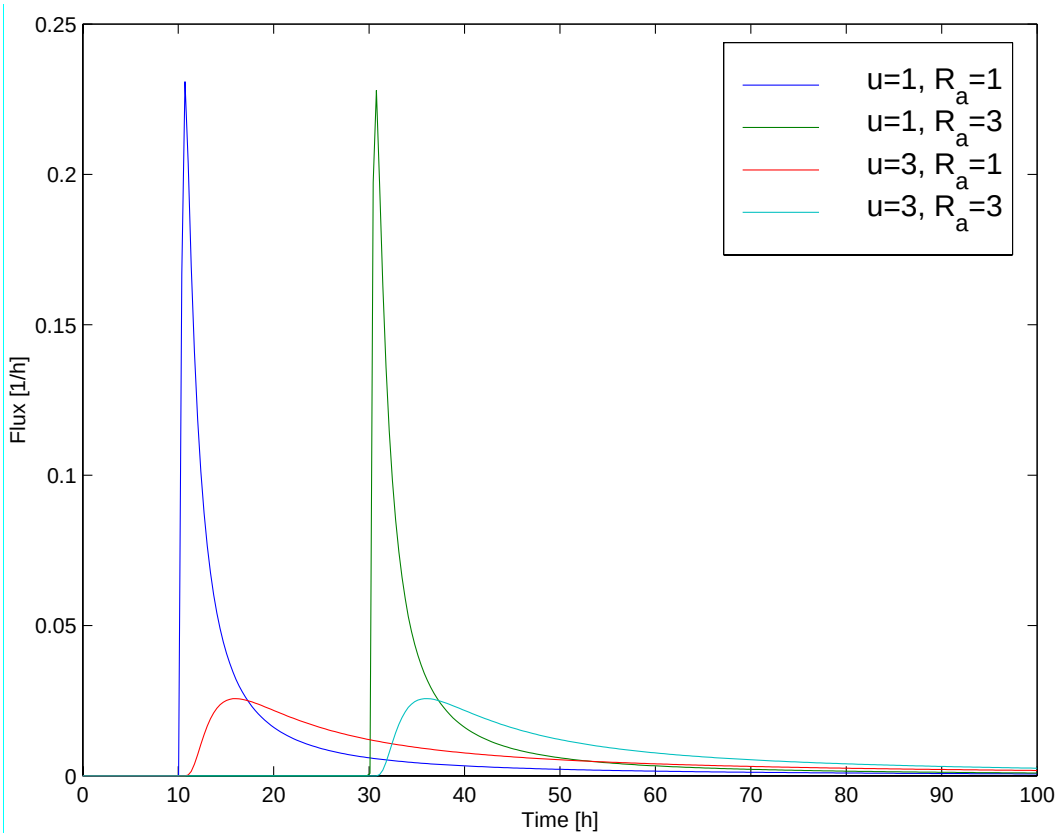

Figure 7-6. *Discharge rate calculated using Equation (7-3) for different* u *and* R_a *pairs.* R_a *determines the time of the early breakthrough.*

Equation (7-3) is solved for a single streamline i.e. there is only one groundwater transit time t_w present in Equation (7-3). Embedded in the actual breakthrough curves there are different transit times. Surface sorption causes linear scaling of the breakthrough times by a factor R_a. In the case of surface sorption only, two breakthrough curves of different sorbing tracers have similar shape. This means that it should be possible to get the breakthrough curves coincide by just scaling the time axes with $1/R_a$ (assuming, of course, that they have the same source function). However, if R_a>>1 it is difficult to identify the first breakthrough time and correspondingly the uncertainty in R_a is large. It is also noted that the first breakthrough time may be affected also by other phenomena than advection and equilibrium sorption, which means that this method should be applied with caution for strongly sorbing tracers.

Luckily, the solution (7-3) can be presented as

$$j(t,t_w,u,R_a) = \frac{j(t/R_a,t_w,u/\sqrt{R_a},1)}{R_a} \quad . \tag{7-6}$$

This means that, if the breakthrough curve of the non-sorbing (here this means surface sorption, i.e. R_a=1) is

$$k(t) = \int_0^t j(t,t_w,u,1)b(t_w)dt_w \quad , \tag{7-7}$$

then the scaled sorbing ($R_a \geq 1$) breakthrough can be presented as

$$k(t) = \int_0^t j(t,t_w,\frac{u}{\sqrt{R_a}},1)b(t_w)dt_w \quad . \tag{7-8}$$

This also means that in the case of a groundwater transit time distribution of t_w's the R_a can be estimated by scaling the measured breakthrough curves. However, the width of the scaled breakthrough with equilibrium sorption ($R_a \geq 1$) is narrower than the non-sorbing ($R_a = 1$) if the retardation factor in the matrix, R_p, is smaller than R_a and broader if $R_p > R_a$. In the special case that $R_p = R_a$ the scaled sorbing and non-sorbing breakthrough curves should coincide. One should also note that R_a is not completely independent of u as is assumed here. Especially, for strongly sorbing tracers R_a depends linearly on the flow field dependent part of the u (i.e. WL/Q or $t_w/2b$). If we consider a single velocity channel and short duration of injection we can write, for the time of the maximum discharge in the case of equilibrium sorption

$$t_{\max} = \left(1+\frac{2}{2b}K_a\right)t_w = t_w + 2K_a\frac{t_w}{2b} = t_w + 2K_a\frac{WL}{Q} \quad . \tag{7-9}$$

Similarly in case of the diffusion to the immobile zone we get

$$t_{\max} = t_w + \frac{2}{3}u^2 = t_w + \frac{2}{3}D_e\varepsilon R_p\left(\frac{WL}{Q}\right)^2 \quad . \tag{7-10}$$

This means that if the same flow path is tested using different flow rates the observed breakthrough time as a function of the flow rate should turn from linear behaviour to quadratic behaviour when the diffusion to the stagnant zones begins to dominate the

retention. In practice this should show the behaviour that the calculated retardation coefficient is constant as long as the equilibrium sorption dominates but begins to increase when the diffusion process dominates.

7.3 Evaluation process

The aim of the evaluation is simply to find reasonable combination of the individual physical parameters so that the retention measured in the experiments can be explained. Naturally, the evaluation is constrained by the applied conceptual and retention model. This means that the observed retention is tried to explain by linear equilibrium sorption (both on the fracture surfaces and in the matrix) and matrix diffusion to the semi-infinite immobile zones using a single streamtube to describe the flow. These basic assumptions have not been tested in the present modelling.

7.3.1 Fitting of the parameters

Evaluation of the Phase C tracer tests is based on the advection-matrix diffusion model (Equation (7-5)) that is fitted to the measured breakthrough curves. Physical retention parameters are determined in two stages. First, in the curve fitting stage the parameter groups of the matrix diffusion model are fitted. This stage gives numerical values for the parameter groups U_t and R_a (cf. Equations (3-16), (7-3) and (7-4)) for each test and each tracer.

It is easy to compare the sorption coefficients R_a to the measured laboratory values of the Äspö fractures. According to the Equation (7-11) R_a depends on the aperture ($2b$) and surface sorption coefficient (K_a).

$$R_a = 1 + \frac{2}{(2b)} K_a \ . \qquad (7\text{-}11)$$

Parameter group U_t is more complicated. It is presented in Equation (7-12).

$$U_t = \frac{\sqrt{D_w G \varepsilon^2 \left(1 + \frac{(1-\varepsilon)}{\varepsilon} K_d \rho\right)}}{2b} \ , \qquad (7\text{-}12)$$

where D_w is the coefficient of molecular diffusion in free water, G is the geometric factor for diffusion in the immobile zone (this is calculated from the formation factor cf. Table 7-1) , ε is the porosity of the immobile zone, K_d is the sorption coefficient in the immobile zone, $2b$ is the fracture aperture and ρ is the bulk density of the immobile zone.

For the stagnant zones U_t is presented in a little bit different form, U_{ts}, that is given in Equation (7-13). Stagnant zones are assumed to be in the fracture plane. This means that the diffusion to the stagnant zones takes place in the lateral direction in the fracture plane instead of normal to the fracture plane.

$$U_{ts} = \frac{\sqrt{D_w \varepsilon_s R_a}}{2a_s} \ , \qquad (7\text{-}13)$$

where ε_s the portion of the stagnant zone available along the channel compared to the channel length and $2a_s$ is the mean lateral distance between the stagnant zones.

The geometry of the transport channel is determined by the width of the transport channel when the channel aperture is fitted using Equation (7-12). The flow velocity and the flow rate through the flow path are fixed. It is assumed that the flow velocity changes linearly from zero velocity to maximum (see Section 7.2.1). Integration of the total flow rate through the channel gives

$$Q = \frac{v_0 W (2b)}{2} \quad , \qquad (7\text{-}14)$$

where Q is the flow rate, v_0 is the maximum flow velocity, W is the channel width and $2b$ is the channel aperture.

The measured breakthrough curves of the Phase C tracer tests contain 6 different breakthrough curves for injection C1, 2 breakthrough curves for C2 and 3 breakthrough curves for C3. This makes a total number of 11 fitted values of parameters U_t. The unknown parameters are K_d's for the tracers, matrix porosity ε, geometric factor G of the pore diffusion and aperture $2b$. Aperture is fitted separately for each of the three flow paths but the porosity and geometric factor are assumed to be the same for all flow paths. This means that 14 different parameters should be determined. Surface sorption coefficients K_a are calculated directly using Equation (7-11) and channel aperture that is fitted from U_t.

Fitting K_d, ε, G and $2b$ values is achieved by minimising the difference between the fitted parameter U_t values and parameter U_t values resulting from Equation (7-12). The minimisation is constrained by the laboratory data on the K_d's, G and ε. The applied constraints for the K_d's, G and ε for the two immobile zone alternatives that are geological material (rock matrix and fault gouge) are given in Table 7-1.

Table 7-1. Limits of the acceptable values for constraining K_d, matrix porosity and geometric factor in the fitting of the retention parameters.

Parameter	Alternative 1, Rock Matrix Acceptable values [m^3/kg]	Source	Alternative 2, Fault gouge Acceptable values [m^3/kg]	Source
K_d,HTO	0	Non-sorbing	0	Non-sorbing
K_d,Re	0	Non-sorbing	0	Non-sorbing
K_d, Br	0	Non-sorbing	0	Non-sorbing
K_d,Na	$\leq 2.2 \cdot 10^{-4}$	Table 6-3[1]	$\leq 2.2 \cdot 10^{-4}$	slightly over the value $2.0 \cdot 10^{-4}$ m^3/kg given in Table 7-4[2]
K_d,Ca	$\leq 6.3 \cdot 10^{-4}$	Table 6-3[1]	$\leq 1.3 \cdot 10^{-3}$	Table 7-4[2]
K_d,K	$\leq 4 \cdot 10^{-4}$	K_d of Na in Table 6-3[1], in the fitting stage this has been increased slightly over the K_d of Na	$\leq 5.2 \cdot 10^{-3}$	Table 7-4[2]
K_d,Rb	$\leq 2.53 \cdot 10^{-3}$	Table 6-3[1]	$\leq 2.8 \cdot 10^{-2}$	Table 7-4[2]
K_d,Cs	$\leq 1.52 \cdot 10^{-2}$	Table 6-3[1]	$\leq 2.8 \cdot 10^{-1}$	Table 7-4[2]
K_d,Sr	$\leq 2.6 \cdot 10^{-4}$	Table 6-3[1]	$\leq 1.3 \cdot 10^{-3}$	Table 7-4[2]
Porosity, ε	0.1 ... 0.6 %	Table 7-1[2] and Section 7.2.6[2]	1.5 ... 3.5 %	Based on Table 7-1[2]
Geometric factor, G	0.0125 ... 0.017	see below	0.0125 ... 0.017	see below

The acceptable range of the values for the geometric factor G is selected based on the data given by Andersson et al. (2002b). Effective diffusion coefficient can be written as

$$D_e = D_w G \varepsilon = D_w F \ , \qquad (7\text{-}15)$$

where F is the formation factor. Values given in Andersson et al. (2002b) are $F = 5 \cdot 10^{-5}$ and $\varepsilon \approx 4 \cdot 10^{-3}$ for unaltered Äspö diorite and $F = 1.7 \cdot 10^{-5}$ and $\varepsilon \approx 1 \cdot 10^{-3}$ for Feature A. Using Equation (7-15) these values give $G = 0.0125$ and $G = 0.017$ for Äspö diorite and Feature A, respectively. The range between these two values has been applied as acceptable range of the geometric factor G.

7.3.2 Selected model parameters

Parameters in Table 7-1 were varied between the given limits to achieve reasonable fit between the measured and modelled breakthrough curves. Some parameters have varied

[1] Byegård et al. (1998)

[2] Andersson et.al (2002b)

using a few á priori selected values. This kind of parameter has been the correlation length of the velocity profile (four different correlation lengths were tested). Finally, a group of model parameters were kept fixed during the modelling. Selected parameters are presented in Table 7-2.

Table 7-2. Parameters fixed á priori to the modelling or varied during the modelling.

Parameter **Test**		**Source**	**comment**
Path length, *L*			
C1	16	Table 6-1[3]	
C2	97	Table 6-1[3]	
C3	35	Table 6-1[3]	
Correlation length of the velocity profile {C1, C2, C3}	{0.01, 0.02, 0.05, 0.1} m	Selected parameter	Selected 4 different variants within the range [0.01, 0.1] m that is considered reasonable
Injection flow rate, *Q*			
C1	2700 ml/h	Table 2-2[4]	C1 forced injection
C2	600 ml/h	Table 2-2[4]	C2 forced injection
C3	112 ml/h	Calculated from HTO injection curve	
Extraction flow rate	117.6 litres/h	TRUE Block Scale Communication #184	From file: "Phase C BTC data 010110.xls"
Molecular diffusion coefficient in free water, D_w	$1.0 \cdot 10^{-9}$ m^2/s	Commonly applied value.	$2.4 \cdot 10^{-9}$ m^2/s is used in [5]

7.3.3 Adjustment of tracer mass recovery

The channel model applied in the evaluation inevitably leads always to complete recovery of the tracers. In the tracer tests the recoveries may vary because other sinks also exist at the experimental site than the pumped section of the borehole. This need to be taken into account when the modelled breakthrough curves are compared with the measured breakthrough curves. In the evaluation this is taken into account by

[3] Andersson et al. (2002a)

[4] Andersson et al. (2001)

[5] Andersson et al. (2002b)

extrapolating the recoveries of the experimental breakthrough curves to very long observation times and adjusting the modelled recovery to correspond to the extrapolated experimental recoveries.

Extrapolation of the experimental recoveries to long observation time is performed by assuming that the flow condition induced by the pumping of the experimental sink is maintained forever. Two different models are fitted to describe the tailings of the measured breakthrough curves. These are exponential and power-law ($t^{-3/2}$) behaviour. To extrapolate the final recovery the breakthrough curves are extrapolated to 10^7 hours. The calculated recoveries are compared to the injected masses given in Table 7-3. Results of the extrapolation are presented in Figures 7-7 to 7-9. The two alternative extrapolated curves are assumed to bound a region for feasible final recoveries. In all cases the exponential expression gives lower recoveries and $t^{-3/2}$-extrapolation gives upper recoveries.

In many cases the extrapolated recoveries exceed the 100% limit. This happens for the Br-82 in the C1 test already in the measured part of the recovery curve. Clearly, this indicates full recovery. The problem is that in the single channel model the integrated recovery of the breakthrough should eventually correspond to the total injected mass. To be comparable with the measured breakthrough curve the calculated recovery should coincide with the integrated mass of the measured breakthrough curve. The extrapolation using $t^{-3/2}$ tailing shows more consistent recoveries, for example, among the different tracers of the C1 test. One clear exception is Re-186 in C2 that shows very high recovered mass. However in this case the double peak shape of the breakthrough curve may indicate that there possible also has been problems with this tracer in the C2 experiment. Based on the more consistent behaviour the recoveries calculated using $t^{-3/2}$-tailing this scheme has been selected for the evaluation calculations. For all tracers the simulated recovered masses are scaled to the extrapolated mass although the extrapolated recovered mass can be higher than the corresponding injected total mass.

Table 7-3. Injected masses in the C1, C2 and C3 tracer tests and extrapolated recovered mass. Total injected mass has been extracted from file "Phase C INJ data 010110.XLS" (TRUE Block Scale Communication #184).

Test	Tracer	Injected mass [Bq]	Recovery [%] Exponential extrapolation	Recovery [%] Power law extrapolation
C1	**Br-82**	$1.38 \cdot 10^8$	113	124
C1	**Na-24**	$1.56 \cdot 10^7$	102	129
C1	**K-42**	$2.29 \cdot 10^8$	84	124
C1	**Ca-47**	$1.07 \cdot 10^7$	101	123
C1	**Rb-86**	$1.33 \cdot 10^7$	81	119
C1	**Cs-134**	$7.79 \cdot 10^6$	63	89
C2	**Re-186**	$1.71 \cdot 10^8$	108	168
C2	**Ca-47**	$5.64 \cdot 10^7$	60	90
C3	**HTO**	$2.44 \cdot 10^8$	76	91
C3	**Na-22**	$2.16 \cdot 10^7$	81	110
C3	**Sr-85**	$2.21 \cdot 10^7$	77	116

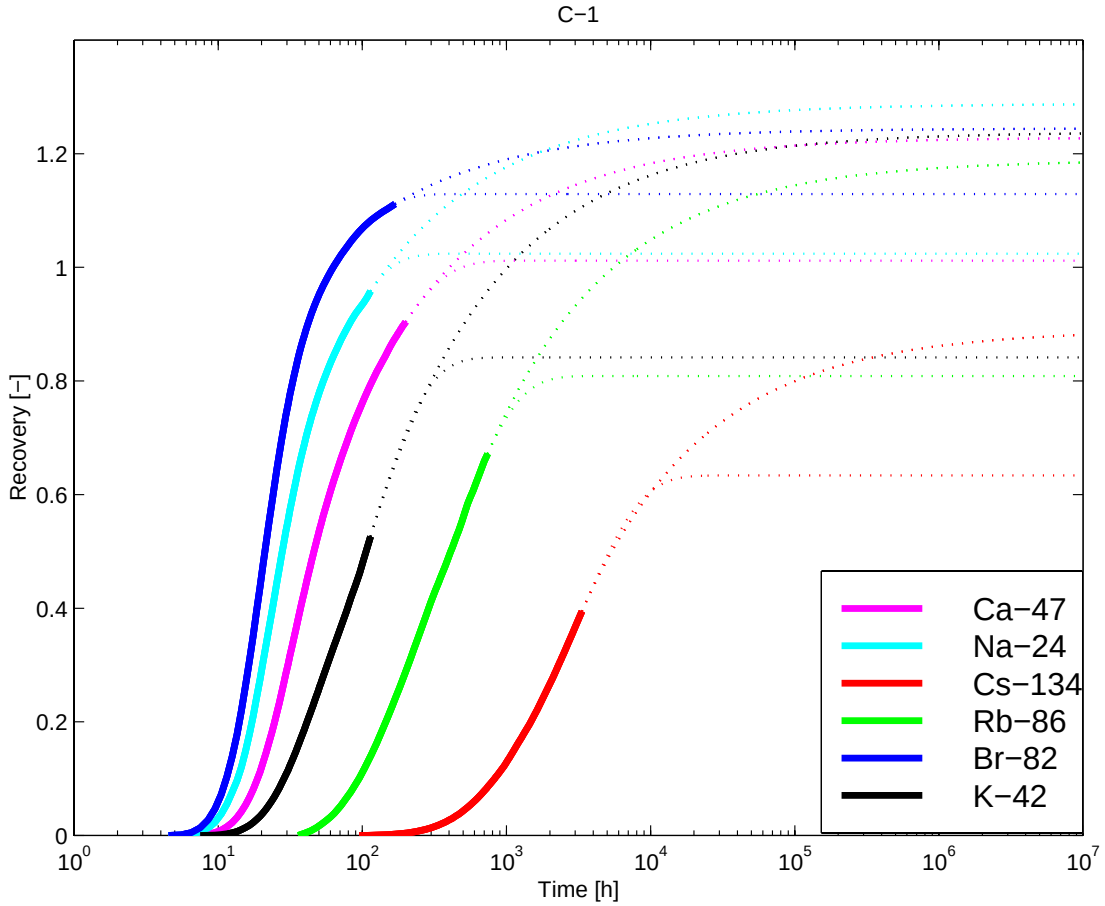

Figure 7-7. *Recoveries of the C1 test extrapolated from the measured breakthrough curves. Solid lines represent the measured recovery curve. Dotted lines are for the $t^{-3/2}$-extrapolation (upper lines) and exponential extrapolation (lower lines).*

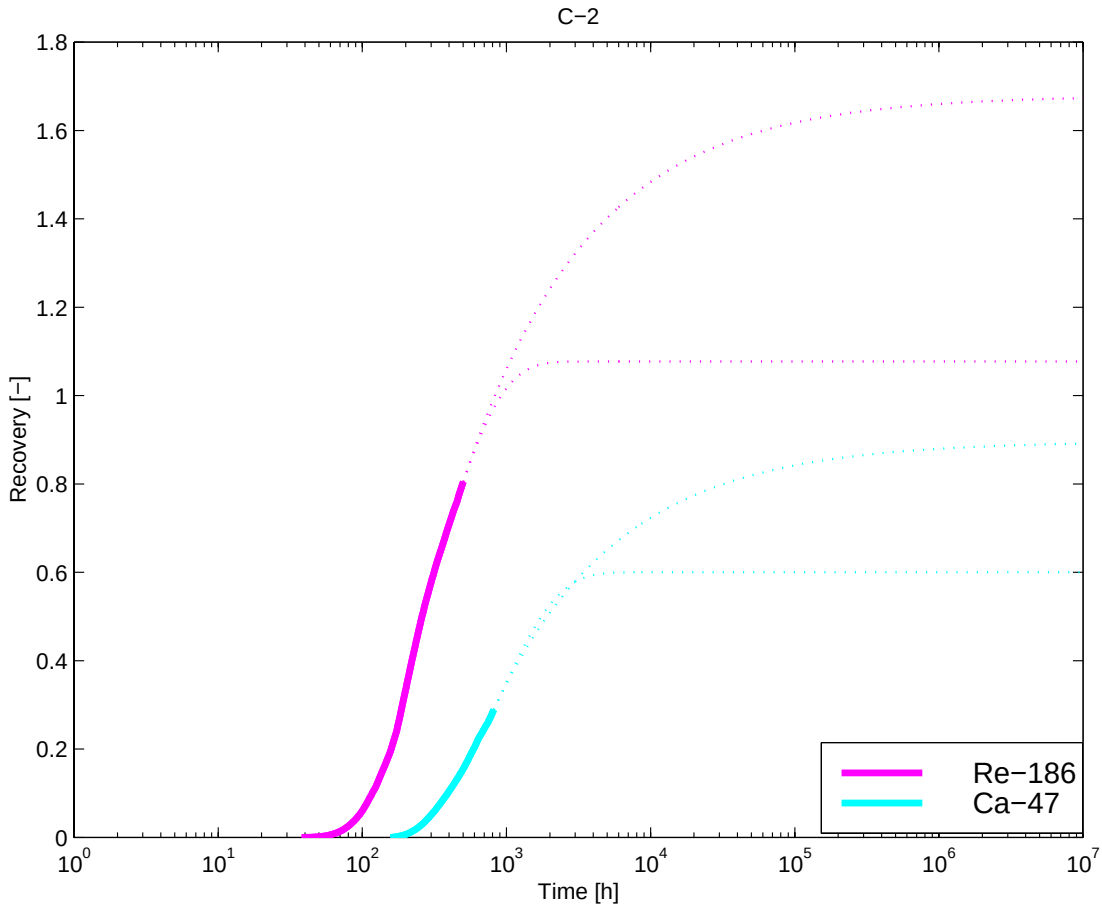

Figure 7-8. *Recoveries of the C2 test extrapolated from the measured breakthrough curves. Solid lines represent the measured recovery curve. Dotted lines are for the* $t^{-3/2}$*-extrapolation (upper lines) and exponential extrapolation (lower lines).*

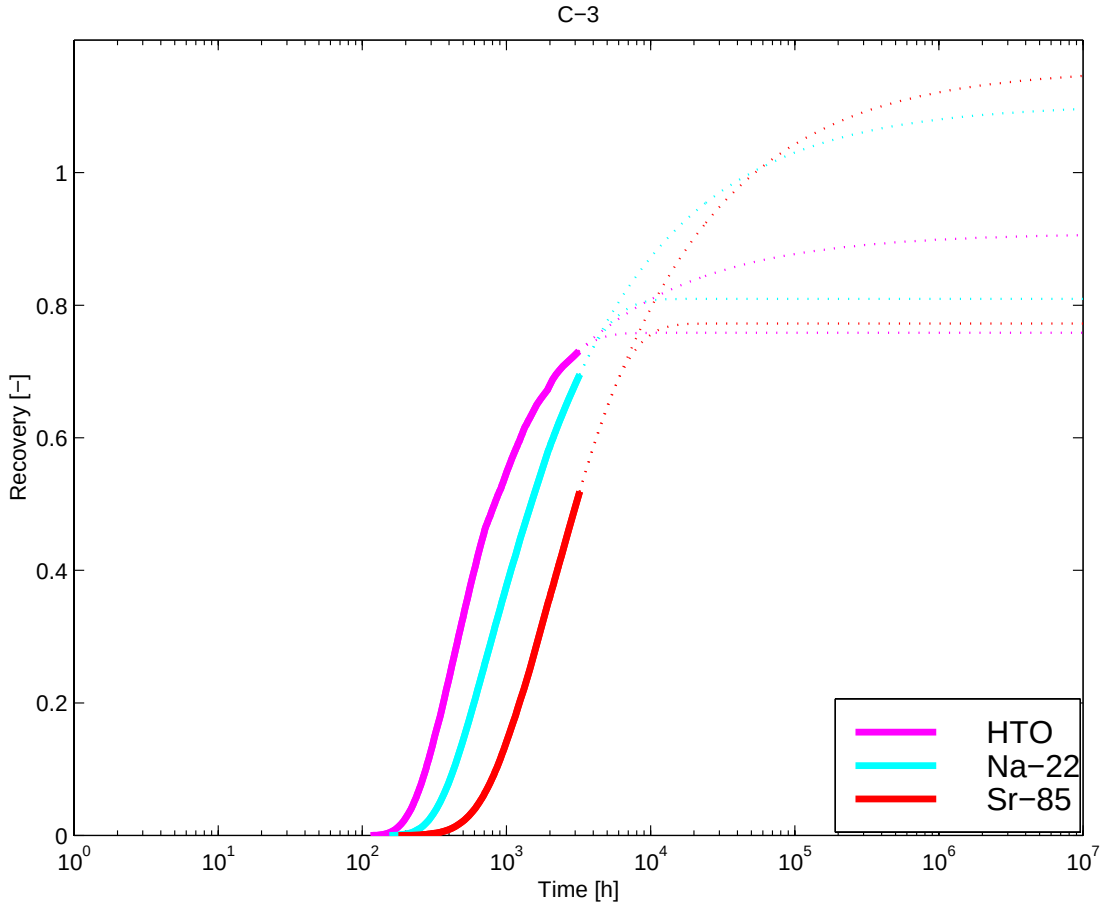

Figure 7-9. *Recoveries of the C3 test extrapolated from the measured breakthrough curves. Solid lines represent the measured recovery curve. Dotted lines are for the* $t^{-3/2}$*-extrapolation (upper lines) and exponential extrapolation (lower lines).*

8 Results of the evaluation

8.1 Simulated cases

Length, width and aperture of the channels determine the geometry of the transport channels. Channel lengths are calculated using in-plane distances of the TRUE Block Scale hydrostructural model (Hermanson and Doe, 2000). Channel length is the only geometry parameter that is selected before the modelling. The non-sorbing tracers breakthrough curves fix the volume of the transport channel and the matrix diffusion of the sorbing tracers for the fixed flow rates determine the width of the channel. Based on this, the uncertainty in the channel length and in the channel width is coupled. Clearly wrong path length should show unrealistic channel width. Apertures and widths of the channel follow from the evaluation. Channel apertures are calculated from the fitted U_t parameters (Equation (7-12)). The width of the channel is calculated using the fitted aperture, flow rate through the transport channel is calculated from the tracer injection curve and the flow velocity is fitted using (Equation (7-14)).

Velocity fields are calculated for four different alternatives. The alternatives have different correlation length of the velocity variation: 0.01 m, 0.02 m, 0.05 m and 0.1 m (cf. Table 7-2). The flow field parameters are calibrated using the breakthrough curves of the non-sorbing tracers. The correlation length has influence on the calibrated maximum flow velocity.

The different simulation cases are presented in Table 8-1. As it can be noted, it has been assumed that flow in the injection borehole section goes entirely through the transport channel to the sink.

Table 8-1. Simulated alternative flow fields in the Phase C tracer tests. Alternatives "recov. 1" refer to extrapolated final recovery using $t^{-3/2}$ tailing and alternatives "recov. 2" refer to exponential tailing, cf. Section 7.3.3.

Test	Flow rate [ml/h]	Max. flow velocity [m/h]	Channel Length [m]	Correlation length in the velocity profile [m]
C1, recov. 1	2700	2.76	16	0.01
C1, recov. 2	2700	2.73	16	0.01
C1, recov. 1	2700	1.67	16	0.02
C1, recov. 2	2700	1.67	16	0.02
C1, recov. 1	2700	1.67	16	0.05
C1, recov. 2	2700	1.67	16	0.05
C1, recov. 1	2700	1.67	16	0.1
C1, recov. 2	2700	1.67	16	0.1
C2, recov. 1	600	2.90	97	0.01
C2, recov. 2	600	2.30	97	0.01
C2, recov. 1	600	2.31	97	0.02
C2, recov. 2	600	1.93	97	0.02
C2, recov. 1	600	1.54	97	0.05
C2, recov. 2	600	1.40	97	0.05
C2, recov. 1	600	1.54	97	0.1
C2, recov. 2	600	1.30	97	0.1
C3, recov. 1	112	0.56	35	0.01
C3, recov. 2	112	0.52	35	0.01
C3, recov. 1	112	0.47	35	0.02
C3, recov. 2	112	0.44	35	0.02
C3, recov. 1	112	0.32	35	0.05
C3, recov. 2	112	0.31	35	0.05
C3, recov. 1	112	0.28	35	0.1
C3, recov. 2	112	0.26	35	0.1

8.2 Transport in the advective field of the channel

Influence of the selected channel geometry and velocity variation on the transport can be analysed using Equation (7-1). Molecular diffusion averages the tracer transit time distribution compared to the transit time distribution due to the velocity variation alone. The averaging is more profound for shorter correlation lengths of the velocity variation or lower flow velocity. Because of the diffusional averaging the breakthrough curve is symmetric if the velocity correlation length is short enough or the flow velocity is low enough. If the diffusion to the longitudinal direction is omitted the breakthrough curve gets narrower with shorter correlation length, eventually approaching plug flow. The opposite case is a very long correlation length or fast flow when the influence of the molecular diffusion disappears and the breakthrough curve is characterised by the underlying velocity field. A linear velocity profile leads to strongly skewed breakthrough curves as presented in Figure 7-5. This behaviour is characterised by the dimensionless parameter X that has been introduced in Equation (7-1) (Hautojärvi 1989)

$$X = \frac{D_w L}{a^2 v_0} \quad , \qquad (8\text{-}1)$$

where D_w is the molecular diffusion coefficient in water, L is the channel length, v_0 is the maximum flow velocity and a is the correlation length of the velocity variation. Values $X < 0.1$ represent advection dominated transport (Hautojärvi 1989). In the model these cases are replaced by purely advective transport. The selected range of the correlation lengths produces flow fields that are dominated both by the advection and advection-dispersion behaviour. The value of the parameter X and interpretation of the transport characteristics for different alternative models are presented Table 8-2.

Table 8-2. Characteristics of the flow field. Dimensionless parameter X describes the character of the transport. Cases X < 0.1 are characterised by purely advective transport. Alternatives "recov. 1" refer to extrapolated recovery using $t^{-3/2}$ tailing and "recov. 2" refer to exponential tailing.

Tracer test and recovery extrapolation	Path length [m]	Velocity correlation [m]	Maximum velocity [m/h]	X	Character of the transport in flow path
C1, recov. 1	16	0.01	2.76	0.21	Advection-dispersion
C1, recov. 2	16	0.01	2.73	0.21	Advection-dispersion
C1, recov. 1	16	0.02	1.67	0.086	Advection
C1, recov. 2	16	0.02	1.67	0.086	Advection
C1, recov. 1	16	0.05	1.67	0.014	Advection
C1, recov. 2	16	0.05	1.67	0.014	Advection
C1, recov. 1	16	0.1	1.67	0.0034	Advection
C1, recov. 2	16	0.1	1.67	0.0034	Advection
C2, recov. 1	97	0.01	2.90	1.20	Advection-dispersion
C2, recov. 2	97	0.01	2.30	1.52	Advection-dispersion
C2, recov. 1	97	0.02	2.31	0.38	Advection-dispersion
C2, recov. 2	97	0.02	1.93	0.45	Advection-dispersion
C2, recov. 1	97	0.05	1.54	0.091	Advection
C2, recov. 2	97	0.05	1.40	0.10	Advection
C2, recov. 1	97	0.1	1.54	0.023	Advection
C2, recov. 2	97	0.1	1.30	0.027	Advection
C3, recov. 1	35	0.01	0.56	2.25	Advection-dispersion
C3, recov. 2	35	0.01	0.52	2.42	Advection-dispersion
C3, recov. 1	35	0.02	0.47	0.67	Advection-dispersion
C3, recov. 2	35	0.02	0.44	0.72	Advection-dispersion
C3, recov. 1	35	0.05	0.32	0.16	Advection-dispersion
C3, recov. 2	35	0.05	0.31	0.16	Advection-dispersion
C3, recov. 1	35	0.1	0.28	0.045	Advection
C3, recov. 2	35	0.1	0.26	0.048	Advection

8.3 Surface sorption

The retardation coefficients that are caused by the surface sorption on the fracture surfaces have been estimated by scaling the time axis of the measured breakthrough curves (see Section 7.2.2). The breakthrough curves of non-sorbing tracers' have been left unchanged as reference breakthrough curves. In C1 test the reference tracer has been Br-82, in C2 and C3 Re-186 and HTO, respectively. Sorbing breakthrough curves have been transformed by scaling linearly the time axis until the first breakthrough time coincide with the first breakthrough time of the reference tracer (keeping the mass of the tracer unchanged). The inverse values of the resulting dimensionless scaling factors have been selected as the surface retardation factors.

Results of the scaling are presented in Figures 8-1 through 8-3. All breakthrough curves have been normalised to the unit mass to make the comparison easier. Estimated retardation coefficients are presented in Table 8-3. Table 8-3 includes also calculated surface sorption coefficient in the case of 1 mm aperture. The calculated sorption coefficients are clearly higher than the values reported Andersson et al. (2002b). This may indicate smaller aperture than 1 mm or different material on the fracture surface than investigated by Andersson et al. (2002b).

Table 8-3. Estimated retardation coefficients of the surface sorption. As an example the sorption coefficient are calculated for a 1 mm aperture.

Experiment	Tracer	Retardation coefficient, Ra	Aperture [mm]	Sorption coefficient [m]
C1	**Br-82**	1.0	1	0
C1	**Na-24**	1.05	1	5.00E-05
C1	**K-42**	1.3	1	3.00E-04
C1	**Ca-47**	1.4	1	4.00E-04
C1	**Rb-86**	3.0	1	2.00E-03
C1	**Cs-134**	16	1	1.50E-02
C2	**Re-186**	1.0	1	0
C2	**Ca-47**	2.4	1	1.40E-03
C3	**HTO**	1.0	1	0
C3	**Na-22**	1.3	1	3.00E-04
C3	**Sr-85**	1.5	1	5.00E-04

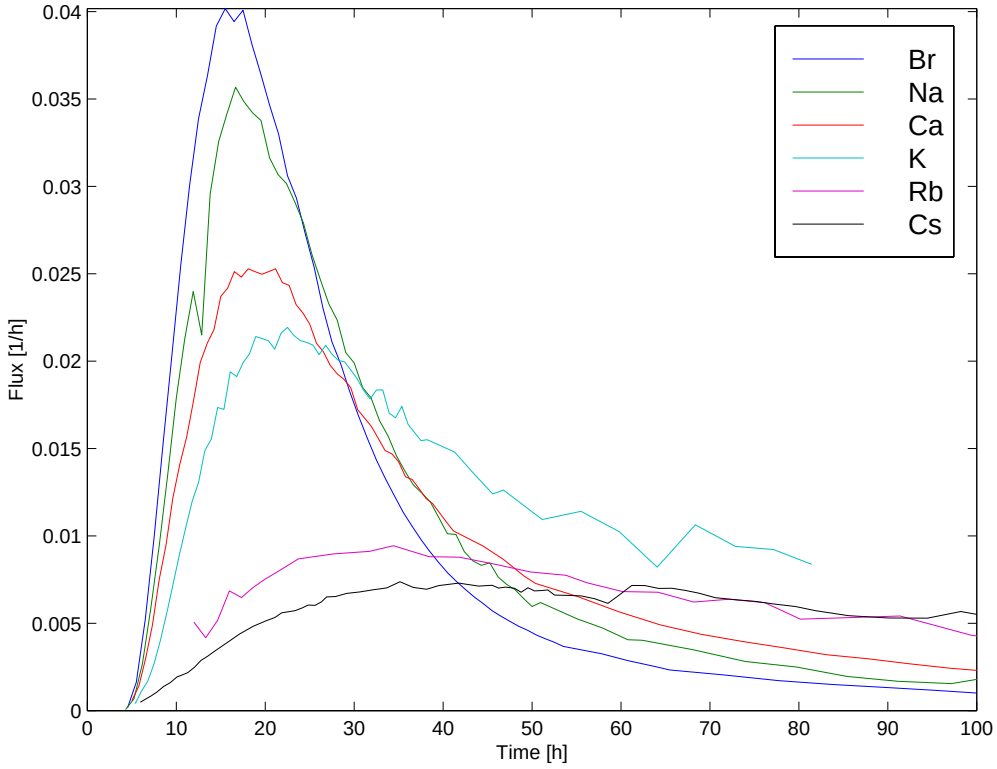

Figure 8-1. *Scaling of the C1 test breakthrough curves. Br-82 is the reference breakthrough (assumed to be closest to the ideal non-sorbing tracer) that is left unchanged. Scaling factors of the tracers are adjusted to give the same first breakthrough time as the reference breakthrough curve. All breakthrough curves are normalised to unit mass.*

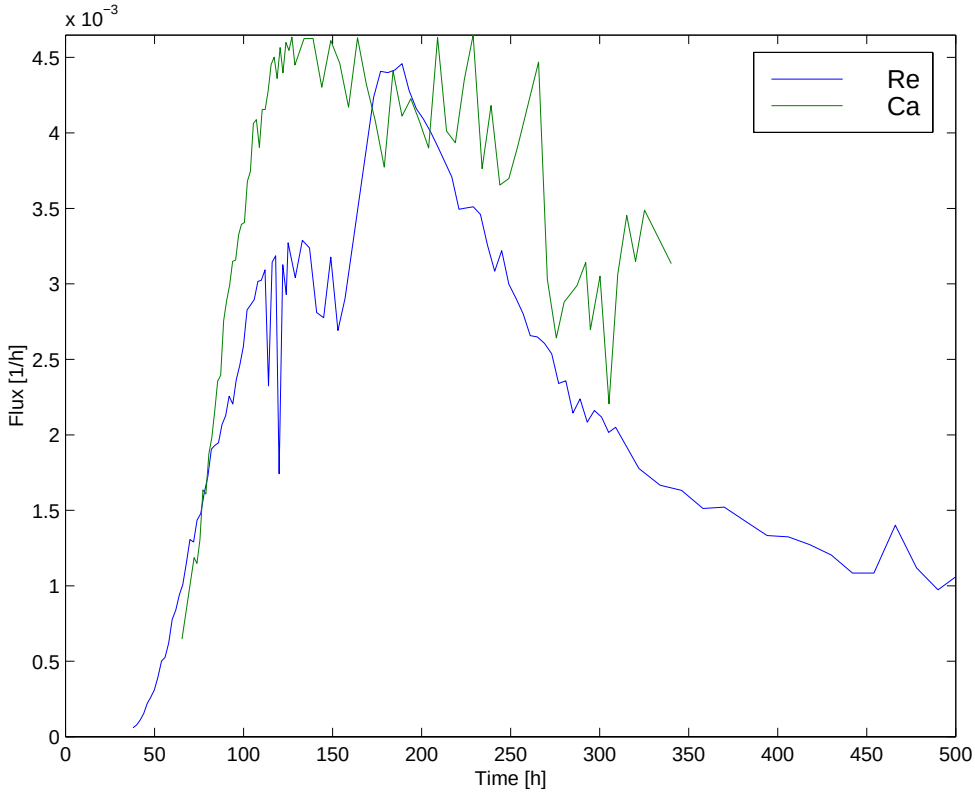

Figure 8-2. *Scaling of the C2 test breakthrough curves. Re-186 is the reference breakthrough that is left unchanged. Scaling factors of the tracers are adjusted to give the same first breakthrough time as the reference breakthrough curve. All breakthrough curves are normalised to unit mass.*

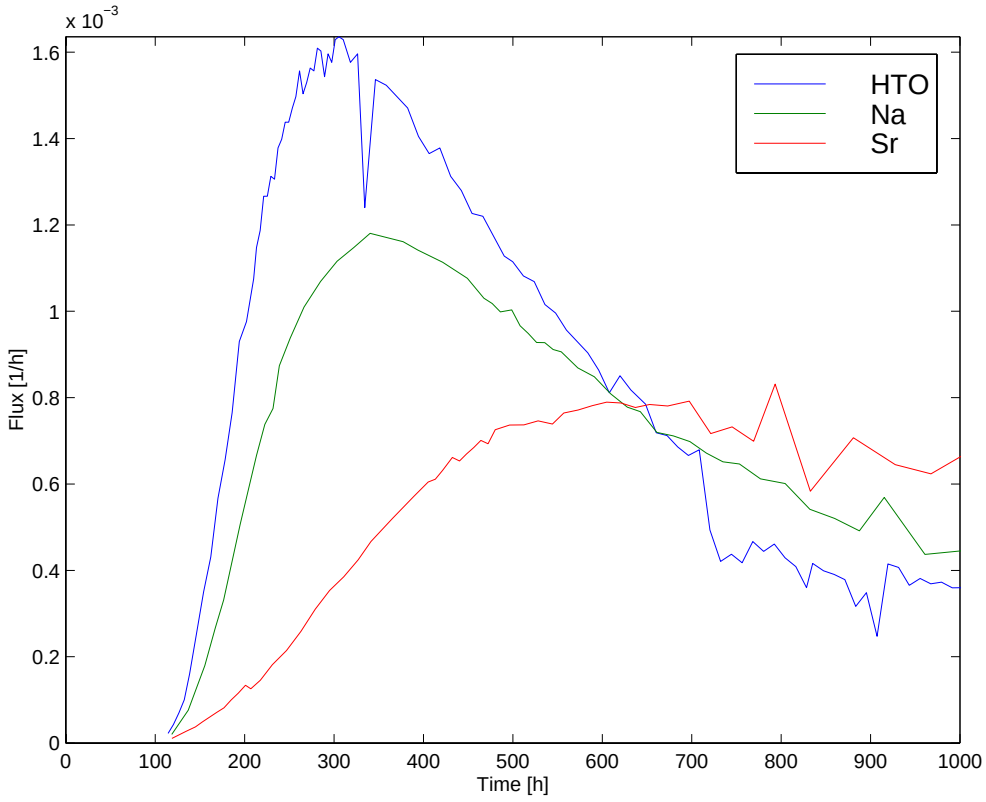

Figure 8-3. *Scaling of the C3 test breakthrough curves. HTO is the reference breakthrough that is left unchanged. Scaling factors of the tracers are adjusted to give the same first breakthrough time as the reference breakthrough curve. All breakthrough curves are normalised to unit mass.*

8.4 Matrix diffusion

Simulated breakthrough curves are calculated by applying Equations (7-4) and (7-5). By adjusting parameter group U_t (matrix diffusion) and R_a (surface sorption) the simulated breakthrough curves are fitted to the measured breakthrough curves. The surface sorption R_a has already been estimated (see Table 8-3). However, at this stage the curve fitting of the sorbing tracers is allowed to fine tune to the surface sorption too. In the fitting the retardation factors in Table 8-3 are used as a lower limit of the R_a. The matrix retention properties are evaluated by comparing the underlying physical retention parameters in the parameter group U_t (Equations (7-12) and (7-13)) to the corresponding laboratory measurements.

Each tracer test is simulated for 8 different cases. These are four different correlation lengths of the velocity profile (0.01 m, 0.02 m, 0.05 m and 0.1 m) and two alternatives of the extrapolated final recovery. Variation of the recovered mass is not expected to have significant influence on the matrix diffusion parameters. However, basically the outcome of the evaluation depends on the curve fitting to the measured breakthrough curves, which means that this kind of sensitivity study is useful.

The four different correlation lengths of the velocity profile cause the transport to cover both advective and advection-dispersion type transport behaviour (cf. Table 8-2). In many cases the measured breakthrough curve is characterised by a skewed long tailing. The advection-dispersion model alone cannot produce this kind of breakthrough curve. However, both matrix diffusion and the advective flow field can produce a breakthrough curve with long tailing, but in the model the advection dominated transport cause steeper rise of the breakthrough curve than it has been measured. It seems that advection alone can not explain the measured breakthrough curves.

8.4.1 Fitted breakthrough curve

Fitted breakthrough curves are presented in Figures 8-4 to 8-14. Simulations that are based on the final recoveries extrapolated using $t^{-3/2}$ tailing seem to give a little bit better fit. Exponential tailing leads to smaller recovered mass and correspondingly the fitted curves tend to be lower than the measured ones.

Fitted parameters U_t and R_a are presented in Appendix C in Tables C-1 to C-4. Fitted R_a does not vary as much as the matrix diffusion parameter U_t. Reason for this is that the estimated R_a values in Table 8-3 have been used as the lower limit of the R_a. In most of the cases this lower limit has also been reached. The parameter U_t varies mainly within a factor of two. Higher values of parameter U_t are obtained using shorter correlation length of the velocity variation. In those cases the advective flow field cause symmetric, advection-dispersion type, breakthrough curves because molecular diffusion can average the flow velocities over the short correlation length. The actual measured breakthrough curves are asymmetric with long tailing that can be, in these cases, produced only by increased matrix diffusion (parameter U_t). In the case of the larger correlation length the advective transport that causes asymmetric tailing is more dominating thus leading to a smaller strength of the matrix diffusion..

The higher recovery estimates ($t^{-3/2}$ tailing) seem to give consistently better fits for every test. In the C1 test the shape of the early breakthrough can be reproduced better by shorter correlation length. The C2 and C3 tests do not show that clear difference between the different correlation lengths of the velocity profile.

Table 8-4. Range of fitted retention parameters U_t and R_a for simulated breakthrough curves using four different alternatives for the velocity correlation length in the channel and two different alternatives for the extrapolation of the final recovery. In total, results are based on eight alternative simulations for each tracer and test.

		U_t [$h^{-1/2}$]		R_a	
Test		**Min**	**Max**	**Min**	**Max**
	Tracer				
C1	**Br-82**	0.05	0.08	1.00	1.01
C1	**Na-24**	0.08	0.16	1.05	1.21
C1	**K-42**	0.17	0.23	1.30	1.31
C1	**Ca-47**	0.27	0.39	1.40	1.40
C1	**Rb-86**	0.55	0.89	3.00	3.52
C1	**Cs-134**	1.60	2.46	16.00	20.09
C2	**Re-186**	0.05	0.13	1.00	1.00
C2	**Ca-47**	0.10	0.25	2.40	2.40
C3	**HTO**	0.03	0.09	1.00	1.00
C3	**Na-22**	0.06	0.14	1.30	1.34
C3	**Sr-85**	0.09	0.24	1.50	3.40

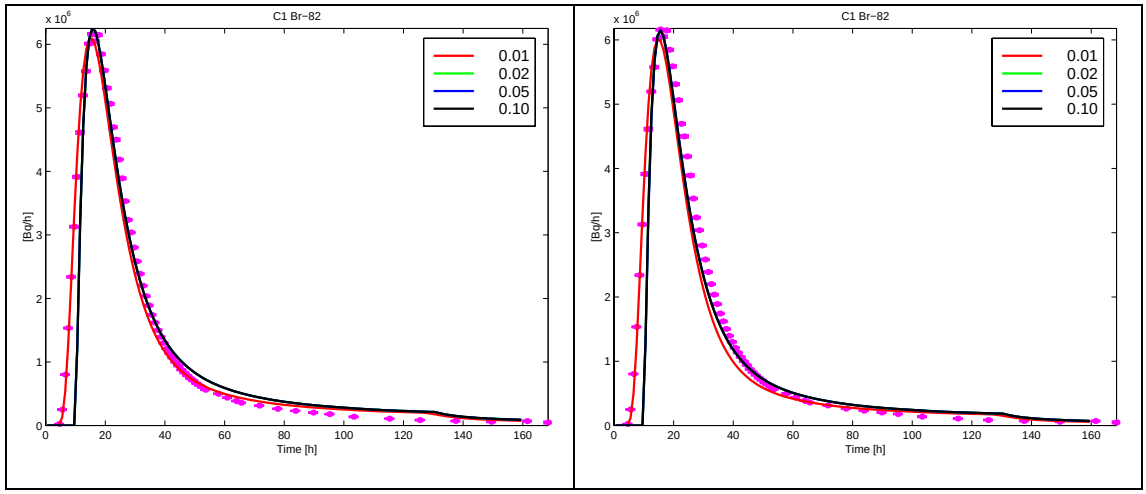

Figure 8-4. *Fitted breakthrough curves for Br-82 in C1. Results for the extrapolation of the final recovery by using $t^{-3/2}$ tailing (left) and exponential tailing (right). Blue dots and bars indicate measured breakthrough and the given uncertainty region of the measurement. Coloured lines represent fitted breakthrough curves for different correlation lengths of the velocity profile. In both figures curves for the 0.02, 0.05 and 0.1 m correlation lengths overlap.*

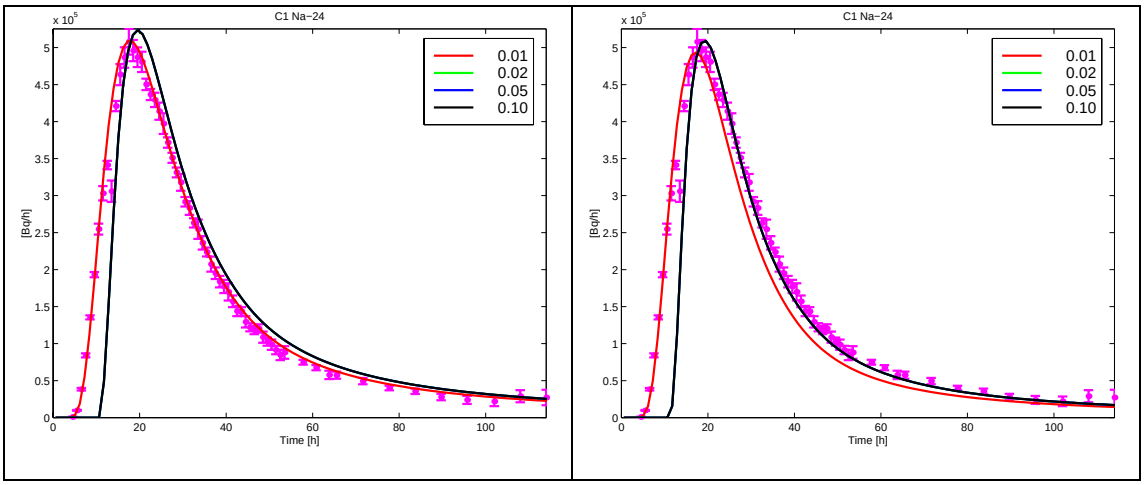

Figure 8-5. *Fitted breakthrough curves for Na-24 in C1. Results for the extrapolation of the final recovery by using $t^{-3/2}$ tailing (left) and exponential tailing (right). Blue dots and bars indicate measured breakthrough and the given uncertainty region of the measurement. Coloured lines represent fitted breakthrough curves for different correlation lengths of the velocity profile. In both figures curves for the 0.02, 0.05 and 0.1 m correlation lengths overlap.*

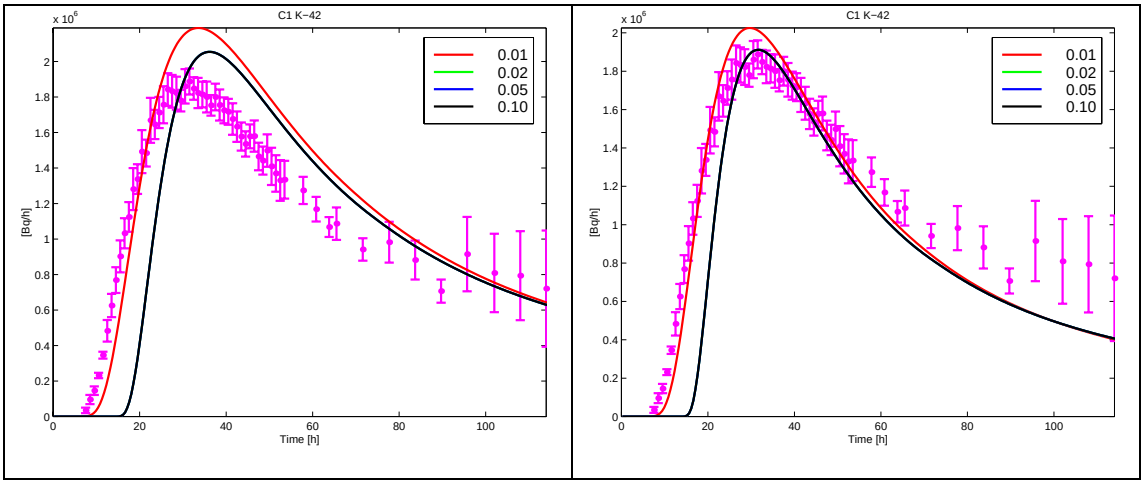

Figure 8-6. *Fitted breakthrough curves for K-42 in C1. Results for the extrapolation of the final recovery by using $t^{-3/2}$ tailing (left) and exponential tailing (right). Blue dots and bars indicate measured breakthrough and the given uncertainty region of the measurement. Coloured lines represent fitted breakthrough curves for different correlation lengths of the velocity profile. In both figures curves for the 0.02, 0.05 and 0.1 m correlation lengths overlap.*

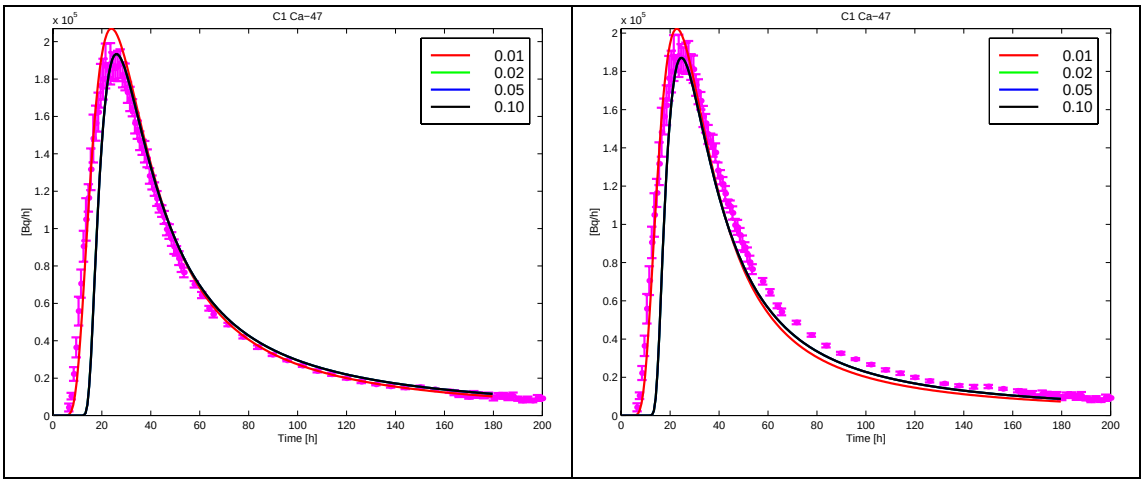

Figure 8-7. *Fitted breakthrough curves for Ca-47 in C1. Results for the extrapolation of the final recovery by using $t^{-3/2}$ tailing (left) and exponential tailing (right). Blue dots and bars indicate measured breakthrough and the given uncertainty region of the measurement. Coloured lines represent fitted breakthrough curves for different correlation lengths of the velocity profile. In both figures curves for the 0.02, 0.05 and 0.1 m correlation lengths overlap.*

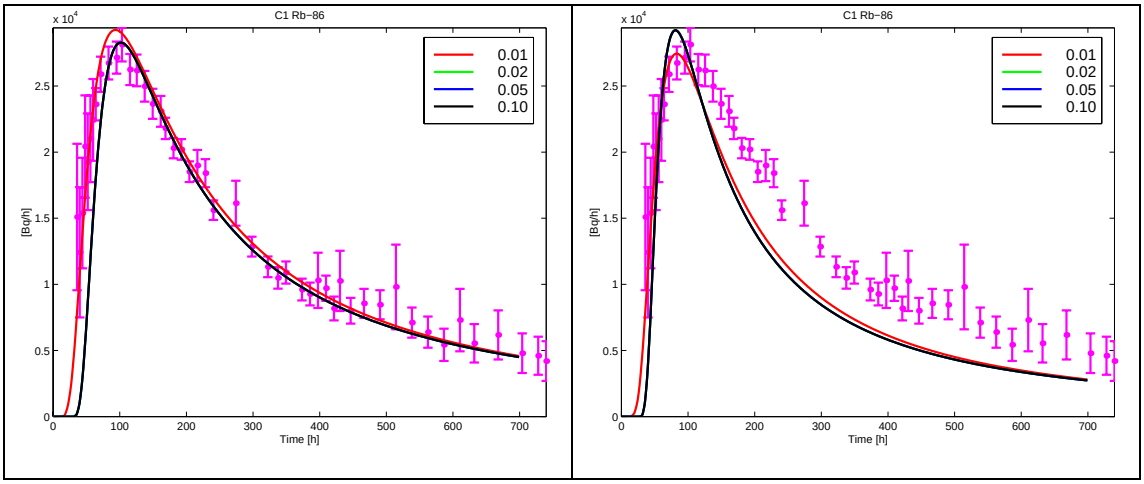

Figure 8-8. *Fitted breakthrough curves for Rb-86 in C1. Results for the extrapolation of the final recovery by using $t^{-3/2}$ tailing (left) and exponential tailing (right). Blue dots and bars indicate measured breakthrough and the given uncertainty region of the measurement. Coloured lines represent fitted breakthrough curves for different correlation lengths of the velocity profile. In both figures curves for the 0.02, 0.05 and 0.1 m correlation lengths overlap.*

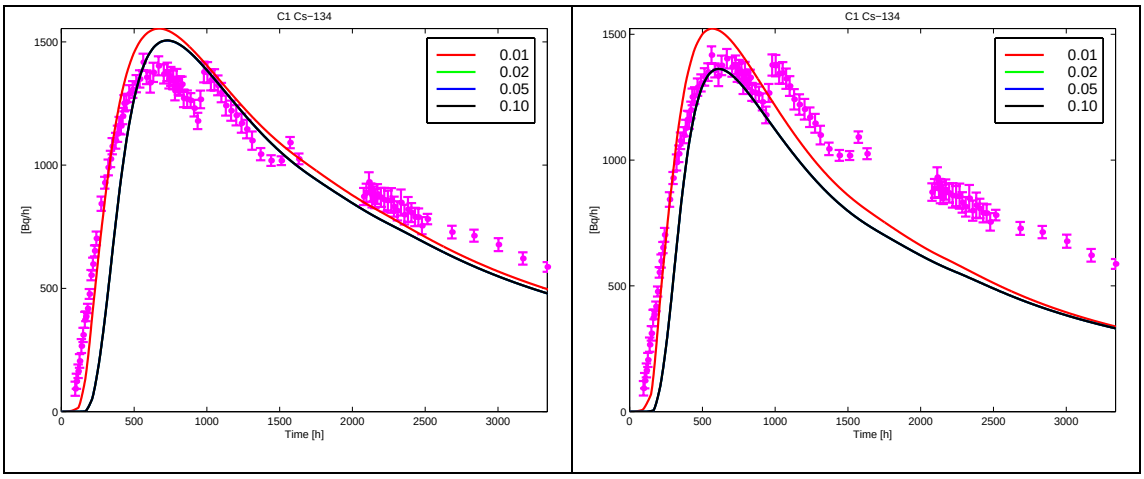

Figure 8-9. *Fitted breakthrough curves for Cs-134 in C1. Results for the extrapolation of the final recovery by using $t^{-3/2}$ tailing (left) and exponential tailing (right). Blue dots and bars indicate measured breakthrough and the given uncertainty region of the measurement. Coloured lines represent fitted breakthrough curves for different correlation lengths of the velocity profile. In both figures curves for the 0.02, 0.05 and 0.1 m correlation lengths overlap.*

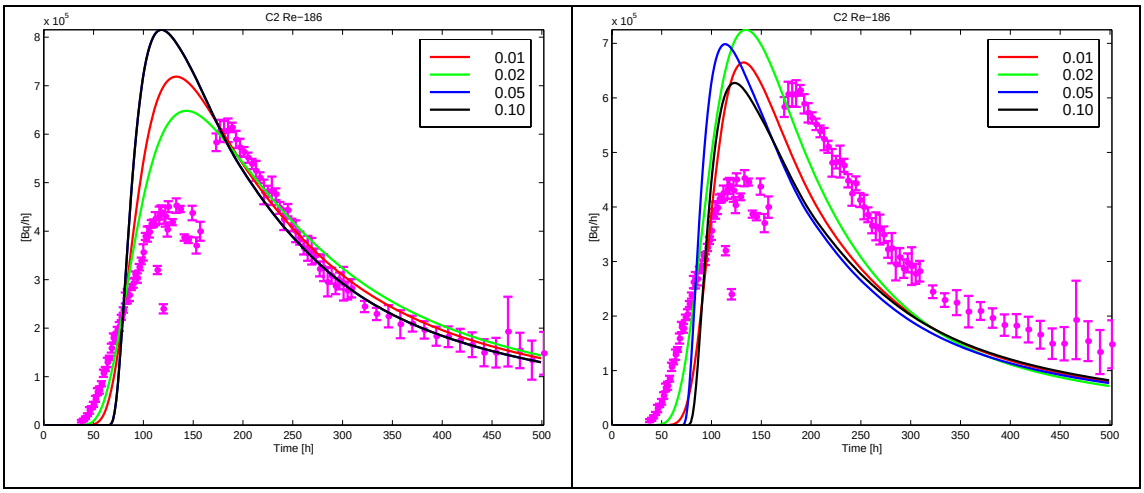

Figure 8-10*. Fitted breakthrough curves for Re-186 in C2. Results for the extrapolation of the final recovery by using $t^{-3/2}$ tailing (left) and exponential tailing (right). Blue dots and bars indicate measured breakthrough and the given uncertainty region of the measurement. Coloured lines represent fitted breakthrough curves for different correlation lengths of the velocity profile. In left figure curves for the 0.05 and 0.1 m correlation lengths overlap.*

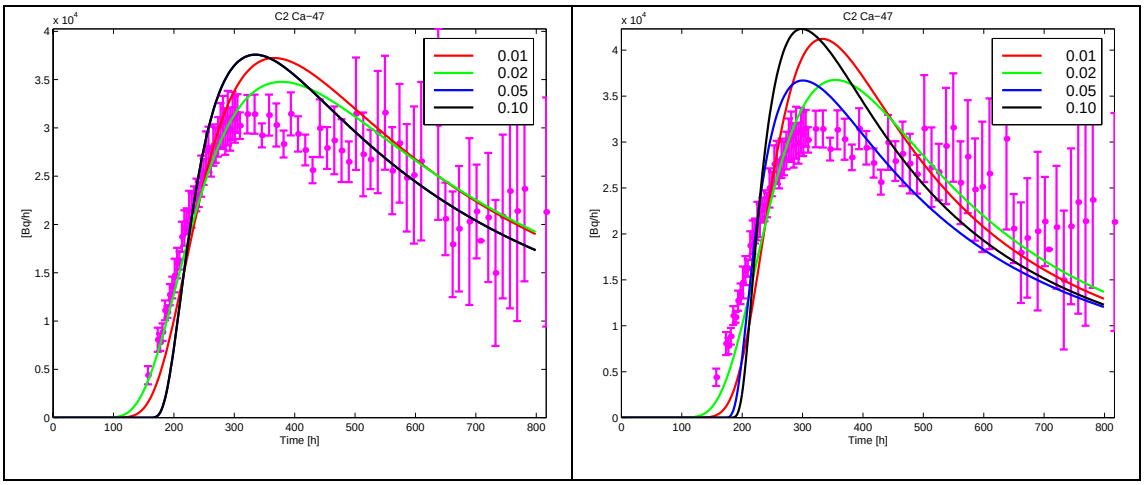

***Figure 8-11**. Fitted breakthrough curves for Ca-47 in C2. Results for the extrapolation of the final recovery by using $t^{-3/2}$ tailing (left) and exponential tailing (right). Blue dots and bars indicate measured breakthrough and the given uncertainty region of the measurement. Coloured lines represent fitted breakthrough curves for different correlation lengths of the velocity profile. In left figure curves for the 0.05 and 0.1 m correlation lengths overlap.*

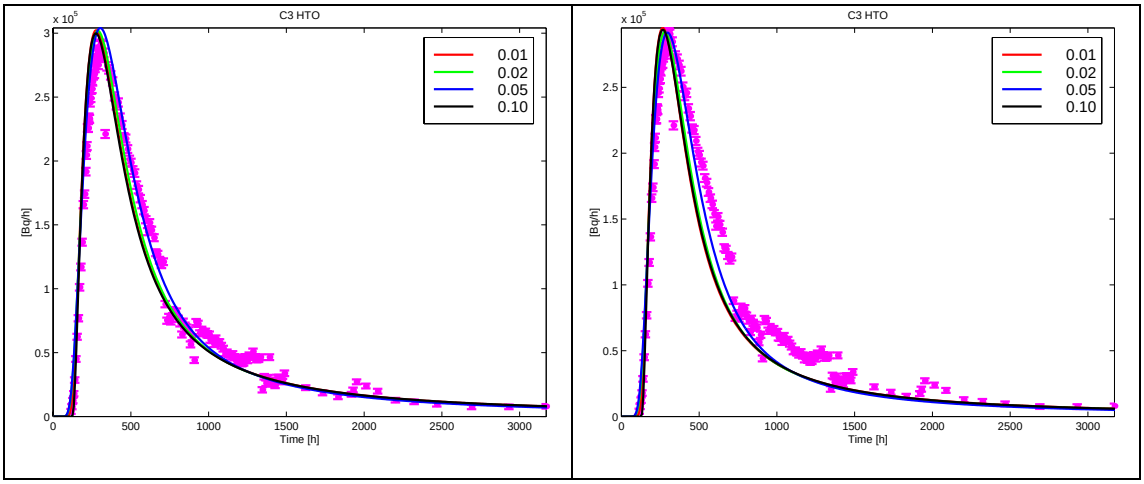

***Figure 8-12.** Fitted breakthrough curves for HTO in C3. Results for the extrapolation of the final recovery by using $t^{-3/2}$ tailing (left) and exponential tailing (right). Blue dots and bars indicate measured breakthrough and the given uncertainty region of the measurement. Coloured lines represent fitted breakthrough curves for different correlation lengths of the velocity profile. In left figure curves for the 0.02, 0.05 and 0.1 m correlation lengths overlap.*

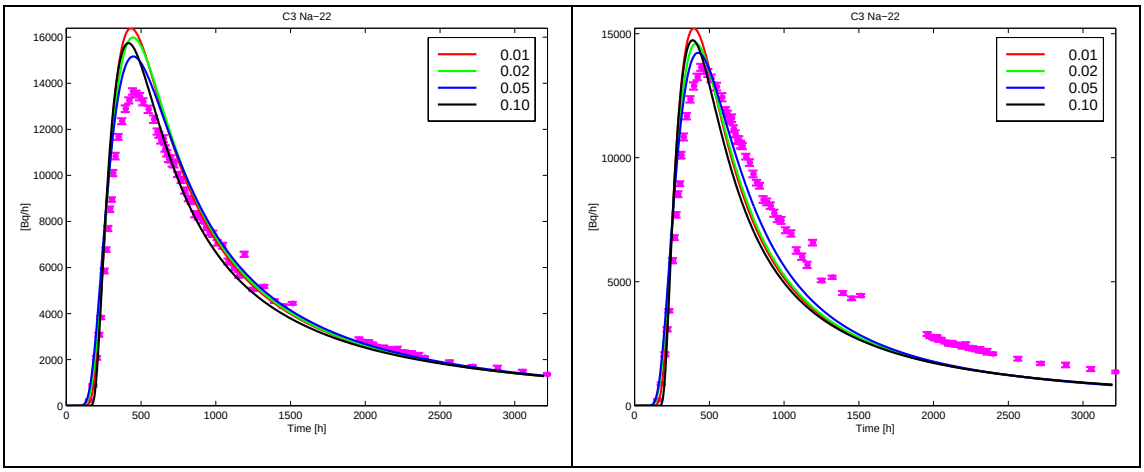

Figure 8-13. *Fitted breakthrough curves for Na-22 in C3. Results for the extrapolation of the final recovery by using $t^{-3/2}$ tailing (left) and exponential tailing (right). Blue dots and bars indicate measured breakthrough and the given uncertainty region of the measurement. Coloured lines represent fitted breakthrough curves for different correlation lengths of the velocity profile.*

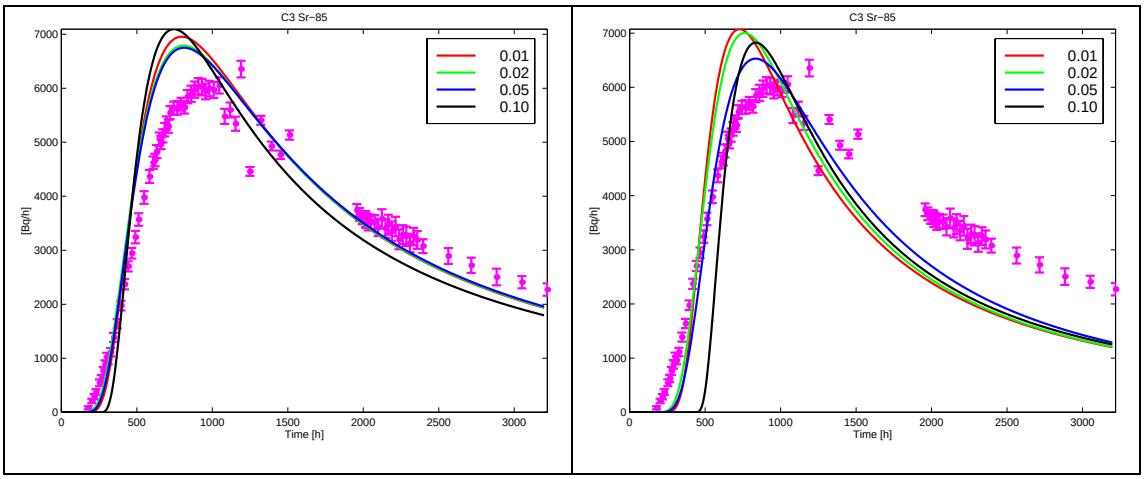

Figure 8-14*. Fitted breakthrough curves for Sr-85 in C3. Results for the extrapolation of the final recovery by using $t^{-3/2}$ tailing (left) and exponential tailing (right). Blue dots and bars indicate measured breakthrough and the given uncertainty region of the measurement. Coloured lines represent fitted breakthrough curves for different correlation lengths of the velocity profile.*

8.4.2 Rock matrix

First, an attempt was made to explain the measured breakthrough curves by diffusion into the rock matrix. Laboratory data of the sorption and porosity properties in the rock matrix is available (altered and unaltered Äspö diorite, Byegård et. al., 1998). The laboratory data was used to narrow down the variability of the evaluated sorption properties along the transport paths. In practice, the laboratory data was applied as upper limit of the K_d and porosity values (see Table 7-1).

Transport of the tracers is modelled using Equations (7-4) and (7-12). This means that transport is parametrised by U_t and R_a (given in Appendix C, Tables C-1 to C-4). This part of the evaluation has not been carried out for all eight alternative cases. Retention parameters have been calculated only for the better fitting alternative of the extrapolated final recovery ($t^{-3/2}$ tailing, alternative 1 in the tables). Results of the interpretation are presented in Table 8-5. As can be seen the K_d, porosity and geometric factor reach the upper limit that was allowed for them in the evaluation. In addition, a quite small aperture is required to reproduce the observed retention. The flow rate through the channel is fixed which means that a small aperture leads to a wide channel.

Reasonableness of the diffusion to the rock matrix to explain the observed retention is judged based on the required channel geometry. The approach is to accumulate the uncertainty in the grouped retention parameter U_t to the flow field part of the parameter. It is here noted that the flow field part of the retention parameter cannot be constrained by using independent data, because there is information on the flow field only at the injection and pumping locations. What happens between these locations can be seen only in the tracer retention that we try to explain. The channel geometry is parametrised by the effective width of the transport channel. The evaluation show that if the whole observed retention is assigned to the diffusion into the rock matrix then in a single channel model the width will be unrealistic large, almost in the same order of magnitude as the transport distance. It therefore seems unrealistic that the observed retention has been caused by diffusion to the rock matrix alone.

Table 8-5. Retention parameters in the case of diffusion into the pore space of the rock matrix. The correlation length of the velocity field is denoted by a_v, the calculated retention parameter of the rock matrix is U_{tr} and the retention parameter fitted to the measured breakthrough curve is U_{tf}.

Test Tracer	K_d [m^3/kg]	Channel characteristics flow rate [ml/h]	v_0 [m/h]	Aperture [m]	width [m]	a_v [m]	U_{tr} [$h^{-1/2}$]	U_{tf} [$h^{-1/2}$]
C1, Br-82	0	2700	1.67	6.50E-05	49.64	0.02	0.023	0.0600
C1, Na-24	6.00E-05	2700	1.67	6.50E-05	49.64	0.02	0.120	0.1149
C1, Ca-47	1.45E-04	2700	1.67	6.50E-05	49.64	0.02	0.185	0.1990
C1, K-42	4.00E-04	2700	1.67	6.50E-05	49.64	0.02	0.306	0.3351
C1, Rb-86	2.00E-03	2700	1.67	6.50E-05	49.64	0.02	0.683	0.7071
C1, Cs-134	1.52E-02	2700	1.67	6.50E-05	49.64	0.02	1.883	1.8407
C2, Re-186	0	600	1.54	7.30E-05	10.70	0.05	0.020	0.0738
C2, Ca-47	1.45E-04	600	1.54	7.30E-05	10.70	0.05	0.165	0.1652
C3, HTO	0	112	0.32	1.07E-04	6.50	0.05	0.014	0.0387
C3, Na-22	6.00E-05	112	0.32	1.07E-04	6.50	0.05	0.073	0.0727
C3, Sr-85	1.80E-04	112	0.32	1.07E-04	6.50	0.05	0.125	0.1251

8.4.3 Fault gouge

There has been found fault gouge in the structures of the TRUE Block Scale site (Andersson et al., 2002b). It is possible that the flow paths examined in the Phase C tracer tests contain also fault gouge. This means that diffusion to the pore space of the fault gouge is also a possible retention mechanism for the tracer particles. Estimates on the K_d and porosity of the gouge material at the Äspö Hard Rock Laboratory exists (see Table 7-1). As in the case of the rock matrix the data measured in the laboratory has been used as upper limit of the porosity and K_d values.

Transport of the tracers is modelled using Equations (7-4) and (7-12). This means that transport is parametrised by U_t and R_a (given in Appendix C, Tables C-1 to C-4). In the fault gouge case the fitted parameters are interpreted by assuming that matrix diffusion takes place to fault gouge. The interpretation has not been carried out for all alternative parameter U_t values but only for the alternative of the higher recovery ($t^{-3/2}$ tailing, alternative 1 in the tables). Results of the interpretation are presented in Table 8-6. As in the case of the rock matrix the K_d, porosity and geometric factor of the pore diffusivity reach the upper limit that was set for them based on the data in Table 7-1.

Similar behaviour as in the case of the diffusion to the rock matrix has been observed. It is not possible to fit the entire set of the tracers equally well. It is possible to get the sorbing tracers behave quite consistently, but then the non-sorbing tracers do not show enough mass transfer to the pore space of the fault gouge (i.e. the U_{tf} fitted to the breakthrough curve is larger than the U_{tg} that is calculated from the selected parameters).

The channel width required to produce the observed retention is for the case of the fault gouge much more reasonable than in case of retention mainly attributed to the rock matrix. In the C1 test, where the flow rate is the highest, the channel need to be about 4 m wide and should be about 1 m for C2 and C3. Based on the evaluated channel geometry it seems more reasonable that the observed retention is mainly a result of the diffusion to the fault gouge than to the rock matrix. At least, this may explain the retention of the sorbing tracers, but some additional pieces of explanation should be sought for the non-sorbing tracers.

It is noted that the diffusion to the pore space of the fault gouge is evaluated using a model that is based on infinite depth of the immobile pore space. In the case of the fault gouge the laboratory data is based on the results of very small particle size (less than 0.125 mm). The small particle size data gave stronger retention, but it is questionable whether the laboratory data is representative for the case evaluated and to what extent the applied approach is applicable. It is possible that the smallest fault gouge particles get saturated by the tracer, which means that it is not possible to estimate the retention capacity in them using matrix diffusion model but rather using equilibrium sorption.

Table 8-6. Retention parameters in the case of diffusion to the pore space of the fault gouge that are less than 0.125 mm in diameter. The correlation length of the velocity field is denoted by a_v, the calculated retention parameter of the fault gouge is U_{tg} and the retention parameter fitted to the measured breakthrough curve is U_{tf}.

Test	K_d	Channel characteristics				a_v	U_{tg}	U_{tf}
Tracer	[m^3/kg]	flow rate [ml/h]	v_0 [m/h]	Aperture [m]	width [m]	[m]	[h$^{-1/2}$]	[h$^{-1/2}$]
C1, Br-82	0	2700	1.67	6.20E-04	5.20	0.02	0.012	0.0600
C1, Na-24	2.20E-04	2700	1.67	6.20E-04	5.20	0.02	0.054	0.1149
C1, Ca-47	1.30E-03	2700	1.67	6.20E-04	5.20	0.02	0.128	0.1990
C1, K-42	5.20E-03	2700	1.67	6.20E-04	5.20	0.02	0.255	0.3351
C1, Rb-86	2.80E-02	2700	1.67	6.20E-04	5.20	0.02	0.592	0.7071
C1, Cs-134	2.80E-01	2700	1.67	6.20E-04	5.20	0.02	1.872	1.8407
C2, Re-186	0	600	1.54	4.80E-04	1.63	0.05	0.015	0.0738
C2, Ca-47	1.30E-03	600	1.54	4.80E-04	1.63	0.05	0.165	0.1652
C3, HTO	0	112	0.32	4.50E-04	1.54	0.05	0.016	0.0387
C3, Na-22	2.20E-04	112	0.32	4.50E-04	1.54	0.05	0.074	0.0727
C3, Sr-85	6.50E-04	112	0.32	4.50E-04	1.54	0.05	0.125	0.1251

8.4.4 Stagnant zones

Diffusion to the stagnant zones, cf. Section 7.3.1, was examined mainly because the non-sorbing tracers showed too low retention for diffusion to the fault gouge or rock matrix. The approach is the same that was applied in the case of the rock matrix and fault gouge. As in the case of the rock matrix and fault gouge the values of the retention parameter U_t are now explained by diffusion to the stagnant zones are given in Appendix C (Tables C-1 to C-4). The difference compared to the fault gouge and rock matrix cases is that diffusion does not take place in the direction of the fracture aperture but laterally in the fracture plane from the flow channel. This means that the fracture geometry, i.e. aperture, should be predetermined. Stagnant zone calculations are based on the aperture estimates of the fault gouge case.

The porosity constraint for the stagnant zone is arbitrary selected to be 50%. This means that on the average stagnant zone is available half of the length of the flow path. The retention parameter for the stagnant zone case is presented in Equation (7-13). All other parameters than the mean lateral distance between the stagnant zones ($2a_s$) are fixed (ε_s=0.5, D_w=10^{-9} m^2/s, R_a fitted c.f. Appendix C).

The stagnant water case appears to be quite consistent with the modelling resulting from variable velocity correlation lengths. This model also gives the required addition to the retention of the non-sorbing tracers but at the same time keeps the contribution to the retention of the sorbing tracers at a reasonable low level so that fault gouge and stagnant zone cases jointly (i.e. U_{tg}+U_{ts} in Tables 8-6 and 8-7) may explain the observed retention. However, as in the case of the fault gouge the dimension of the stagnant zones may cause problem in some cases. The calculations are based on the unproven assumption that the stagnant zones do not get saturated.

Table 8-7. Retention parameters in the case of diffusion to the stagnant zones. Correlation length of the velocity field is denoted by a_v, calculated mean lateral distance between stagnant zones in the fracture is a_s, calculated retention parameter of the stagnant zones is U_{ts} and retention parameter that is fitted to the measured breakthrough curve is U_{tf}.

Test Tracer	R_a [-]	Channel characteristics flow rate v_0 [ml/h]	[m/h]	Aperture [m]	a_s [m]	a_v [m]	U_{ts} [$h^{-1/2}$]	U_{tf} [$h^{-1/2}$]
C1, Br-82	1.00	2700	1.67	6.20E-04	0.0245	0.02	0.055	0.0600
C1, Na-24	1.12	2700	1.67	6.20E-04	0.0245	0.02	0.058	0.1149
C1, Ca-47	1.30	2700	1.67	6.20E-04	0.0245	0.02	0.062	0.1990
C1, K-42	1.40	2700	1.67	6.20E-04	0.0245	0.02	0.065	0.3351
C1, Rb-86	3.00	2700	1.67	6.20E-04	0.0245	0.02	0.095	0.7071
C1, Cs-134	16.05	2700	1.67	6.20E-04	0.0245	0.02	0.219	1.8407
C2, Re-186	1.00	600	1.54	4.80E-04	0.028	0.05	0.048	0.0738
C2, Ca-47	2.40	600	1.54	4.80E-04	0.028	0.05	0.074	0.1652
C3, HTO	1.00	112	0.32	4.50E-04	0.055	0.05	0.024	0.0387
C3, Na-22	1.30	112	0.32	4.50E-04	0.055	0.05	0.028	0.0727
C3, Sr-85	2.09	112	0.32	4.50E-04	0.055	0.05	0.035	0.1251

8.5 Integrated retention model of the Phase C tracer tests

An integrated retention model infers collection of the transport properties due to the advection, advection-dispersion and diffusion to the immobile pore space. The aim is to build models of the C1, C2 and C3 flow paths that can explain the observed retention and at the same time give concrete and consistent picture of the flow paths and main retention processes. The approach is to take the results from Sections 8.3 and 8.4 and build models of the respective transport channels by starting from the flow field and then taking into account the joint effects of surface sorption and diffusion to the immobile pore space and sorption in the immobile pore space.

8.5.1 Flow field

The tracer residence time distribution in the advective flow field is affected also by the molecular diffusion that averages out the variability of the groundwater transit times. How effective the averaging is depends on the correlation length of the velocity field. If the time required for diffusive mixing over the correlation length is clearly smaller than the mean transit time, then the detailed features of the flow field are explained the mean behaviour.

Tracer tests C1, C2 and C3 have been evaluated using different correlation lengths of the velocity variation. The calculated cases cover both purely advective transport and by the molecular diffusion averaged advection-dispersion type transport. Examination of the non-sorbing tracer transport show that in the case of the C1 test the simple advective field used in the modelling cannot explain the breakthrough curve, especially at the early times. Shortening of the correlation length gives a better fit. The conclusion is that the correlation length of the velocity field along the flow path tested by the C1 test is in the order of centimetres. A similar conclusion can also be drawn from the non-sorbing breakthrough curves of the C2 and C3 tests. It is clear that the correlation length cannot be in the decimetre scale in any of the tests.

A conceptual illustration of the flow field is presented in Figure 8-15. Diffusion of the non-sorbing tracers to the rock matrix or fault gouge has been found to be a secondary retention process for the non-sorbing tracers. This means that using non-sorbing tracer data it is not possible for the estimation of the geometry of the flow channel (aperture and width). However, the volume of the flow channel is constrained by the non-sorbing breakthrough times if the velocity field and the flow rate through the channel are fixed (cf. Equation (7-14)).

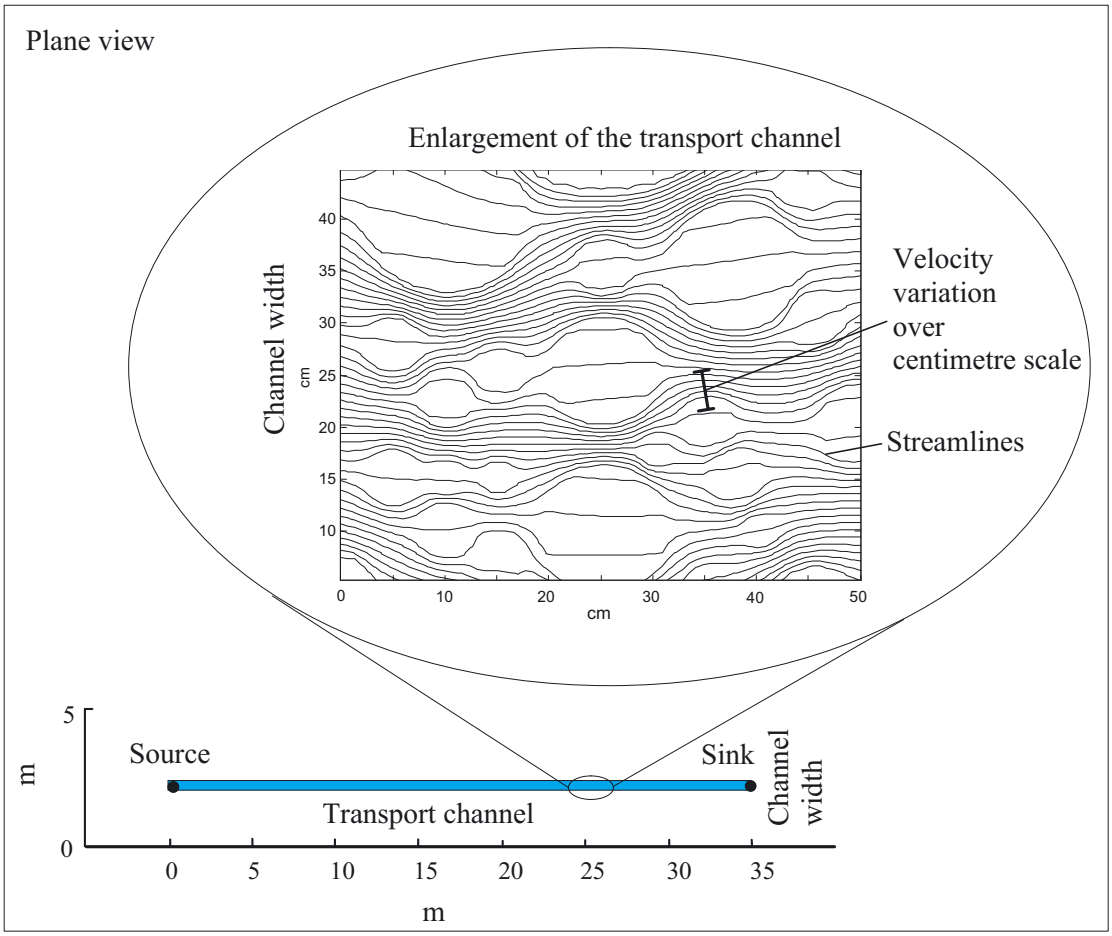

Figure 8-15. *Conceptual illustration of the advective flow field in the transport channels. This conceptualisation is based on the evaluations of the non-sorbing tracer breakthrough data.*

The advective flow field and molecular diffusion between streamlines alone cannot explain the measured breakthrough curves. Best-fit breakthrough curves with and without diffusion to the immobile zones were calculated to test this hypothesis. In Figure 8-16 are presented the best-fit breakthrough curves for the case of flow field only and the case where both flow field and diffusion to the immobile zone are taken into account.

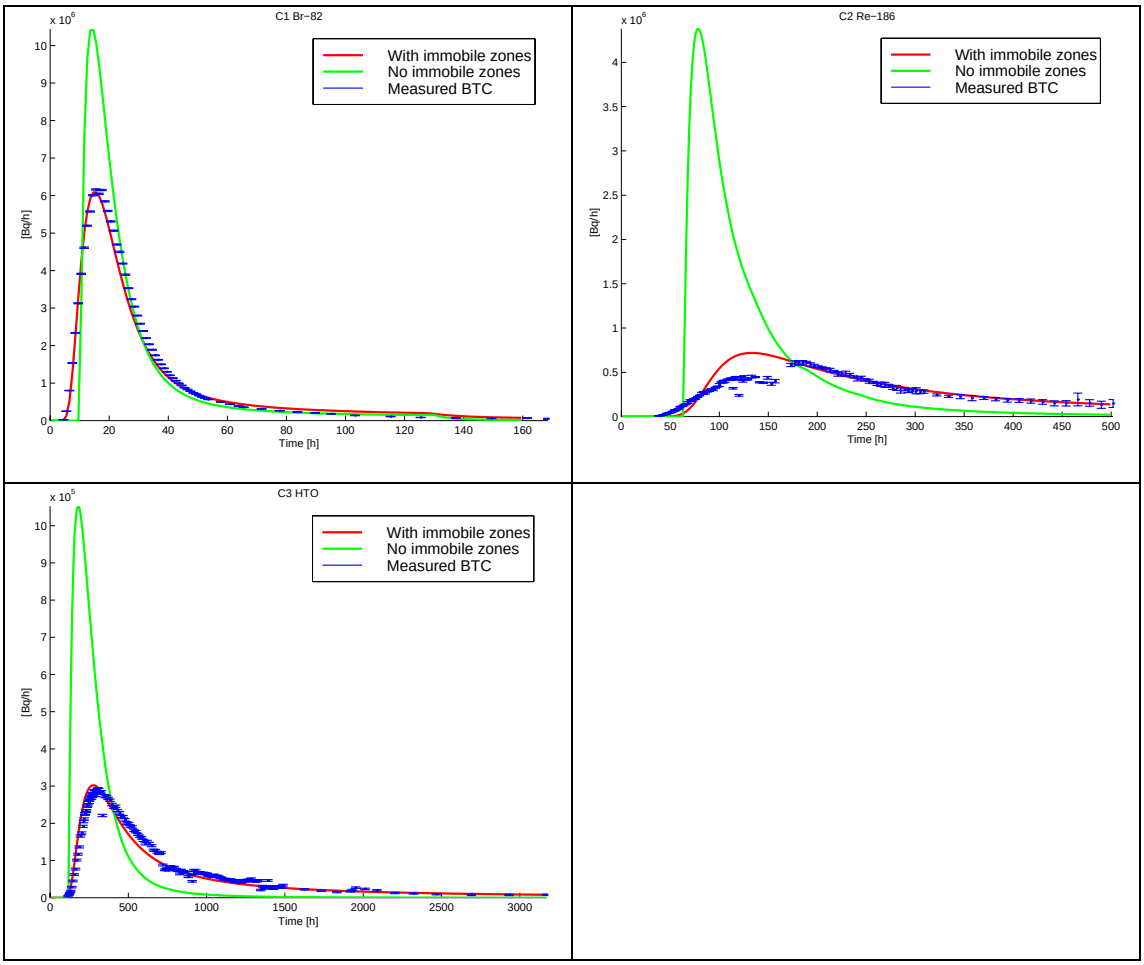

Figure 8-16. *Non-sorbing tracer breakthrough curves with and without diffusion to the immobile zones.*

Clearly the case with diffusion to the immobile zones gives better fit. The evaluation showed that for a non-sorbing tracer diffusion to the rock matrix or fault gouge were not able to produce enough matrix diffusion. This means that diffusion to the stagnant zones of the flow field should also probably be important for the non-sorbing tracers.

8.5.2 Surface sorption

The measured breakthrough curves cannot be explained by the present modelling approach using the flow field and surface sorption alone. This becomes clear from the modelling results of the non-sorbing tracers. It is shown in the Section 8.3 that if the surface sorption is the only retardation mechanism then scaling of the time axis of the sorbing tracer will give the non-sorbing breakthrough curve. This cannot be done for the measured breakthrough curves (see Figures 8-1 to 8-3).

Although surface sorption alone cannot explain the retardation it is still an important part of the overall retention. In the present modelling approach the overall retention is assumed to follow from both surface sorption and matrix diffusion but in practice the division of the overall retention to matrix diffusion and surface sorption cannot be done uniquely. It is possible to get reasonable fits without surface sorption or using very moderate surface sorption but in that case the estimated matrix diffusion parameters show excessively strong matrix diffusion. Then, it is difficult to explain matrix diffusion parameters using e.g. laboratory data of the sorption and porosity properties.

The conclusion from the modelling is that there is surface sorption along the flow paths correlates well with available laboratory data on sorption.

8.5.3 Rock matrix

The analysis in Section 8.4.2 showed that it is quite unlikely that diffusion into rock matrix have caused the observed retention. The strength of the matrix diffusion is determined by a grouped parameter that depends on the flow field and matrix properties. Taking matrix properties from the laboratory measurements means that the retention is fitted using flow field properties, in practice geometry of the flow path. In order to have enough retention due to the diffusion to rock matrix the apertures of the flow channels need to be less than 0.1 mm.

Non-sorbing tracers' residence time and flow rates through the channels indicate volumes of the transport channels. Those together with the estimated apertures give estimates of the widths of the transport channels. The calculated channel widths vary from about 6.5 m to 50 m. This geometry appears to be unrealistic. The effective widths of the channels are quite close to the lengths of the channels. One should also remember that tracers were injected from the boreholes and in spite of the forced injection the effective extent of the source is not large.

8.5.4 Fault gouge

Tracer retention due to diffusion into the fault gouge is assessed similarly as in the rock matrix alternative. Laboratory data are used for the fault gouge properties and the geometry of the flow path is fitted to give the observed tracer retention. The validity of the assumption that the observed tracer retention comes from the diffusion to the pore space of the fault gouge is judged based on the required flow path geometry. In practice the flow path geometry means here the width of the flow path.

The observed retention can be reproduced using the laboratory sorption and porosity data of fault gouge if the apertures of the flow paths are approximately 0.4 mm to 0.6 mm. Determining the volumes of the transport channels using the residence times of the non-sorbing tracers and the path lengths from the structural model results leads to the flow channel widths that ranges from about 1.5 m to 5.2 m.

The required channel widths in the case of retention to fault gouge are much more reasonable than in the case of retention in the rock matrix. Especially, retention of the sorbing tracers is easier to explain by diffusion to the fault gouge. Non-sorbing tracers show more retention than is produced by suitable flow path geometry for the sorbing tracers. This may imply presence of some other retention process that is more dominating for non-sorbing than sorbing tracers. In the evaluation it is assumed that this process is diffusion to the stagnant zones of the flow field.

8.5.5 Summary

The performed evaluation of the observed tracer retention in the Phase C tracer tests has lead to following conceptualisation of the transport channels;

- The main retention processes are surface sorption, diffusion to the pore space of the fault gouge for the sorbing tracers and diffusion to the stagnant zones for the non-sorbing tracers.

- The relative importance of the diffusion into stagnant zones and fault gouge for the least sorbing tracers was not directly examined but Tables 8-6 and 8-7 indicate that diffusion to the stagnant regions may be important process also for the least sorbing tracers.

The developed transport channels are illustrated and quantified by combining the results of the flow field analysis and diffusion to the fault gouge. Channel apertures vary from 0.45 to 0.62 mm and average channel width from 1.5 to 5.2 m, depending on the flow path. The flow field analysis carried out for the non-sorbing tracers give the best results if the correlation length of the velocity variation is in the centimetre scale. On the other hand, diffusion to the stagnant zones gives reasonable retention for the least sorbing and non-sorbing tracers if the mean distance between the stagnant zones that is about 2-5 cm. These two results are mutually consistent if it is assumed that the same phenomena in the flow field produce both stagnant zones and the velocity variation. This kind of process can be, for example, channelling of the flow due to the obstacles or low aperture regions in the flow channels.

A conceptual illustration of the developed transport channels that is based on the evaluation is presented in Figure 8-17.

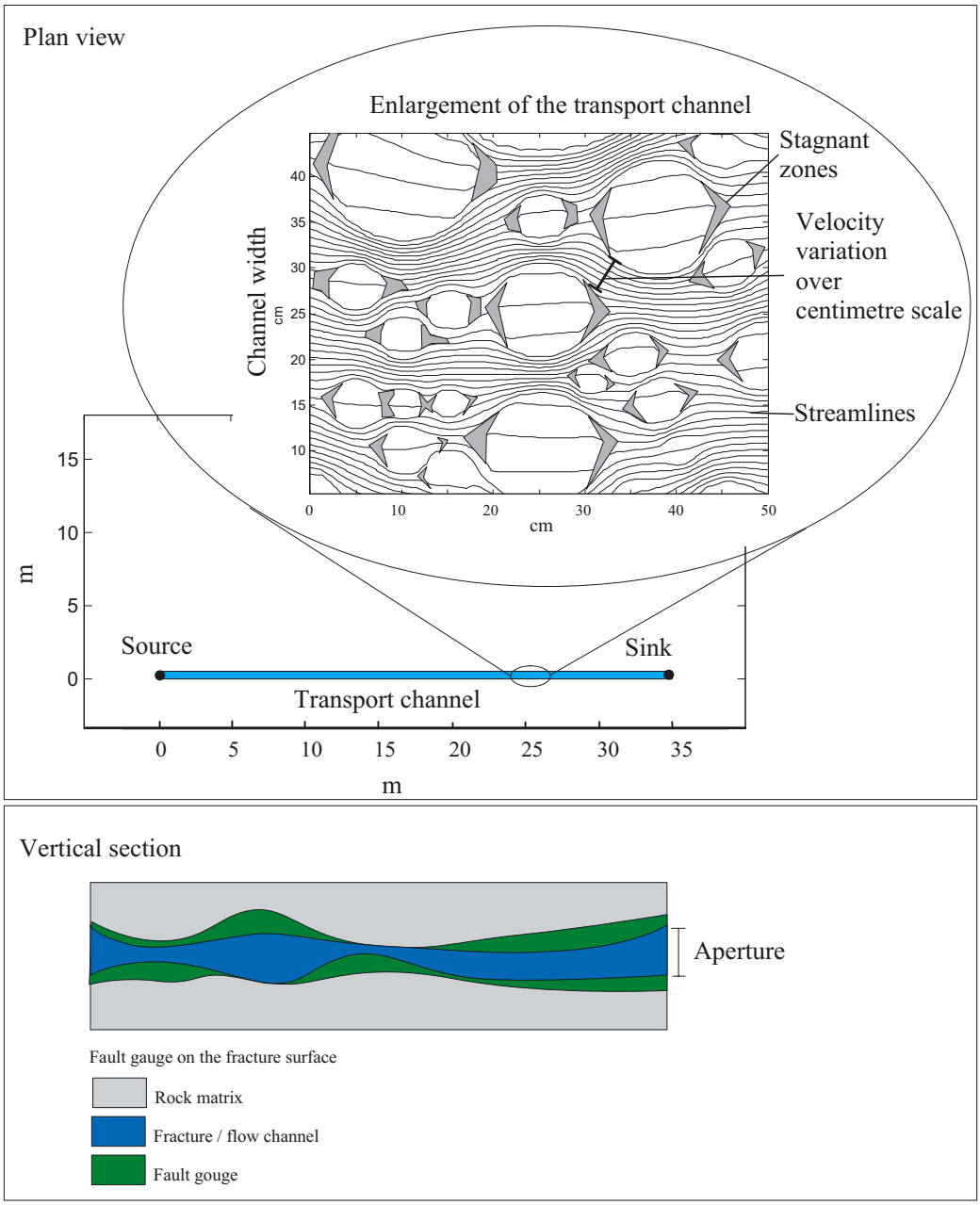

Figure 8-17. *Conceptual illustration of the transport channels based on the evaluation. The evaluation suggests that the main retention processes are diffusion to the fault gouge and stagnant zones.*

9 Summary and discussion

Tracer transport through a network of fractures is evaluated using a simple flow channel (or streamtube) model. It is assumed that the transport takes place due to the advective field that is characterised by a distribution of velocities and the correlation length of the spatial velocity variation. The residence time distribution of the tracer particles is also affected by molecular diffusion in the flow field. It is assumed that surface sorption and diffusion to the immobile zones retard tracer migration. Immobile zones can be located in the pore space of the geological material or in the void space of the fracture.

The modelling of the transport problem is based on the assumption that the immobile zones can be treated as an infinite medium. This assumption has not been verified. It is quite possible that in the case of the stagnant zones of the flow field and smallest particle fraction of the fault gouge this assumption is not fulfilled.

The evaluation shows that the observed retention is quite strong. This can be explained by application of elevated porosity/K_d values compared to the laboratory measurements. However, there is no clear basis for the elevated K_d values though the porosity can be higher close to the fracture surface. It is important to note that the retention depends on grouped parameters. It is not always possible to resolve the retention parameter group to obtain unique values for the individual physical parameters. In the evaluation, the physical parameters were determined by assigning the excess retention capacity, compared to that indicated by the laboratory measurements, to the flow field properties. In the applied simple flow channel model this means evaluation of the effective width of the transport channel. The evaluation indicates that it is not reasonable to explain the retention by diffusion to the rock matrix (unaltered wall rock). Diffusion/sorption to the fault gouge gives more realistic results. However, in both cases it is difficult to reproduce the desired retention using available laboratory data on sorption and porosity.

It is questionable whether the selected laboratory K_d values of the fault gouge, based on measured data for very small size fraction diameter less than 125 μm, are the best choice for all tracers. There may exist an equitable size fraction of fault gouge in the fracture but those particles would most likely get saturated during the tracer tests. This means that then the kinetic diffusion model does not describe the retention correctly. On the other hand, if the retention in the fault gouge is governed by larger particles then the selected K_d data probably are not representative. On the average the K_d values for small size fraction of the gouge are about 10-20 times larger than for the rock matrix. The larger size fraction shows 2-70 times smaller K_d than rock matrix.

Uncertainties related to the flow parameters are also quite large. For example, in the evaluation of the Phase C tracer experiments the lengths of the flow paths are calculated based on the structural model assuming planar. The estimated length of the flow path along the fractures is in some cases much longer than the Euclidean distance between source and sink. In C2 the length of the in-plane flow path is about 97 m whereas the Euclidean distance from source to sink is about 17 m (Andersson et al., 2001). This shows that as an extreme case close to an order of magnitude uncertainty can also be associated with the length of flow path.

The division between retention due to surface sorption and diffusion to the immobile pore space is not obvious and this gives rise to additional uncertainty. The surface sorption is determined as a retardation coefficient not taking into account the actual aperture. The reason for this is that the aperture estimate originates from the retention due to the diffusion to the immobile zones. Strictly, the determination of the surface sorption and other retention parameters should have been done using an iterative approach. In addition, determination of the surface sorption by scaling the breakthrough times to the same first breakthrough time is quite an insensitive method especially for the most sorbing tracers.

There are also uncertainties connected to the source terms of the tracer experiments. This can be seen in the C1 and C2 tests where forced injection has been applied. It seems that the stronger the forced injection applied the larger the discrepancy between the flow rate determined from the tracer dilution and the applied injection flow rate. In C1 the forced injection has been 2700 ml/h but dilution of the K-42 and Na-24 show only about 1500 ml/h flow rate. Predictions were calculated applying flow rates that are calculated from the dilution curves but in the evaluation the forced injection flow rates have been applied.

The evaluation has not been able to resolve the governing retention processes in the Phase C tracer tests. It is likely that distinctly different processes have been major retention processes for non-sorbing and sorbing tracers, respectively. It also seems evident that diffusion to the rock matrix alone cannot explain the retention seen for the sorbing tracers'. Probably, the retention follows from two parallel superimposed processes: surface sorption and diffusion to the fault gouge, stagnant zones or rock matrix.

Over the time scales of the tracer tests the system altered wall rock of higher porosity and unaltered rock matrix of lower porosity may have caused significant effects. This heterogeneity has not been taken into evaluation. It can, for example, lead to the effective retention properties that vary tracer by tracer along the same flow path in such a way that model based on single effective immobile zone (altered or unaltered) cannot explain all the tracers simultaneously.

References

Andersson, P., Ludvigson, J.-E., Wass, E., and Holmqvist, M., 2000a. TRUE Block Scale Project Tracer Test Stage. Interference tests, dilution tests and tracer tests, Phase A. Äspö Hard Rock Laboratory, SKB International Progress Report IPR-00-28.

Andersson, P., Wass, E., Holmqvist, M. and Fierz, T., 2000b. Tracer tests, Phase B. Äspö Hard Rock Laboratory, TRUE Block Scale Project. SKB International Progress Report, IPR-00-29.

Andersson, P., Byegård, J., Holmqvist, M., Skålberg, M., Wass, E., and Widestrand, H., 2001. TRUE Block Scale tracer test stage. Tracer tests, Phase C. SKB International Progress Report IPR-01-33.

Andersson, P., Byegård, J., and Winberg, A., 2002a. Final report of the TRUE Block Scale project, 2. Tracer tests in the block scale. SKB Technical Report TR-02-14, May 2002.

Andersson, P., Byegård, J., Dershowitz, B., Doe, T., Hermanson, J., Meier, P., Tullborg, E.-L. and Winberg, A. (ed), 2002b. Final report of the TRUE Block Scale project, 1. Characterisation and model development. SKB Technical Report TR-02-13, April 2002.

Byegård, J., Johansson, H., Skålberg, M., and Tullborg, E-L., 1998. The interaction of sorbing and non-sorbing tracers with different Äspö rock types. Sorption and diffusion experiments in the laboratory scale. SKB Technical Report TR-98-18

Hautojärvi, A., 1989. Dispersion in transport through fractures. Technical Research Centre of Finland, Nuclear Engineering Laboratory. Espoo, Finland. Technical Report, TOKA-26/89.

Hautojärvi, A. and Taivassalo, V., 1994. The Intraval Project -Analysis of the Tracer Experiments at Finnsjön by the VTT/TVO Project Team. Nuclear Waste Commission of Finnish Power Companies. Report YJT-94-24.

Hermanson, J., and Doe, T., 2000. TRUE Block Scale Project Tracer test stage. March'00 structural and hydraulic model based on borehole data from KI0025F03. SKB, Äspö Hard Rock Laboratory. International Progress Report IPR-00-34.

Winberg, A. (ed), 2000. Final report of the detailed characterisation stage- Compilation of premises and outline of programme for tracer tests in the block scale. ICR-00-02 - Report on detailed characterisation stage. Äspö Hard Rock laboratory, SKB International Cooperation Report ICR-00-02.

Winberg, A., Andersson, P., Hermanson, J., Byegård, J., Cvetkovic, V., and Birgersson, L., 2000. Äspö Hard Rock Laboratory, Final report of the first stage of the tracer retention understanding experiments. SKB Technical Report TR-00-07. March 2000.

Appendix A: Fitted breakthrough curves of the STT-1, STT-1b and STT-2 tests

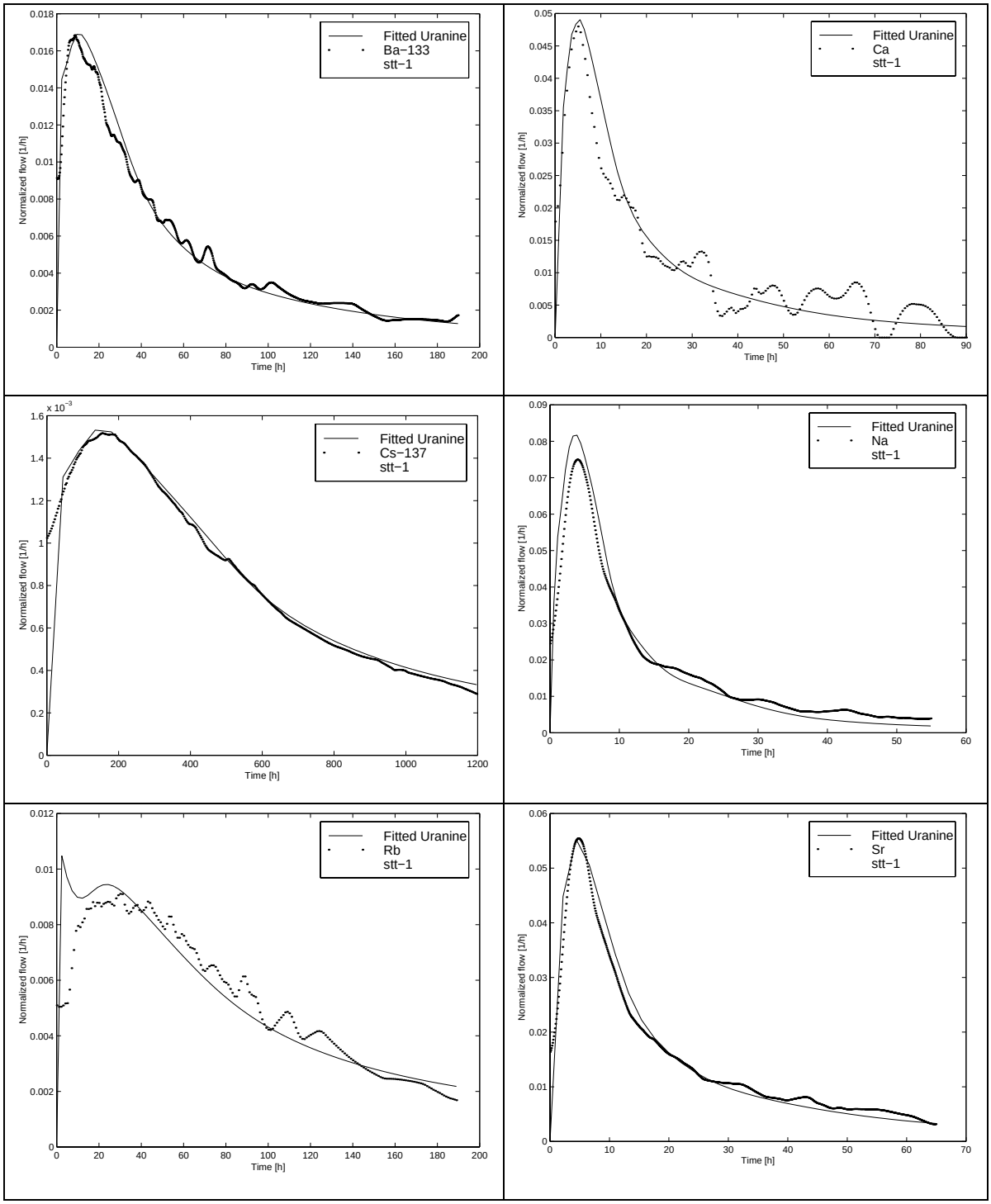

Figure A-1m*. Modelled breakthrough curves fitted to the TRUE-1 STT-1 in situ test results. Para eter* U_t *and retardation coefficient* R_a *are given in Table 4-3.*

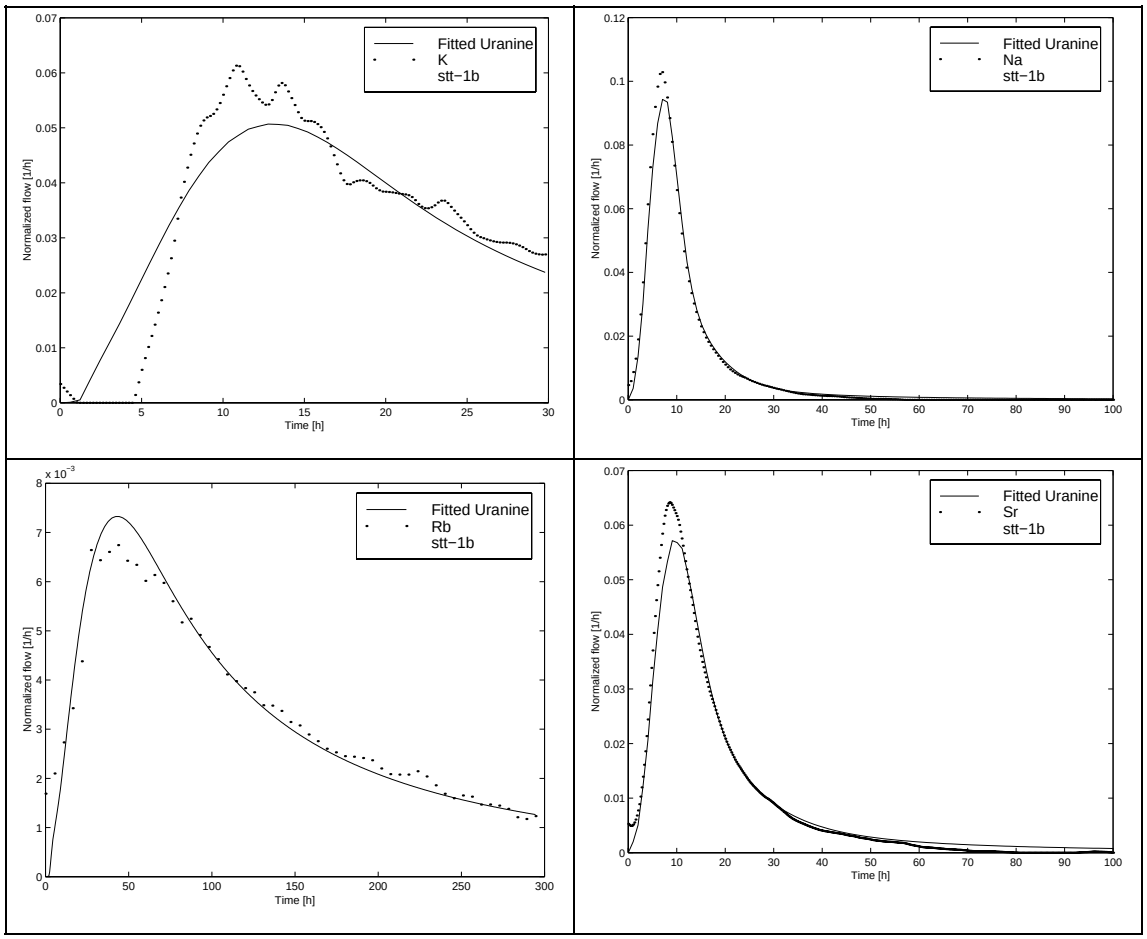

***Figure A-2**. Modelled breakthrough curves fitted to the TRUE-1 STT-1b in situ test results. Parameter* U_t *and retardation coefficient* R_a *are given in Table 4-3.*

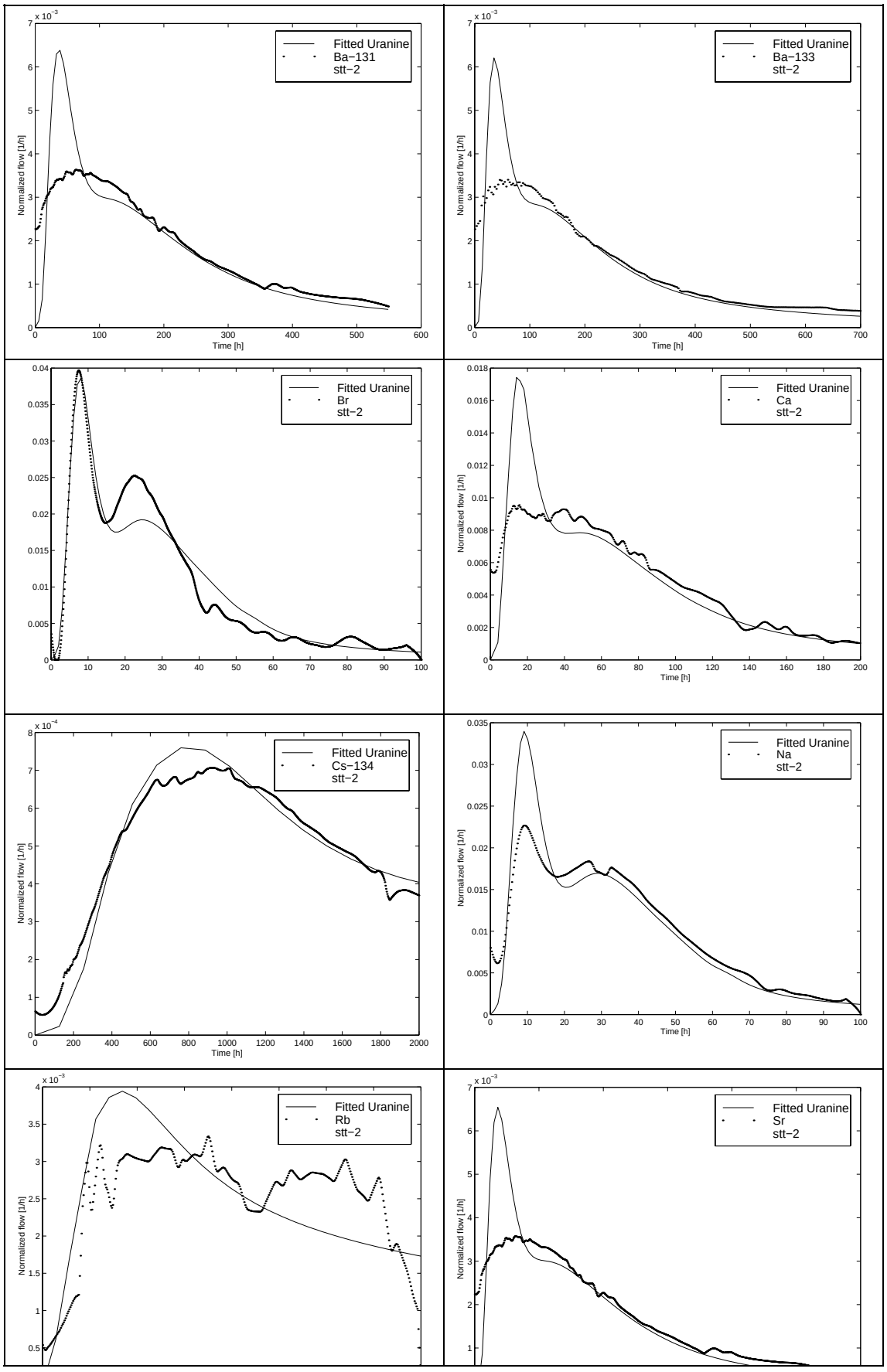

***Figure A-3**. Modelled breakthrough curves fitted to the TRUE-1 STT-2 in situ test results. Parameter* U_t *and retardation coefficient* R_a *are given in Table 4-3.*

Appendix B: Additivity of the retention parameters *u* and R_a

The governing equations for the transport in the case of advection and diffusion to the immobile pore water are

$$\begin{aligned} R_a \frac{\partial c_f}{\partial t} + v\frac{\partial c_f}{\partial x} - 2\frac{D_e}{2b}\frac{\partial c_m}{\partial z}\bigg|_{z=0} &= 0 \\ R_p \frac{\partial c_m}{\partial t} - D_p \frac{\partial^2 c_m}{\partial z^2} &= 0 \end{aligned} \qquad \text{(B-1)}$$

with boundary conditions

$$\begin{aligned} c_f &= \delta(t), x = 0 \\ c_m &= c_f, z = 0 \quad . \\ \lim_{z->\infty} c_m &= 0 \end{aligned} \qquad \text{(B-2)}$$

The solution for c_f can be obtained by using Laplace transforms. In the transformed domain the solution is

$$\ell\{c_f\} = \bar{c}_f = \exp\left(-\frac{R_a x}{v}p\right)\exp\left(-2\frac{D_e x}{v2b}\sqrt{\frac{R_p}{D_p}}\sqrt{p}\right) \quad . \qquad \text{(B-3)}$$

The solution (B-3) can be simplified by defining two parameters

$$\begin{aligned} t_w &= \frac{R_a x}{v} \\ u &= \frac{D_e x}{v2b}\sqrt{\frac{R_p}{D_p}} \end{aligned} \qquad \text{(B-4)}$$

Equation (B-3) can be now written as

$$\bar{c}_f(p, t_w, u) = \exp(-t_w p)\exp\left(-2u\sqrt{p}\right) \quad . \qquad \text{(B-5)}$$

The inverse of the transformation (B-5) gives the solution for the solute breakthrough in the case of a single homogeneous transport channel and Dirac input of unit mass of the solute

$$c_f(t, t_w, u) = \theta(t - t_w)\frac{u}{\sqrt{\pi}}(t - t_w)^{-3/2}\exp\left(-\frac{u^2}{t - t_w}\right), \qquad \text{(B-6)}$$

where θ is the Heaviside's step function.

Transport channels in series

If two transport channels are connected in series then the outlet of the first channel is given as an input to the second channel. Outlet the two-channel system can be now given as a convolution integral

$$c'_f(t) = \int_0^t c_f(\tau, t_{w1}, u_1) c_f(t-\tau, t_{w2}, u_2) d\tau \ , \qquad \text{(B-7)}$$

where the function c_f, outlet of a single homogeneous channel, is defined in Equation (B-6). Properties of the first channel are u_1 and t_{w1} and for the second channel u_2 and t_{w2}. According to the Faltung theorem

$$\ell\{c'_f(t)\} = \ell\{c_f(t, t_{w1}, u_1)\}\ \ell\{c_f(t, t_{w2}, u_2)\}, \qquad \text{(B-8)}$$

where ℓ denotes the Laplace transform. Applying Equation (B-5) gives now

$$\begin{aligned} \bar{c}'_f(p) &= \exp(-t_{w1}p)\exp\left(-2u_1\sqrt{p}\right)\exp(-t_{w2}p)\exp\left(-2u_2\sqrt{p}\right) \\ &= \exp(-(t_{w1}+t_{w2})p)\exp\left(-2(u_1+u_2)\sqrt{p}\right) \end{aligned} . \qquad \text{(B-9)}$$

The result of the Equation (B-7) can now be written as

$$c'_f(t) = \int_0^t c_f(\tau, t_{w1}, u_1) c_f(t-\tau, t_{w2}, u_2) d\tau = c_f(t, t_{w1}+t_{w2}, u_1+u_2) \ . \qquad \text{(B-10)}$$

where c_f is the breakthrough from a single homogeneous channel and the parameters t_{w1} and t_{w2} refer to the transit times and the parameters u_1 and u_2 refer to the matrix diffusion properties of the channels 1 and 2, respectively.

Parallel diffusion processes

Equation (B-1) assumes that there is a single one dimensional diffusion process between the migrating solute and surroundings. Let us now assume that there are two such a processes occurring in parallel and independently in the transport channel. Equations (B-1) and (B-2) can now be rewritten as

$$\begin{aligned} & R_a \frac{\partial c_f}{\partial t} + v\frac{\partial c_f}{\partial x} - 2\frac{D_{e_1}}{2b_1}\frac{\partial c_{m_1}}{\partial z_1}\bigg|_{z_1=0} - 2\frac{D_{e_2}}{2b_2}\frac{\partial c_{m_2}}{\partial z_2}\bigg|_{z_2=0} = 0 \\ & R_{p_1}\frac{\partial c_{m_1}}{\partial t} - D_{p_1}\frac{\partial^2 c_{m_1}}{\partial {z_1}^2} = 0 \\ & R_{p_2}\frac{\partial c_{m_2}}{\partial t} - D_{p_2}\frac{\partial^2 c_{m_2}}{\partial {z_2}^2} = 0 \end{aligned} \qquad \text{(B-11)}$$

and for the boundary conditions

$$\begin{aligned} & c_f = \delta(t)\,,\, x = 0 \\ & c_{m_1} = c_{m_2} = c_f\,,\, z_1 = 0,\, z_2 = 0 \\ & \lim_{z_1 \to \infty} c_{m_1} = \lim_{z_2 \to \infty} c_{m_2} = 0 \end{aligned} \quad . \qquad \text{(B-12)}$$

The Laplace transforms of the Equations (B-1) are

$$\begin{aligned} & R_a\, p\bar{c}_f + v\frac{\partial \bar{c}_f}{\partial x} - 2\frac{D_{e_1}}{2b_1}\frac{\partial \bar{c}_{m_1}}{\partial z_1}\bigg|_{z_1=0} - 2\frac{D_{e_2}}{2b_2}\frac{\partial \bar{c}_{m_2}}{\partial z_2}\bigg|_{z_2=0} = 0 \\ & R_{p_1}\, p\bar{c}_{m_1} - D_{p_1}\frac{\partial^2 \bar{c}_{m_1}}{\partial {z_1}^2} = 0 \\ & R_{p_2}\, p\bar{c}_{m_2} - D_{p_2}\frac{\partial^2 \bar{c}_{m_2}}{\partial {z_2}^2} = 0 \end{aligned} \quad , \qquad \text{(B-13)}$$

where p is the variable of the Laplace transfered domain. Solution in the transfered domain for the $\bar{c}_f$ can be solved similarly as in the case of the Equation (B-1). The equation for the $\bar{c}_f$ becomes following

$$R_a\, p\bar{c}_f + v\frac{\partial \bar{c}_f}{\partial x} + 2\frac{D_{e_1}}{2b_1}\sqrt{\frac{R_{p_1}}{D_{p_1}}}\sqrt{p}\,\bar{c}_f + 2\frac{D_{e_2}}{2b_2}\sqrt{\frac{R_{p_2}}{D_{p_2}}}\sqrt{p}\,\bar{c}_f = 0 \quad , \qquad \text{(B-14)}$$

that can be written as

$$\frac{d\bar{c}_f}{\bar{c}_f} = \left(-\frac{R_a\, p}{v} - 2\frac{D_{e_1}}{v\,2b_1}\sqrt{\frac{R_{p_1}}{D_{p_1}}}\sqrt{p} - 2\frac{D_{e_2}}{v\,2b_2}\sqrt{\frac{R_{p_2}}{D_{p_2}}}\sqrt{p} \right) dx \quad . \qquad \text{(B-15)}$$

Integration of the Equation (B-15) gives the solution for $\bar{c}_f$, that satisfies also the boundary conditions given in Equations (B-12).

$$\bar{c}_f = \exp\left(-\frac{R_a x}{v} p\right)\exp\left(-2\left\{\frac{D_{e_1} x}{v 2b_1}\sqrt{\frac{R_{p_1}}{D_{p_1}}} + \frac{D_{e_2} x}{v 2b_2}\sqrt{\frac{R_{p_2}}{D_{p_2}}}\right\}\sqrt{p}\right). \quad \text{(B-16)}$$

Using definitions in Equation (B-4) the solution (B-16) can be written as

$$\bar{c}_f = \exp(-t_w p)\exp\left(-2[u_1 + u_2]\sqrt{p}\right) \quad , \quad \text{(B-17)}$$

where

$$u_i = \frac{D_{e_i} x}{v 2b_i}\sqrt{\frac{R_{p_i}}{D_{p_i}}} \quad , \; i = 1, 2 \quad . \quad \text{(B-18)}$$

Based on the Equations (B-5) and (B-6) the solution for the breakthrough from two parallel transport channels, c'_f, can be written as

$$c'_f(t) = c_f(t, t_w, u_1 + u_2), \quad \text{(B-19)}$$

where c_f is the solution for a single homogeneous channel and parameters u_1 and u_2 refer to channels 1 and 2, respectively.

Appendix C: Retention parameters fitted to the Phase C tracer experiments

Table C-1. Fitted retention parameters u and R_a for simulated breakthrough curves of Br-82, Na-24 and Ca-47 in test C1. Recovery estimate 1 refers to extrapolated recovery using $t^{-3/2}$ fit to the tailing of the measured breakthrough curves and estimate 2 refers to an exponential fit to the tailing.

Channel width	Recovery estimate *)	Br-82		Na-24		Ca-47	
		U_t [$h^{-1/2}$]	R_a	U_t [$h^{-1/2}$]	R_a	U_t [$h^{-1/2}$]	R_a
0.04 m	1	0.0844	1.0001	0.1560	1.0500	0.2324	1.3000
	2	0.0711	1.0000	0.1183	1.0904	0.1948	1.3000
0.10 m	1	0.0600	1.0000	0.1149	1.1180	0.1990	1.3005
	2	0.0506	1.0000	0.0841	1.2105	0.1712	1.3087
0.20 m	1	0.0600	1.0000	0.1148	1.1180	0.1988	1.3038
	2	0.0501	1.0053	0.0841	1.2105	0.1712	1.3087
0.30 m	1	0.0600	1.0000	0.1149	1.1177	0.1988	1.3038
	2	0.0506	1.0000	0.0841	1.2106	0.1712	1.3087

Table C-2. Fitted retention parameters u and R_a for simulated breakthrough curves of K-42, Rb-86 and Cs-134 in test C1. Recovery estimate 1 refers to extrapolated recovery using $t^{-3/2}$ fit to the tailing of the measured breakthrough curves and estimate 2 refers to an exponential fit to the tailing.

Channel width	Recovery estimate *)	K-42		Rb-86		Cs-134	
		U_t [$h^{-1/2}$]	R_a	U_t [$h^{-1/2}$]	R_a	U_t [$h^{-1/2}$]	R_a
0.04 m	1	0.3938	1.4000	0.8861	3.0000	2.4565	16.0000
	2	0.3113	1.4000	0.7154	3.5184	1.9829	20.0927
0.10 m	1	0.3351	1.4000	0.7071	3.0000	1.8407	16.0500
	2	0.2685	1.4000	0.5547	3.0000	1.6000	16.0000
0.20 m	1	0.3351	1.4000	0.7071	3.0000	1.8407	16.0500
	2	0.2685	1.4000	0.5547	3.0000	1.6000	16.0000
0.30 m	1	0.3352	1.4000	0.7071	3.0000	1.8401	16.1000
	2	0.2685	1.4000	0.5547	3.0000	1.6000	16.0000

Table C-3. Fitted retention parameters u and R_a for simulated breakthrough curves of Re-186 and Ca-47 in test C2. Recovery estimate 1 refers to extrapolated recovery using $t^{-3/2}$ fit to the tailing of the measured breakthrough curves and estimate 2 refers to an exponential fit to the tailing.

Channel width Recovery estimate *)		Re-186		Ca-47	
		U_t [$h^{-1/2}$]	R_a	U_t [$h^{-1/2}$]	R_a
0.04 m	1	0.1281	1.0000	0.2516	2.4000
	2	0.0800	1.0041	0.1495	2.4000
0.10 m	1	0.0988	1.0001	0.1939	2.4048
	2	0.0516	1.0041	0.1185	2.4000
0.20 m	1	0.0738	1.0000	0.1652	2.4000
	2	0.0516	1.0041	0.1158	2.4030
0.30 m	1	0.0738	1.0000	0.1652	2.4000
	2	0.0516	1.0041	0.0957	2.4000

Table C-4. Fitted retention parameters u and R_a for simulated breakthrough curves of HTO, Na-22 and Sr-85 in test C3. Recovery estimate 1 refers to extrapolated recovery using $t^{-3/2}$ fit to the tailing of the measured breakthrough curves and estimate 2 refers to an exponential fit to the tailing.

Channel width Recovery estimate *)		HTO		Na-22		Sr-86	
		U_t [$h^{-1/2}$]	R_a	U_t [$h^{-1/2}$]	R_a	U_t [$h^{-1/2}$]	R_a
0.04 m	1	0.0912	1.0008	0.1438	1.3000	0.2419	1.5000
	2	0.0743	1.0009	0.1141	1.3000	0.1759	2.3099
0.10 m	1	0.0716	1.0003	0.1166	1.3325	0.1993	1.6886
	2	0.0595	1.0005	0.0952	1.3000	0.1435	2.4999
0.20 m	1	0.0387	1.0007	0.0727	1.3000	0.1251	2.0941
	2	0.0315	1.0007	0.0569	1.3407	0.0877	2.8814
0.30 m	1	0.0507	1.0008	0.0883	1.3000	0.1505	1.9839
	2	0.0396	1.0008	0.0681	1.3199	0.1050	3.4000